

# Towards the firsts compelling signs of vacuum dynamics in modern cosmological observations

Joan Solà<sup>1, 2, 3,\*</sup>, Javier de Cruz Pérez<sup>1, 2, †</sup> and Adrià Gómez-Valent<sup>1, 2, ‡</sup>

<sup>1</sup>*Departament de Física Quàntica i Astrofísica (FQA), Universitat de Barcelona,  
Av. Diagonal 647, E-08028 Barcelona, Catalonia, Spain*

<sup>2</sup>*Institute of Cosmos Sciences, Universitat de Barcelona (ICCUB).*

<sup>3</sup>*Institute of Advanced Studies (IAS), Nanyang Technological University, Singapore.*

(Dated: June 30, 2022)

In this paper we assess the possibility that a rigid cosmological constant,  $\Lambda$ , and hence the traditional concordance  $\Lambda$ CDM model, might not be the best phenomenological description of the current cosmological data. We show that a large class of dynamical vacuum models (DVMs), whose vacuum energy density  $\rho_\Lambda = \rho_\Lambda(H)$  consists of a nonvanishing constant term and a series of powers of the Hubble rate, provides a substantially better phenomenological account of the overall SNIa+BAO+ $H(z)$ +LSS+CMB cosmological observations. We find that some models within the class of DVMs, particularly the running vacuum model (RVM), appear significantly much more favored than the  $\Lambda$ CDM, at an unprecedented confidence level of  $\sim 4\sigma$ . We further support this claim by computing the Akaike and Bayesian information criteria and confirm that the RVM is strongly preferred as compared to the  $\Lambda$ CDM. In addition, we compare the dynamical vacuum signature encoded in the RVM to the behavior of the generic XCDM and CPL parametrizations of the dark energy, as well as to realistic  $\phi$ CDM (quintessence) models with specific potentials (e.g. the Peebles & Ratra potential). In all cases the most telltale sign of dynamical vacuum energy in our expanding universe lies in the combined triad of modern BAO+LSS+CMB observations. In the absence of any of these three crucial data sources, the dynamical signature could not be perceived at a significant confidence level. This comprehensive paper is the expanded, and fully updated, backup version of the previously submitted, Letter-type, presentation of our results in arXiv:1606.00450.

PACS numbers: 98.80.-k, 98.80.Es, 95.36.+x

## I. INTRODUCTION

The presence of dark energy (DE) in our universe seems to be a well established empirical reality in modern cosmology. The facts supporting its existence are robust, innumerable and overwhelming. They are compellingly expressed through the observational body of evidence confirming the accelerated expansion of the universe, evidence that has been piling up in the last two decades from a large variety of cosmological sources, see [1–6] and references therein. On these grounds it all looks as if the historical investigation on the DE has been a research path full of color and successes. It is so, in part, but not exactly so. For one thing, real knowledge and understanding of the physical quantities being measured seems to lag “a bit” behind the outstanding record achieved by the modern observations. It is disquieting to recognize that our theoretical conceptions, bold as they are in some cases, did not live up to our expectations. In fact, they did not follow a pace comparable to the astounding developments undergone by the observational tools and highly sophisticated instruments that have been (and are being) used to explore our patch of surrounding cosmos. That this dual pace between empirical and theoretical knowl-

edge is a factual reality in cosmology becomes apparent when we try to answer the next obvious scientific question at stake: what is the dark energy that we observe? Is it a substance, is it a field, may be an effect associated to something else more fundamental than matter and fields? Or perhaps it is the quantum vacuum in action, maybe behaving in a way that we are not sufficiently prepared to fully understand it yet? Cosmologists have worked hard to decipher the dark energy code, but the bare facts tell us that despite the staggering technological victories in exploring the universe in the last twenty years, we are still facing a longstanding, stubbornly persistent, almost hopeless ignorance about the physical nature of the DE and hence on the ultimate cause of the observed acceleration of the universe. This profound and distressing conflict is, of course, at the root of the Cosmological Constant Problem (CCP) [7–12], most likely the biggest theoretical conundrum of Fundamental Physics of all times.

Such a situation becomes all the more worrisome when witnessed from the deep and broad perspective of the historical facts, and especially in the very year when the cosmological constant (CC),  $\Lambda$ , in Einstein’s equations turns hundred years old [13]. The  $\Lambda$ -term, or equivalently the vacuum energy density associated to it,  $\rho_\Lambda = \Lambda/(8\pi G)$  ( $G$  being Newton’s gravitational coupling), is usually regarded as the simplest possible explanation for the DE. A positive, constant, tiny value (in particle physics units) of order  $\rho_\Lambda \sim 10^{-47} \text{ GeV}^4 \sim (10^{-3} \text{ eV})^4$  can explain the needed speed up of our cosmos according to the

\*Electronic address: [sola@fqa.ub.edu](mailto:sola@fqa.ub.edu)

†Electronic address: [decruz@fqa.ub.edu](mailto:decruz@fqa.ub.edu)

‡Electronic address: [adriagova@fqa.ub.edu](mailto:adriagova@fqa.ub.edu)

aforementioned wealth of cosmological observations. The standard or “concordance” cosmological model embodies such an assumption as a fundamental built-in principle, together with the hypothesis of dark matter (DM), and for this reason is called the  $\Lambda$ CDM model. Phrased in terms of the current cosmological parameters, the  $\Lambda$ CDM assumes that  $\rho_\Lambda = \text{const.}$  throughout the history of the universe, with  $\Omega_\Lambda \simeq 0.7$  and  $\Omega_m \simeq 0.3$  at present. However, no convincing theoretical explanation is provided about the measured value of  $\rho_\Lambda$ . In actual fact, no fundamental theory, not even quantum field theory (QFT), can explain this value; and, what is worse, the typical prediction is preposterously large as compared to the measured value. This is recognized as such as of the time when Y.B. Zeldovich first observed [14] that the contribution from QFT to the vacuum energy density should be of order  $\sim m^4$  for any quantum field of mass  $m$ , and therefore many orders of magnitude bigger than the existing upper bound on  $\rho_\Lambda$  in those days. This observation by Zeldovich, made just half-century ago, can be reckoned as the actual birth of the CCP. The realization that the problem becomes further aggravated by the spontaneous symmetry breaking mechanism (or Higgs mechanism [15]) in modern gauge theories, a key ingredient of our beloved standard model of electroweak interactions, came only a few years later [16–18]. A lot has been said and done since, but despite numerous and strenuous efforts no convincing resolution to the “ $\Lambda$ -enigma” is available at present yet.

It is well-known that G. Gamow asserted in his autobiography [19] that Einstein considered the introduction of  $\Lambda$  in his equations as the greatest “blunder” made in his life. Right next, however, Gamow wrote the following prescient words, which still resonate in our ears with undamped strength: ‘But this “blunder”, rejected by Einstein, is still sometimes used by cosmologists even today, and the cosmological constant denoted by the Greek letter  $\Lambda$  rears its ugly head again and again and again’ [19].

Not too surprisingly, cosmologists have felt motivated to look for many other explanations for the DE beyond a rigid cosmological constant  $\Lambda$ . The most popular option came with the use of *ad hoc* scalar fields  $\phi$  in cosmology, such as in the Brans-Dicke context [20] as well as in general scalar-tensor theories [21]. The scalar field paradigm was then profusely used also to make the cosmic vacuum dynamical:  $\Lambda = \Lambda(\phi)$ . In the old days the main aim was to adjust the large value of  $\Lambda$  typically predicted in QFT to zero. Among the proposed dynamical mechanisms, the cosmon model [22] played an influential role and was discussed as a prototype model by Weinberg in his famous review [7]. There were many early proposals, see e.g. [23–30]. In spite of the hopes raised by these works at solving the “old CC Problem”, it was later shown by Weinberg (through the so-called “no-go theorem” [7]) that most if not all the dynamical adjustment mechanisms existing in the literature to date were afflicted by a more or less obvious form of subtly hidden fine tuning. For this reason the subsequent use of scalar

fields in cosmology was mostly focused on trying to explain another aspect of the CCP: the cosmic coincidence problem (viz. the fact that  $\rho_\Lambda$  happens to be so close to the matter density  $\rho_m$  right now), see e.g. [10]. The new wave of dynamical scalar fields in cosmology crystalized in the notions of quintessence, phantom fields and the like, which have had a tremendous influence in cosmology till our days: see e.g. [31–38], the reviews [10, 11] and the many references therein. More or less simultaneously to that new revival of the scalar field fashion, a blooming crest of models based on ascribing a direct phenomenological time-dependence to the the CC term,  $\Lambda = \Lambda(t)$ , broke with impetus into the market [39–46]. For reviews, see e.g. [47], [48], and corresponding references. It is fair to mention that the oldest proposal along these lines stems from the work by M. Bronstein, as early as 1933 [49], who first pointed out that matter and vacuum could be exchanging energy.

The cosmological constant problem stays unsolved right now, even a full century after  $\Lambda$  was first introduced by Einstein [13], and precisely fifty years after the CCP was first formulated as such [14]. Most likely the mystery will remain for a long time still. In this work, we will not attempt to solve neither the old CCP nor the cosmic coincidence problem. Truly, our main aim is much more humble. Somehow we wish to follow the original phenomenological approach that made possible to unveil that  $\Lambda$  is nonvanishing, irrespective of its ultimate physical nature. The method to substantiate that  $\Lambda$  is non-null was largely empirical, namely  $\Lambda$  was assumed to be a parameter and then fitted directly to the data. Of course a minimal set of assumptions had to be made, such as the validity of the Cosmological Principle and hence of the Friedmann-Lemaître-Robertson-Walker (FLRW) metric, with the ensuing set of Friedmann equations for the scale factor [50]. In our case, we wish of course to keep these minimal assumptions and make a phenomenological case study of the next-to-leading possibility on the nature of  $\Lambda$ , to wit: that  $\Lambda$  might be not just a parameter but a slowly varying cosmic variable that stays close to a constant for cosmic spans of time and therefore capable of mimicking the  $\Lambda$ CDM-like behavior.

This is perfectly respectful with the Cosmological Principle and it could help to improve the fit to the overall cosmological data versus the  $\Lambda$ CDM. One cannot exclude that the peculiarities of important cosmological processes, for instance those related with structure formation, are conspicuously sensitive and even positively receptive, to a mild dynamical variation of the cosmic vacuum, which certainly influences the gravitational interaction of matter. Recall that a positive  $\Lambda$  suppresses the growth of structure formation and this explains why the  $\Lambda$ CDM model is highly preferred to the CDM one, in which  $\Lambda = 0$ . The next natural step, therefore, would be to introduce some time modulation of the growth suppression through  $\rho_\Lambda = \rho_\Lambda(t)$ . This might help to ameliorate the description of the large scale structure (LSS) formation data, so it is worthwhile testing it. On the

other hand, a slowly evolving vacuum energy density is a much more natural expectation for a possible fundamental QFT picture of the cosmic vacuum than just a strict cosmological constant, which is completely indifferent to the universe's expansion.

In point of fact, we do not wish to abandon the vacuum hypothesis since we want to stay as close as possible to the  $\Lambda$ CDM. Thus, we retain the vacuum equation of state (EoS)  $p_\Lambda = -\rho_\Lambda$ , but we make allowance for  $\rho_\Lambda$  to have a moderate time variation as a definite function of a cosmic variable  $\zeta$ , i.e.  $\rho_\Lambda = \rho_\Lambda(\zeta)$ . The variation near our time is around a constant value  $C_0$ , namely  $\rho_\Lambda(\zeta) = C_0 + \delta\rho_\Lambda(\zeta)$ , with  $|\delta\rho_\Lambda(\zeta)/C_0| \ll 1$ , and hence  $C_0$  is essentially (but not quite) the current value of  $\rho_\Lambda$ . Here  $\zeta$  is not just the cosmic time  $t$  (even though ultimately any cosmic variable is of course a function of  $t$ ). In the class of dynamical vacuum models (DVMs) being dealt with here,  $\zeta$  can be in all cases the scale factor since they are analytically solvable in terms of it. However, only in one of the DVMs the dynamical variable  $\zeta$  can be further promoted, and be identified from the very beginning, with the full Hubble rate  $H$ , which can eventually be expressed analytically as a function of  $a$ . This especial situation corresponds to the “running vacuum model” (RVM). The fact that  $\zeta = H(a)$  for this model will allow us to further characterize it from the theoretical point of view.

As a matter of fact, the dynamical vacuum models being investigated here can be addressed on mere phenomenological grounds, but in the case of the RVM it can also be motivated within the context of QFT in curved spacetime (see [12, 51–53] and references therein). One can think of this framework as one in which the  $\Lambda$ CDM is replaced by the  $\bar{\Lambda}$ CDM [51], with  $\bar{\Lambda} = \bar{\Lambda}(H)$ , or equivalently  $\rho_\Lambda = \rho_\Lambda(H)$ , playing the role of “running” vacuum energy density. Interestingly, such a running with the expansion rate,  $H$ , can be related to the renormalization group. For previous investigations along these lines, see e.g. [54–65], and the closely related works [66–69]. In some of these cases it is contemplated the possibility that  $G$  also participates in the running, together with  $\rho_\Lambda$ . While this is allowed by the Bianchi identity, we shall not elaborate on this option here. Furthermore, contrary to previous studies we will assume now that baryon number and radiation are strictly conserved and do not have any whatever interaction with the vacuum. Only dark matter will support some dynamical energy exchange with vacuum. This is a reasonable assumption and will allow us to compare the RVM with related DVMs, all of which will be fitted to the data. At the same time, by adopting the mentioned conservation laws will enable us to better confront the DVMs with the traditional  $\phi$ CDM models (viz. the scalar field models accounting for quintessence and phantom DE [10, 11]), and also with the generic XCDM [70] and CPL [71] parametrizations of the dynamical DE [72]. The joint comparison of these models against the current SNIa+BAO+ $H(z)$ +LSS+CMB data will demonstrate not only that some of the DVMs render a very good quality fit that amply surpasses the

performance of the  $\Lambda$ CDM, but it will serve also to emphasize that the dynamical DE signal can be captured (at different strengths) using a variety of models and parametrizations. Needless to say, this is very important since it sheds more light on the possibility that the DE of our universe is most likely dynamical in the light of modern observations. We will show that the peak confidence level of such an evidence is  $\sim 4\sigma$  at present. The main results put forward here were advanced in the Letter-type work [68]. Since then new support to the dynamical DE from the observational point of view has appeared in the literature very recently, see [73].

The guidelines of our work are as follows. In Sect. II we describe the different dynamical vacuum models (DVMs) under consideration. In Sect. III we report on the main fitting results and the set of cosmological data used, on distant type Ia supernovae (SNIa), baryonic acoustic oscillations (BAOs), the Hubble parameter values at different redshifts, the LSS data, and the cosmic microwave background (CMB) distance priors from Planck. In Sect. IV we discuss aspects of structure formation with dynamical vacuum. The numerical analysis of the DVMs and a comparison with the standard XCDM and CPL parametrizations is the object of Sect. V. An ample discussion of the results along with a reanalysis under different conditions, including a comparison with the traditional  $\phi$ CDM models, is developed in Sect. VI. Finally, in Sect. VII we present our conclusions. Two appendices at the end, viz. on the cosmological constant problem and running vacuum (A), and on cosmological observables and statistical analysis (B), complete our presentation.

## II. DYNAMICAL VACUUM MODELS

The gravitational field equations with cosmological term  $\Lambda$  are

$$G_{\mu\nu} - \Lambda g_{\mu\nu} = 8\pi G T_{\mu\nu}, \quad (1)$$

where  $G_{\mu\nu} = R_{\mu\nu} - \frac{1}{2}g_{\mu\nu}R$  is the Einstein tensor. Defining the vacuum energy density (in natural units) as  $\rho_\Lambda = \Lambda/(8\pi G)$ , the full energy-momentum tensor involving the effect of both matter and the vacuum energy density, reads  $\tilde{T}_{\mu\nu} \equiv T_{\mu\nu} + g_{\mu\nu}\rho_\Lambda$ . The original field equations can then be brought to the same form as in the case without  $\Lambda$ -term:  $G_{\mu\nu} = 8\pi G \tilde{T}_{\mu\nu}$ . Notice from the structure of  $\tilde{T}_{\mu\nu}$  that the vacuum is dealt with as a perfect fluid, with EoS  $p_\Lambda = -\rho_\Lambda$ . When the matter can also be treated as an ideal fluid and is distributed homogeneously and isotropically, as postulated by the Cosmological Principle, we can write

$$\tilde{T}_{\mu\nu} = (\rho_\Lambda - p_m)g_{\mu\nu} + (\rho_m + p_m)U_\mu U_\nu, \quad (2)$$

where  $U_\mu$  is the 4-velocity of the cosmic fluid,  $\rho_m$  is the proper energy density of matter and  $p_m$  its isotropic pressure. We assume the standard cosmological framework grounded on the FLRW metric with flat three-dimensional slices:  $ds^2 = dt^2 - a^2(t) d\mathbf{x}^2$ , where  $t$  is the

cosmic time and  $a(t)$  the scale factor. However, we admit that matter can be in interaction with vacuum, which is tantamount to saying that  $\rho_\Lambda = \rho_\Lambda(\zeta)$  is a function of some cosmic variable evolving with time,  $\zeta = \zeta(t)$ . While this, of course, implies that  $\dot{\rho}_\Lambda \equiv d\rho_\Lambda/dt \neq 0$  we assume that  $\dot{G} = 0$  in our study. Such a dynamics of vacuum is compatible with the Bianchi identity (see below) provided there is some energy exchange between vacuum and matter. In other words, matter cannot be strictly conserved in these circumstances. The Friedmann and acceleration equations for the present universe are nonetheless formally identical to the standard  $\Lambda$ CDM case:

$$3H^2 = 8\pi G (\rho_m + \rho_r + \rho_\Lambda(\zeta)) \quad (3)$$

$$3H^2 + 2\dot{H} = -8\pi G (\rho_r - \rho_\Lambda(\zeta)). \quad (4)$$

Here  $H = \dot{a}/a$  is the usual Hubble rate,  $\rho_m = \rho_b + \rho_{dm}$  involves the pressureless contributions from baryons and cold dark matter (DM) in the current epoch, and  $\rho_r$  is the radiation density (with the usual EoS  $p_r = \rho_r/3$ ). We emphasize once more that in the above equations we stick to the EoS,  $p_\Lambda = -\rho_\Lambda$ , although the vacuum is dynamical,  $\rho_\Lambda(t) = \rho_\Lambda(\zeta(t))$ , and its evolution is tied to the cosmic expansion. In all of the dynamical vacuum models (DVMs) being considered here, the cosmic variable  $\zeta$  is either the scale factor or can be expressed analytically in terms of it,  $\zeta = \zeta(a)$ , or equivalently in terms of the cosmological redshift,  $z = a^{-1} - 1$ , where we adopt the normalization  $a = 1$  at present.

From the basic pair of Friedmann and acceleration equations (3)-(4), a first integral of the system follows:

$$\sum_{N=dm,b,r,\Lambda} [\dot{\rho}_N + 3H(\rho_N + p_N)] = 0. \quad (5)$$

Of course, the last term being summed over (for the  $\Lambda$  component) is zero owing to the vacuum EoS. Such a first integral ensues also from the divergenceless property of the full energy-momentum tensor  $\tilde{T}_{\mu\nu}$ , see Eq.(2), in the FLRW metric, i.e.  $\nabla^\mu \tilde{T}_{\mu\nu} = 0$ . The last property is a consequence of the Bianchi identity satisfied by the Einstein tensor,  $\nabla^\mu G_{\mu\nu} = 0$ , and the assumed constancy of the Newtonian coupling  $G$ . It reflects the local conservation law of the compound system formed by matter and vacuum, and the consequent nonconservation of each of these components when taken separately. For our purposes it will be more convenient to reexpress the combined conservation law in a way that reflects more explicitly the interaction between the particular components of the cosmic fluid. Thus, by introducing the vacuum-matter interaction source,  $Q$ , and using the vacuum EoS we can conveniently split (5) into two coupled equations:

$$\dot{\rho}_{dm} + 3H\rho_{dm} + \dot{\rho}_b + 3H\rho_b + \dot{\rho}_r + 4H\rho_r = Q, \quad (6)$$

$$\dot{\rho}_\Lambda = -Q. \quad (7)$$

Rephrased in this form, it will be easier to sort out the types of DVMs we will be dealing with in terms of the different proposed forms for  $Q$ . For example, in the  $\Lambda$ CDM

case the vacuum energy density is  $\rho_\Lambda = \text{const.}$  and therefore  $Q = 0$ . The concordance model assumes also that matter and radiation are self-conserved after equality. It also assumes that baryons and CDM are separately conserved. Hence their respective energy densities satisfy  $\dot{\rho}_b + 3H\rho_b = 0$ ,  $\dot{\rho}_r + 4H\rho_r = 0$  and  $\dot{\rho}_{dm} + 3H\rho_{dm} = 0$ . Nevertheless, it is obvious that in the presence of vacuum dynamics at least one of these equations cannot hold. Following our definite purpose to remain as close as possible to the  $\Lambda$ CDM, we would like to leave the most sensitive and accessible components of the cosmic fluid completely unaltered by the vacuum dynamics. Thus, in the considered DVMs, we will assume that the first two of the above conservation equations still hold good but that the last does not, meaning that the vacuum exchanges energy only with DM. The dilution laws for baryons and radiation as a function of the scale factor therefore take on the conventional  $\Lambda$ CDM forms:

$$\rho_b(a) = \rho_{b0} a^{-3}, \quad \rho_r(a) = \rho_{r0} a^{-4}, \quad (8)$$

where  $\rho_{b0}$  and  $\rho_{r0}$  are the corresponding current values. In contrast, the density of DM is tied to the dynamics of the vacuum through Eqs. (6)-(7), which now become simplified:

$$\dot{\rho}_{dm} + 3H\rho_{dm} = Q, \quad \dot{\rho}_\Lambda = -Q, \quad (9)$$

after the conservation laws (8) have been taken into account. The solution of these equations will depend on the particular form assumed for  $Q$ , which determines the leakage rate of vacuum energy into dark matter or vice versa. Such a leakage must certainly be much smaller than the standard dilution rate of nonrelativistic matter associated to the cosmic expansion (i.e. much smaller than  $\sim a^{-3}$ ), as otherwise these anomalous effects would be too sharp at the present time. Therefore, we must have  $0 < |Q| \ll \dot{\rho}_m$ . The different DVMs will be characterized by different functions  $Q_i$  ( $i = 1, 2, \dots$ ) that are proportional to a small dimensionless coupling,  $|\nu_i| \ll 1$ . In some cases the interaction source  $Q_i$  will be merely phenomenological, but in one of the cases (the running vacuum model) we have a more theoretical motivation.

### A. The running vacuum model (RVM)

One of the DVMs under study is the so-called running vacuum model (RVM), which can be motivated in the context of QFT in curved space-time (cf. [12, 51] and references therein). The model has some virtues and can be extended to afford an effective description of the cosmic evolution starting from inflation up to our days [12, 51, 74–78]. For instance, in [76] it is suggested that the RVM could positively impinge on solving some of the fundamental cosmological problems, including the entropy problem. Intriguingly, the inherent tiny leakage of vacuum energy into matter within the RVM could also furnish an explanation for the possible slow time

variation of the fundamental constants, an issue that has been examined in detail in [79–81]. In the Appendix A we summarize some of the theoretical motivations behind the RVM. We shall not discuss here the implications for the early universe, but only for the part of the cosmic history that is accessible to our measurements and can therefore be tested phenomenologically with the current data.

As advertised, for the specific RVM case the cosmic variable  $\zeta$  in the field equations (3)-(4) can be identified with the Hubble rate  $H$ . The general form of the RVM can be parametrized as follows:

$$\rho_\Lambda(H) = \frac{3}{8\pi G} \left[ c_0 + \nu H^2 + 3\alpha \frac{H^4}{M^2} + \dots \right]. \quad (10)$$

where  $\nu, \alpha, \dots$  are dimensionless parameters,  $M$  is an average (large) mass scale and the dots would include in general the  $\mathcal{O}(H^6/M^4)$  terms and higher. The structure of (10) can be linked to a renormalization group (RG) equation for the vacuum energy density, in which the running scale  $\mu$  of the RG is associate with the characteristic energy scale of the FLRW metric, i.e.  $\mu = H$ . In the Appendix A we present a summarized discussion, see e.g. [12, 51, 79] for more details.

Well after inflation and up to our days, the dynamical terms of (10) other than  $\sim H^2$  remain negligible and the vacuum energy density of the RVM can be simply written

$$\rho_\Lambda(H) = \frac{3}{8\pi G} (c_0 + \nu H^2). \quad (11)$$

The additive constant  $c_0 = H_0^2(\Omega_\Lambda - \nu)$  appears because one integrates the RG equation satisfied by  $\rho_\Lambda(H)$ . It is fixed by the boundary condition  $\rho_\Lambda(H_0) = \rho_{\Lambda 0}$ , where  $\rho_{\Lambda 0}$  and  $H_0$  are the current values of these quantities; similarly  $\Omega_\Lambda = \rho_{\Lambda 0}/\rho_{c0}$  and  $\rho_{c0} = 3H_0^2/(8\pi G)$  are the values of the vacuum density parameter and the critical density today. The dimensionless coefficient  $\nu$  encodes the dynamics of the vacuum at low energy and can be related with the  $\beta$ -function of the running of  $\rho_\Lambda$ . Thus, we naturally expect  $|\nu| \ll 1$ . An estimate of  $\nu$  at one loop in QFT indicates that is of order  $10^{-3}$  at most [53], but here we will treat it as a free parameter. This means we shall deal with the RVM on pure phenomenological grounds, hence fitting actually  $\nu$  to the observational data (cf. Sect. III).

In the RVM case, the source function  $Q$  in (9) is not just put by hand (as in the case of the *ad hoc* DVMs we will introduce in short). It is a calculable expression from (11), using Friedmann's equation (3) and the local conservation laws (6)-(9). We find:

$$\text{RVM} : \quad Q = -\dot{\rho}_\Lambda = \nu H(3\rho_m + 4\rho_r), \quad (12)$$

where we recall that  $\rho_m = \rho_{dm} + \rho_b$ , and that  $\rho_b$  and  $\rho_r$  are known functions of the scale factor – see Eq. (8). The remaining densities,  $\rho_{dm}$  and  $\rho_\Lambda$ , must be determined upon further solving the model explicitly, see the next subsection. If baryons and radiation would also possess a small interaction with vacuum, their densities in Eq. (12) would not follow the standard conservation laws and the cosmological solution would be different [60–62, 66, 67].

## B. Other dynamical vacuum models

Next we include in our study two *ad hoc* DVMs in which the source function  $Q$  is introduced by hand, i.e. without any special theoretical motivation. Two possible phenomenological ansatzs are the following:

$$\text{Model } Q_{dm} : \quad Q_{dm} = 3\nu_{dm} H \rho_{dm} \quad (13)$$

$$\text{Model } Q_\Lambda : \quad Q_\Lambda = 3\nu_\Lambda H \rho_\Lambda. \quad (14)$$

Model  $Q_\Lambda$  was previously addressed in [82], but as we shall see we do not agree with their analysis, in accordance also with [83]. Model  $Q_{dm}$  was recently studied in [84]; it is closer to the RVM than  $Q_\Lambda$ , but certainly not identical, confer equations (12) and (13). There are many more choices for  $Q$ , see e.g. [85] and [86], but it will suffice to focus on the RVM and on the two additional variants (13)-(14) to assess the possible impact of the DVMs in the light of the modern observational data.

The dimensionless parameters  $\nu_i = (\nu, \nu_{dm}, \nu_\Lambda)$  for each model (RVM,  $Q_{dm}$ ,  $Q_\Lambda$ ) determine the strength of the dark-sector interaction in the sources  $Q_i$  and enable the evolution of the vacuum energy density. In all cases we have a similar structure  $Q_i \propto \nu_i H \mathcal{Q}_i$ , but the density function  $\mathcal{Q}_i$  varies from one model to the other, as it is plain from the above formulae. For  $\nu_i > 0$  the vacuum decays into DM (which is thermodynamically favorable) whereas for  $\nu_i < 0$  is the other way around. This will be an important argument (see Sect. IV E) to judge the viability of these models, as only the first situation is compatible with the second law of thermodynamics (SLT).

## C. Solving explicitly the dynamical vacuum models

The matter and vacuum energy densities of the DVMs can be computed straightforwardly upon solving the coupled system of differential equations (9), given the explicit forms (12)-(14) for the interacting source in each case and keeping in mind that, in the current framework, the baryon ( $\rho_b$ ) and radiation ( $\rho_r$ ) parts are separately conserved. After some calculations the equations for the DM energy densities  $\rho_{dm}$  for each model (RVM,  $Q_{dm}$ ,  $Q_\Lambda$ ) can be explicitly solved in terms of the scale factor. Below we quote the final results for each case:

**RVM :**

$$\begin{aligned} \rho_{dm}(a) &= \rho_{dm0} a^{-3(1-\nu)} + \rho_{b0} \left( a^{-3(1-\nu)} - a^{-3} \right) \\ &\quad + \frac{4\nu}{1+3\nu} \rho_{r0} \left( a^{-3(1-\nu)} - a^{-4} \right) \end{aligned} \quad (15)$$

**$Q_{dm}$  :**

$$\rho_{dm}(a) = \rho_{dm0} a^{-3(1-\nu_{dm})} \quad (16)$$

**$Q_\Lambda$  :**

$$\rho_{dm}(a) = \rho_{dm0} a^{-3} + \frac{\nu_\Lambda}{1-\nu_\Lambda} \rho_{\Lambda 0} \left( a^{-3\nu_\Lambda} - a^{-3} \right). \quad (17)$$

In solving the differential equations (9) we have traded the cosmic time variable for the scale factor using the chain rule  $d/dt = aHd/da$ .

The corresponding vacuum energy densities can also be solved in the same variable, and yield:

**RVM :**

$$\begin{aligned} \rho_\Lambda(a) &= \rho_{\Lambda 0} + \frac{\nu}{1-\nu} \left( a^{-3(1-\nu)} - 1 \right) \\ &+ \frac{\nu \rho_{r0}}{1-\nu} \left( \frac{1-\nu}{1+3\nu} a^{-4} + \frac{4\nu}{1+3\nu} a^{-3(1-\nu)} - 1 \right) \end{aligned} \quad (18)$$

**Q<sub>dm</sub> :**

$$\rho_{dm}(a) = \rho_{dm 0} + \frac{\nu_{dm} \rho_{dm 0}}{1-\nu_{dm}} \left( a^{-3(1-\nu_{dm})} - 1 \right) \quad (19)$$

**Q<sub>Λ</sub> :**

$$\rho_\Lambda(a) = \rho_{\Lambda 0} a^{-3\nu_\Lambda}. \quad (20)$$

One can easily check that for  $a = 1$  (i.e. at the present epoch) all of the energy densities (15)-(20) recover their respective current values  $\rho_{N0}$  ( $N = dm, b, r, \Lambda$ ). In addition, for  $\nu_i \rightarrow 0$  we retrieve for the three DM densities the usual  $\Lambda$ CDM expression  $\rho_{dm}(a) = \rho_{dm 0} a^{-3}$ , and the corresponding vacuum energy densities  $\rho_\Lambda(a)$  boil down to the constant value  $\rho_{\Lambda 0}$  in that limit. The normalized Hubble rate  $E \equiv H/H_0$  ( $H_0$  being the current value) for each model can be easily obtained by plugging the above formulas, along with the radiation and baryon energy densities, into the Friedmann's equation (3). We find:

**RVM :**

$$\begin{aligned} E^2(a) &= 1 + \frac{\Omega_m}{1-\nu} \left( a^{-3(1-\nu)} - 1 \right) \\ &+ \frac{\Omega_r}{1-\nu} \left( \frac{1-\nu}{1+3\nu} a^{-4} + \frac{4\nu}{1+3\nu} a^{-3(1-\nu)} - 1 \right) \end{aligned} \quad (21)$$

**Q<sub>dm</sub> :**

$$\begin{aligned} E^2(a) &= 1 + \Omega_b (a^{-3} - 1) + \frac{\Omega_{dm}}{1-\nu_{dm}} \left( a^{-3(1-\nu_{dm})} - 1 \right) \\ &+ \Omega_r (a^{-4} - 1) \end{aligned} \quad (22)$$

**Q<sub>Λ</sub> :**

$$\begin{aligned} E^2(a) &= \frac{a^{-3\nu_\Lambda} - \nu_\Lambda a^{-3}}{1-\nu_\Lambda} + \frac{\Omega_m}{1-\nu_\Lambda} (a^{-3} - a^{-3\nu_\Lambda}) \\ &+ \Omega_r \left( a^{-4} + \frac{\nu_\Lambda}{1-\nu_\Lambda} a^{-3} - \frac{a^{-3\nu_\Lambda}}{1-\nu_\Lambda} \right). \end{aligned} \quad (23)$$

In the above expressions, we have used the cosmological parameters  $\Omega_N = \rho_{N0}/\rho_{c0}$  for each fluid component ( $N = dm, b, r, \Lambda$ ), and defined  $\Omega_m = \Omega_{dm} + \Omega_b$ . Altogether, they satisfy the sum rule  $\sum_N \Omega_N = 1$ . The normalization condition  $E(1) = 1$  in these formulas is apparent, meaning that the Hubble function for each model reduces to  $H_0$  at present, as they should; and, of course, for  $\nu_i \rightarrow 0$  we recover the  $\Lambda$ CDM form for  $H$ , as should be expected.

From the structure of equations (18) and (21) we can readily see that the vacuum energy-density for the RVM can be fully written as a function of a cosmic variable  $\zeta$ , which can be chosen to be not only the scale factor but the full Hubble function  $\zeta = H$ . The result is, of course, Eq. (11). In contrast, for the  $Q_{dm}$  and  $Q_\Lambda$  models this is not possible, as it is clear on comparing equations (19)-(20) and the corresponding ones (22)-(23). For these models  $\rho_\Lambda$  can only be written as a function of the scale factor. In fact, the RVM happens to have the greatest level of symmetry since its origin is an RG equation in  $H$  whose solution is precisely (11), see Appendix A.

#### D. XCDM and CPL parametrizations

It will be convenient to fit also the data through the simple XCDM parametrization of the dynamical DE, first introduced by Turner and White [70] shortly after the discovery of the cosmic acceleration with type Ia distant supernovae. Since both matter and DE are self-conserved (i.e., they are not interacting), the DE energy density as a function of the scale factor is simply given by  $\rho_X(a) = \rho_{X0} a^{-3(1+w_0)}$ , with  $\rho_{X0} = \rho_{\Lambda 0}$ , where  $w_0$  is the (constant) equation of state (EoS) parameter of the generic DE entity  $X$  in this parametrization. The normalized Hubble function is:

$$E^2(a) = \Omega_m a^{-3} + \Omega_r a^{-4} + \Omega_\Lambda a^{-3(1+w_0)}. \quad (24)$$

For  $w_0 = -1$  it boils down to that of the  $\Lambda$ CDM with rigid CC term. Borrowing the XCDM parametrization throughout our analysis will be useful to roughly mimic a (noninteractive) DE scalar field with constant EoS. For  $w_0 \gtrsim -1$  the XCDM mimics quintessence, whereas for  $w_0 \lesssim -1$  it mimics phantom DE.

A slightly more sophisticated approximation to the behavior of a noninteractive scalar field playing the role of dynamical DE is afforded by the CPL parametrization [71], in which one assumes that the generic DE entity  $X$  has a slowly varying EoS of the form

$$w_D = w_0 + w_1 (1-a) = w_0 + w_1 \frac{z}{1+z}. \quad (25)$$

The CPL parametrization, in contrast to the XCDM one, makes allowance for a time evolution of the dark energy EoS owing to the presence of the additional parameter  $w_1$ , which satisfies  $0 < |w_1| \ll |w_0|$ , with  $w_0 \gtrsim -1$  or  $w_0 \lesssim -1$ . The expression (25) is seen to have a well-defined limit both in the early universe ( $a \rightarrow 0$ , equivalently  $z \rightarrow \infty$ ) and in the current one ( $a = 1$ , or  $z = 0$ ).

The corresponding normalized Hubble function for the CPL can be easily found:

$$E^2(a) = \Omega_m a^{-3} + \Omega_r a^{-4} + \Omega_\Lambda a^{-3(1+w_0+w_1)} e^{-3w_1(1-a)}. \quad (26)$$

The XCDM and the CPL parametrizations can be conceived as a kind of baseline frameworks to be referred to in the study of dynamical DE. They can be used as

| Model               | $h$               | $\omega_b = \Omega_b h^2$ | $n_s$             | $\Omega_m$        | $\nu_i$               | $w_0$              | $w_1$             | $\chi^2_{\min}/dof$ | $\Delta\text{AIC}$ | $\Delta\text{BIC}$ |
|---------------------|-------------------|---------------------------|-------------------|-------------------|-----------------------|--------------------|-------------------|---------------------|--------------------|--------------------|
| $\Lambda\text{CDM}$ | $0.692 \pm 0.004$ | $0.02253 \pm 0.00013$     | $0.976 \pm 0.004$ | $0.296 \pm 0.004$ | -                     | -1                 | -                 | 84.88/85            | -                  | -                  |
| $\text{XCDM}$       | $0.672 \pm 0.007$ | $0.02262 \pm 0.00014$     | $0.976 \pm 0.004$ | $0.311 \pm 0.007$ | -                     | $-0.923 \pm 0.023$ | -                 | 74.08/84            | 8.55               | 6.31               |
| CPL                 | $0.673 \pm 0.009$ | $0.02263 \pm 0.00014$     | $0.976 \pm 0.004$ | $0.310 \pm 0.009$ | -                     | $-0.944 \pm 0.089$ | $0.063 \pm 0.259$ | 74.03/83            | 6.30               | 1.87               |
| RVM                 | $0.677 \pm 0.005$ | $0.02231 \pm 0.00014$     | $0.965 \pm 0.004$ | $0.303 \pm 0.005$ | $0.00158 \pm 0.00042$ | -1                 | -                 | 69.72/84            | 12.91              | 10.67              |
| $Q_{dm}$            | $0.678 \pm 0.005$ | $0.02230 \pm 0.00015$     | $0.965 \pm 0.004$ | $0.302 \pm 0.005$ | $0.00216 \pm 0.00060$ | -1                 | -                 | 70.50/84            | 12.13              | 9.89               |
| $Q_\Lambda$         | $0.691 \pm 0.004$ | $0.02230 \pm 0.00016$     | $0.966 \pm 0.005$ | $0.298 \pm 0.005$ | $0.00601 \pm 0.00253$ | -1                 | -                 | 79.22/84            | 3.41               | 1.17               |

TABLE I: Best-fit values for the  $\Lambda\text{CDM}$ ,  $\text{XCDM}$ , CPL and the three dynamical vacuum models (DVMs), including their statistical significance ( $\chi^2$ -test and Akaike and Bayesian information criteria, AIC and BIC). The  $\Delta\text{AIC}$  and  $\Delta\text{BIC}$  increments clearly favor the dynamical DE options. In particular, the RVM and  $Q_{dm}$  are strongly favored ( $\sim 4\sigma$  c.l.). Our fit is grounded on a rich and fully updated SNIa+BAO+ $H(z)$ +LSS+CMB data set, see data sources DS1)-DS6) in the text for details and references. The specific fitting parameters for each DVM are  $\nu_i = \nu$  (RVM),  $\nu_{dm}(Q_{dm})$  and  $\nu_\Lambda(Q_\Lambda)$ , whilst for the XCDM and CPL are the EoS parameters  $w_0$  and the pair  $(w_0, w_1)$ , respectively. For the vacuum models, including the  $\Lambda\text{CDM}$ , we have  $w_0 = -1$  and  $w_1 = 0$ . The remaining parameters are standard  $(h, \omega_b, n_s, \Omega_m)$ . The number of degrees of freedom (dof) is equal to the number of data points minus the number of fitting parameters (4 for the  $\Lambda\text{CDM}$ , 5 for the DVMs and the XCDM, and 6 for the CPL parametrization). The parameter M in the SNIa sector [87] was dealt with as a nuisance parameter and has been marginalized over analytically (see Appendix B).

| Model               | $h$               | $\omega_b = \Omega_b h^2$ | $n_s$             | $\Omega_m$        | $\nu_i$               | $w_0$              | $w_1$             | $\chi^2_{\min}/dof$ | $\Delta\text{AIC}$ | $\Delta\text{BIC}$ |
|---------------------|-------------------|---------------------------|-------------------|-------------------|-----------------------|--------------------|-------------------|---------------------|--------------------|--------------------|
| $\Lambda\text{CDM}$ | $0.691 \pm 0.004$ | $0.02251 \pm 0.00013$     | $0.973 \pm 0.004$ | $0.297 \pm 0.005$ | -                     | -1                 | -                 | 80.19/78            | -                  | -                  |
| $\text{XCDM}$       | $0.673 \pm 0.007$ | $0.02261 \pm 0.00014$     | $0.976 \pm 0.004$ | $0.311 \pm 0.007$ | -                     | $-0.929 \pm 0.023$ | -                 | 72.00/77            | 5.92               | 3.78               |
| CPL                 | $0.674 \pm 0.009$ | $0.02261 \pm 0.00015$     | $0.976 \pm 0.004$ | $0.310 \pm 0.009$ | -                     | $-0.938 \pm 0.087$ | $0.026 \pm 0.258$ | 71.99/76            | 3.60               | -0.61              |
| RVM                 | $0.677 \pm 0.005$ | $0.02232 \pm 0.00015$     | $0.965 \pm 0.004$ | $0.302 \pm 0.005$ | $0.00159 \pm 0.00048$ | -1                 | -                 | 67.85/77            | 10.07              | 7.93               |
| $Q_{dm}$            | $0.678 \pm 0.005$ | $0.02230 \pm 0.00015$     | $0.965 \pm 0.004$ | $0.302 \pm 0.005$ | $0.00215 \pm 0.00066$ | -1                 | -                 | 68.59/77            | 9.33               | 7.19               |
| $Q_\Lambda$         | $0.690 \pm 0.004$ | $0.02230 \pm 0.00017$     | $0.966 \pm 0.005$ | $0.299 \pm 0.005$ | $0.00568 \pm 0.00259$ | -1                 | -                 | 75.40/77            | 2.52               | 0.38               |

TABLE II: Same as in Table I, but excluding from our analysis the BAO and LSS data from WiggleZ, see point DS5) in the text.

fiducial models to which we can compare other, more sophisticated, models for the dynamical DE, such as the DVMs under study. The mimicking of the vacuum dynamics through these parametrizations need not be perfect, though, since the DVMs interact with matter whereas the XCDM and CPL do not involve any interaction. Still, since the vacuum dynamics inherent in the DVMs is mild enough, we expect that a significant part of the effects departing from the  $\Lambda\text{CDM}$  should be captured by these parametrizations, either in the form of effective quintessence behavior ( $w \gtrsim -1$ ) or effective phantom behavior ( $w \lesssim -1$ ). The fact that the CPL comprises two parameters ( $w_0, w_1$ ) rather than just  $w_0$  will, however, be in detriment of the accuracy of the fit versus that of the XCDM. The XCDM is in fact more appropriate for a fairer comparison with the DVMs, which also have one single vacuum parameter  $\nu_i$ . We present the main fitting results with these parametrizations, along with the other models, in Table I. A more detailed discussion will be given later on in Sections V and VI.

### III. FITTING THE VACUUM MODELS TO THE DATA

In this work, we fit the  $\Lambda\text{CDM}$ , XCDM, CPL and the three DVMs to the cosmological data from type Ia supernovae, BAOs, the values of the Hubble parameter at various redshifts,  $H(z_i)$ , the LSS formation data embodied in the quantity  $f(z_i)\sigma_8(z_i)$  and, finally, the CMB distance priors from Planck 2015. We denote this cosmological data set by SNIa+BAO+ $H(z)$ +LSS+CMB. A guide to the presentation of our results is the following. The various fitting analyses and contour plots under different con-

ditions (to be discussed in detail in the next sections) are displayed in twelve fitting tables, Tables I,II, V-XIV and in ten figures, Figs. 1-10. Tables III and IV correspond to particular data set inputs that we wish to stand out. The main results of our analysis are those recorded in Table I and Figs. 1-4. The elliptical shapes in the contour plots have been obtained according to the standard statistical technique relying on the Fisher matrix formalism [72, 88]. This is perfectly legitimate in this case, since the deviation of the posterior distribution from an ideal Gaussian one is found to be negligible, as we have checked – similarly as we did in [66] for other models. Details of the  $\chi^2$  function to be minimized, as well as of the covariance matrices for the most significant data sets are specified in the Appendix B. For additional details the reader is referred to specialized references of our bibliography, which we deem is quite generous.

The remaining tables and figures contain complementary information, which can be very helpful to gather a more detailed picture of our rather comprehensive study. For example, Figs. 5-10 are quite revealing of different aspects of the dynamical dark energy signal, together with the complementary tables, which are in support of the figures. A summarized road map to the content of the fitting tables is the following: Table II explores a possible effect of correlations in data sets; Tables V-VII examine the influence of refitting the data by excluding a single one of the three basic observables CMB, LSS or BAO, respectively; Table VIII shows the results when we use only the fitting data employed by the Planck 2015 collaboration, where no dynamical DE signal was detected; Table IX explores the difference between including or not including the data on the three-point correlation function,

| Survey    | $z$   | $f(z)\sigma_8(z)$      | References  |
|-----------|-------|------------------------|-------------|
| 6dFGS     | 0.067 | $0.423 \pm 0.055$      | [95]        |
| SDSS-DR7  | 0.10  | $0.37 \pm 0.13$        | [96]        |
| GAMA      | 0.18  | $0.29 \pm 0.10$        | [97]        |
|           | 0.38  | $0.44 \pm 0.06$        | [98]        |
| DR12 BOSS | 0.32  | $0.427 \pm 0.056$      | [92]        |
|           | 0.57  | $0.426 \pm 0.029$      |             |
| WiggleZ   | 0.22  | $0.42 \pm 0.07$        | [99]        |
|           | 0.41  | $0.45 \pm 0.04$        |             |
|           | 0.60  | $0.43 \pm 0.04$        |             |
|           | 0.78  | $0.38 \pm 0.04$        |             |
| 2MTF      | 0.02  | $0.34 \pm 0.04$        | [100]       |
| VIPERS    | 0.7   | $0.38^{+0.06}_{-0.07}$ | [101]       |
| VVDS      | 0.77  | $0.49 \pm 0.18$        | [102],[103] |

TABLE III: Published values of  $f(z)\sigma_8(z)$ , referred to in the text as the LSS data, see the quoted references and text in point DS5).

i.e. the bispectrum, in addition to the usual spectrum; Table X tests the effect on our results when we replace some of the BAO data in Table I with different BAO data existing in the recent literature; Table XI allows to compare the effect of using a recent (but earlier) release of the BOSS data on BAO and LSS (including the bispectrum) carrying different errors as compared to the most recent BOSS data that we used in Table I; Table XII reports on the fitting results to the same cosmological data when we use the original Peebles & Ratra model as a prototype  $\phi$ CDM model to explore the dynamical DE; and, finally, Table XIII and Table XIV check the impact on our results upon using alternative fitting formulas existing in the literature for the sound horizon at the redshift of the drag epoch. We will discuss all these results in detail in the corresponding sections and in Appendix B. Below we start with a detailed description of the data used.

### A. Data sets

The 89 data points used in our fit stem from six data sources DS1-DS6 that are associated to the chain SNIa+BAO+ $H(z)$ +LSS+CMB of cosmological observations, keeping nonetheless in mind that two of the data sources described below stem from BAOs of different kinds (isotropic and anisotropic). Notice that the selected BAO+LSS points actually encode the information of hundreds of thousands of galaxies corresponding to certain effective redshifts. More precisely, the data sets used in our analysis read as follows:

DS1) Data on distant type Ia supernovae. We take the SNIa data points from the SDSS-II/SNLS3 Joint Light-curve Analysis (JLA) [87]. We have used the 31 binned distance modulus fitted to the JLA sample and the compressed form of the likelihood with the corresponding  $31 \times 31$  covariance matrix.

DS2) Data on isotropic baryonic acoustic oscillations. We use 5 data points on the isotropic BAO at the following redshifts:  $z = 0.106$  [89], obtained from the  $D_V(z)$  estimator; and  $z = 0.15$  [90] and  $z_i = 0.44, 0.6, 0.73$  [91] from the alternative estimator  $D_V(z)/r_s(z_d)$  (with the correlations between the last 3 points). See Appendix B for more details on these estimators.

DS3) Data on anisotropic baryonic acoustic oscillations. We use 6 data points on anisotropic BAO estimators: 4 of them on  $D_A(z_i)/r_s(z_d)$  and  $H(z_i)r_s(z_d)$  at  $z_i = 0.32, 0.57$ , for the LOWZ and CMASS samples, respectively. These data are taken from [92], based on the Redshift-Space Distortions (RSD) measurements of the power spectrum combined with the bispectrum, and the BAO post-reconstruction analysis of the power spectrum (cf. Table 5 of that reference), including the correlations among these data encoded in the provided covariance matrices. We also use 2 data points involving the observables  $D_A(z_i)/r_s(z_d)$  and  $D_H(z_i)/r_s(z_d)$  at  $z = 2.34$ , from the combined Ly $\alpha$ F analysis [93]. The correlation coefficient among these 2 points is taken from [94] (cf. Table II of that reference). We have also taken due account of the correlations among the BAO data and the corresponding  $f\sigma_8$  data of [92] – see DS5) below and Table III with the associated references. We refer the reader to Appendix B and references therein for further technical details on the (isotropic and anisotropic) BAO observables.

DS4) Data on the Hubble parameter at different redshift points. We use 30 data points on  $H(z_i)$  at different redshifts, listed in Table IV. We use only  $H(z_i)$  values obtained by the so-called differential-age (or cosmic chronometer) techniques applied to passively evolving galaxies. That is to say, we use data where one estimates  $H(z)$  from  $(1+z)H(z) = -dz/dt$ . Here  $dz/dt \simeq \Delta z/\Delta t$  is extracted from a sample of passive galaxies (i.e. with essentially no active star formation) whose age and redshift differences,  $\Delta t$  and  $\Delta z$ , are known. See the references also in Table IV. The important point to remark here is that these  $H(z)$  values, although relying on the theory of spectral evolution of galaxies, are uncorrelated with the BAO data points. See also [111–115], where the authors make only use of Hubble parameter data in their analyses. We find, however, indispensable in our analysis to take into account the remaining data sets to derive our conclusions on dynamical vacuum, specially the BAO, LSS and CMB observations. This fact can also be verified quite evidently in Figs. 7–9, to which we shall turn our attention in Sect. VID. See, however, [116] for other tests of dynamical DE using  $H(z)$  data.

DS5) Data on large scale structure formation (LSS). In this paper, the LSS data specifically refers to data points on the product of the ordinary growth rate  $f(z_i)$  with  $\sigma_8(z_i)$  (the root mean square matter fluctuation on  $R_8 = 8h^{-1}$  Mpc spheres) at different (effective) redshifts

| $z$    | $H(z)$           | References |
|--------|------------------|------------|
| 0.07   | $69.0 \pm 19.6$  | [104]      |
| 0.09   | $69.0 \pm 12.0$  | [105]      |
| 0.12   | $68.6 \pm 26.2$  | [104]      |
| 0.17   | $83.0 \pm 8.0$   | [106]      |
| 0.1791 | $75.0 \pm 4.0$   | [107]      |
| 0.1993 | $75.0 \pm 5.0$   | [107]      |
| 0.2    | $72.9 \pm 29.6$  | [104]      |
| 0.27   | $77.0 \pm 14.0$  | [106]      |
| 0.28   | $88.8 \pm 36.6$  | [104]      |
| 0.3519 | $83.0 \pm 14.0$  | [107]      |
| 0.3802 | $83.0 \pm 13.5$  | [108]      |
| 0.4    | $95.0 \pm 17.0$  | [106]      |
| 0.4004 | $77.0 \pm 10.2$  | [108]      |
| 0.4247 | $87.1 \pm 11.2$  | [108]      |
| 0.4497 | $92.8 \pm 12.9$  | [108]      |
| 0.4783 | $80.9 \pm 9.0$   | [108]      |
| 0.48   | $97.0 \pm 62.0$  | [109]      |
| 0.5929 | $104.0 \pm 13.0$ | [107]      |
| 0.6797 | $92.0 \pm 8.0$   | [107]      |
| 0.7812 | $105.0 \pm 12.0$ | [107]      |
| 0.8754 | $125.0 \pm 17.0$ | [107]      |
| 0.88   | $90.0 \pm 40.0$  | [109]      |
| 0.9    | $117.0 \pm 23.0$ | [106]      |
| 1.037  | $154.0 \pm 20.0$ | [107]      |
| 1.3    | $168.0 \pm 17.0$ | [106]      |
| 1.363  | $160.0 \pm 33.6$ | [110]      |
| 1.43   | $177.0 \pm 18.0$ | [106]      |
| 1.53   | $140.0 \pm 14.0$ | [106]      |
| 1.75   | $202.0 \pm 40.0$ | [106]      |
| 1.965  | $186.5 \pm 50.4$ | [110]      |

TABLE IV: Published values of  $H(z)$  in [km/s/Mpc] obtained using the differential-age technique, see the quoted references and text in point DS4).

$z_i$ , see Sect. IV C for more details. We use 13 data points on  $f(z_i)\sigma_8(z_i)$ . Not all are from RSD. The actual fitting results shown in Table I make use of the LSS data listed in Table III, in which we have carefully avoided possible correlations among them (see below). As an example, we do not include the 2dFGRS point at  $z = 0.17$  [103, 117] in our analysis because, as it is stated in [118], it is strongly correlated with the 6dFGS one (cf. Table III). Let us mention that although we are aware of the existence of other LSS data points in the literature concerning some of the used redshift values in our Table III – cf. [103, 117]; [119, 120]; [121] – we have explicitly checked that their inclusion in our numerical fits has no significant impact on the main results of our paper, namely, it does not alter in any significant way the attained level of evidence in favor of the main DVMs under study. Our results are definitely secured in both cases, but we have naturally presented our final results sticking to the most updated data. See also Sect. VI B for more details on the data selection procedure.

The following observation is now pertinent concerning the possible correlations between data sets. In our analysis we have included both the WiggleZ and the

CMASS data sets. We are aware that there exists some overlap region between these two galaxy samples. But the two surveys have been produced independently and the studies on the existing correlations among these observational results, see [122, 123], show that the correlation is small. The overlap region of the CMASS and WiggleZ galaxy samples is actually not among the galaxies that the two surveys pick up, but between the region of the sky they explore. Furthermore, in spite of the fact that almost all of the WiggleZ region (more precisely, 5/6 parts of it) lies inside the CMASS one, it only takes a very small fraction of the whole sky region covered by CMASS, since the latter is much larger than the WiggleZ one (see, e.g. Fig. 1 in [122]). In this paper, the authors are able to estimate the correlation degree among the BAO constraints in CMASS and WiggleZ, and they conclude that it is less than 4%. For this reason we find it perfectly justified to keep the WiggleZ data as part of our BAO and LSS data sets. As an additional check, we have computed the fitting results that are obtained when we remove the WiggleZ data points from the BAO and  $f(z)\sigma_8(z)$  data sets (see Table II). We can see that the differences in the uncertainties and in the central values of the parameters with respect to Table I are small. Therefore, no significant change in the statistical significance of the results is found.

DS6) Data on the CMB distance priors. These comprise:  $R$  (shift parameter),  $\ell_a$  (acoustic length) and their correlations with the reduced baryon mass parameter and the spectral index ( $\omega_b, n_s$ ). It has been shown in [124] that although this compression loses information compared to the full CMB likelihood, such an information loss becomes negligible when more data is added, as in the current analysis. We have used the CMB covariance matrix from the analysis of the Planck 2015 data of [125]. Our fitting results with such a covariance matrix are compiled in all our tables (except in Table V where we test the behavior of our fit in the absence of the CMB distance priors  $R$  and  $\ell_a$ ). We display the final contour plots for the DVMs and the XCDM in Figs. 1-3. Let us point out that we have checked that very similar results ensue for all models if we use the alternative CMB covariance matrix from [6]. We have, for definiteness, chosen that of [125] since it uses the more complete compressed likelihood analysis for Planck 2015 TT,TE,EE + lowP data whereas [6] uses Planck 2015 TT+lowP data only.

Finally, let us examine the Big Bang Nucleosynthesis (BBN) bound (see e.g. [126, 127]), namely the limitation in the value of the BBN speed-up factor, defined as the ratio of the expansion rate predicted in a given model versus that of the  $\Lambda$ CDM model at the BBN epoch. For models of constant  $G$ , it is tantamount to enforcing the condition that the vacuum energy density at the BBN epoch is sufficiently small in comparison to the radiation density, typically less than 5–10%. In the current study,

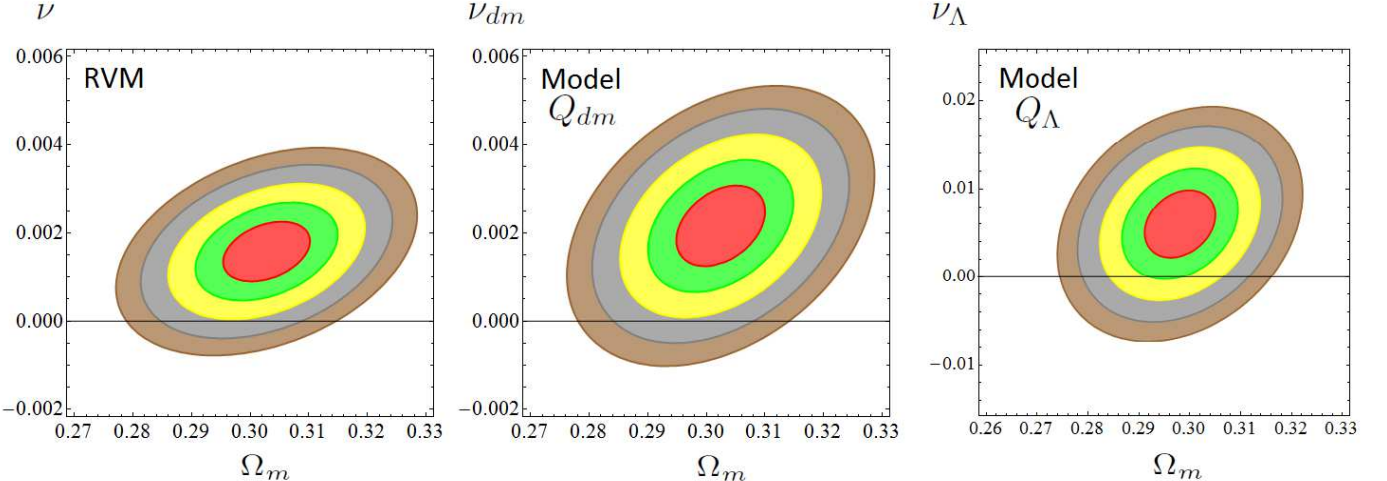


FIG. 1: Likelihood contours for the DVMs in the  $(\Omega_m, \nu_i)$  plane for the values  $-2 \ln \mathcal{L}/\mathcal{L}_{max} = 2.30, 6.18, 11.81, 19.33, 27.65$  (corresponding to  $1\sigma, 2\sigma, 3\sigma, 4\sigma$  and  $5\sigma$  c.l.) after marginalizing over the rest of the fitting parameters indicated in Table I. The elliptical shapes have been obtained applying the standard Fisher matrix approach. We estimate that for the RVM, 94.80% (resp. 89.16%) of the  $4\sigma$  (resp.  $5\sigma$ ) area is in the  $\nu > 0$  region. For the  $Q_{dm}$  we find that 95.24% (resp. 89.62%) of the  $4\sigma$  (resp.  $5\sigma$ ) area is in the  $\nu_{dm} > 0$  region. Finally, for the  $Q_\Lambda$  we estimate that 99.45% (resp. 90.22%) of the  $2\sigma$  (resp.  $3\sigma$ ) area is in the  $\nu_\Lambda > 0$  region. Subsequent marginalization over  $\Omega_m$  increases slightly the c.l. and renders the fitting values collected in Table I. The  $\Lambda$ CDM ( $\nu_i = 0$ ) appears disfavored at  $\sim 4\sigma$  c.l. in the RVM and  $Q_{dm}$ , and at  $\sim 2.5\sigma$  c.l. for  $Q_\Lambda$ .

the BBN bound need not be enforced since it is automatically fulfilled. The reason stems from our assumption that the radiation is conserved for the DVMs analyzed in this paper. As a result, the behavior of the ratio of the vacuum energy density to the radiation density in these models at BBN time ( $a \rightarrow 0$ ) is, in each case, as follows:

$$\left. \frac{\rho_\Lambda(a)}{\rho_r(a)} \right|_{RVM} \rightarrow \frac{\nu}{1+3\nu} \simeq \nu = \mathcal{O}(10^{-3}) \ll 1 \quad (27)$$

$$\left. \frac{\rho_\Lambda(a)}{\rho_r(a)} \right|_{Q_{dm}} \rightarrow \frac{\nu_{dm}}{1-\nu_{dm}} \frac{\rho_{dm0}}{\rho_{r0}} a^{(1+3\nu_{dm})} \rightarrow 0 \quad (28)$$

$$\left. \frac{\rho_\Lambda(a)}{\rho_r(a)} \right|_{Q_\Lambda} \rightarrow \frac{\rho_{\Lambda0}}{\rho_{r0}} a^{(4-3\nu_\Lambda)} \rightarrow 0 \quad , \quad (29)$$

as it can be easily checked from the energy densities explicitly computed in Sect. II C. We use, of course, the fact that  $0 < \nu_i \ll 1$ . In all cases the ratio is very small and therefore the BBN proceeds standard, with no significant difference versus the  $\Lambda$ CDM. Note that this situation is in contradistinction to the models addressed in Refs. [66, 67], where strict BBN bounds had to be applied in the analysis. In particular, when  $G$  can be variable it generally produces an effective change in the BBN speed-up factor, which was duly restrained in these works. For more details, see these references. Recently other models with variable  $G$  have been considered in the literature aiming to cure a certain level of tension between the Planck 2015 measurements and some independent observations in intermediate cosmological scales [128]. See also our discussion in Sect. V B.

## B. Background observables

With the above data sets the fitting results for the main background cosmological observables  $(h, \Omega_m)$  are afforded in Table I, together with the reduced baryon mass parameter  $\omega_b = \Omega_b h^2$ , the spectral index  $n_s$  and the vacuum parameter  $\nu_i$ , or alternatively the XCDM or CPL parameters. We will discuss in detail these parameters throughout the paper. Here we want to comment only on the basic two  $(h, \Omega_m)$  we have just mentioned. The reduced Hubble constant  $h$  is defined as usual from  $H_0 \equiv 100h\varsigma$ , with  $\varsigma \equiv 1 \text{ Km/s/Mpc} = 2.1332 \times 10^{-44} \text{ GeV}$  (in natural units), and the fitting values for  $h$  in our tables correspond to using an uninformative flat prior (in the technical sense). Owing to some tension in the values of  $h$  in the current literature (see Sect. V B), this procedure should be the fairest option rather than adopting some elicited prior.

Concerning the radiation density parameter  $\Omega_r$ , it is taken to be a function of the fitted value of  $h$  in our analysis through  $\Omega_r = \omega_r h^{-2}$ . The value of  $\omega_r$  can be computed from the current temperature of the CMB photons,  $T_{\gamma0} = 2.7255 \text{ K}$  [129], and the effective number of neutrino species,  $N_{\text{eff}} = 3.046$  [130]. Recall that the total radiation density at present is given by

$$\rho_{r0} = \rho_{\gamma0} \left[ 1 + N_{\text{eff}} \frac{7}{8} \left( \frac{4}{11} \right)^{4/3} \right] , \quad (30)$$

where  $T_{\nu0}/T_{\gamma0} = (4/11)^{1/3}$  is the ratio of the current neutrino and photon temperatures [131]. Finally, the density of photons now is  $\rho_{\gamma0} = (\pi^2/15) T_{\gamma0}^4$ . Using the afore-

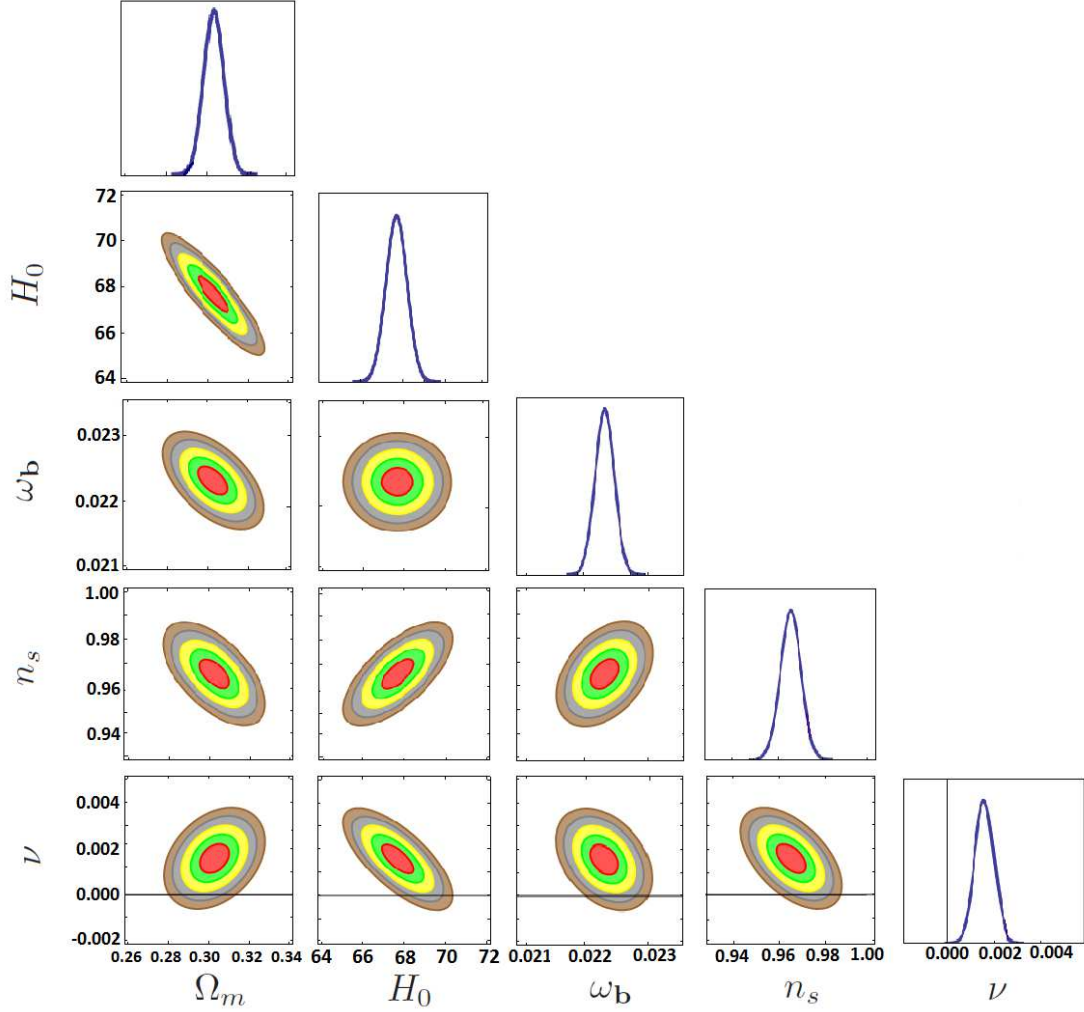


FIG. 2: As in Fig. 1, but projecting the fitting results of the RVM onto the different planes of the involved parameters ( $H_0$  is expressed in Km/s/Mpc). The horizontal line  $\nu = 0$  in the plots of the last row corresponds to the  $\Lambda$ CDM. It is apparent that it is significantly excluded at  $\sim 4\sigma$  c.l. in all cases. The peak in the rightmost plot corresponds to the central value  $\nu = 0.00158$  indicated in Table I.

mentioned numerical values, we obtain

$$\omega_r = \frac{\rho_{r0}}{\rho_{c0}} h^2 = \frac{8\pi G}{3 \times 10^4 \zeta^2} \rho_{r0} = 4.18343 \times 10^{-5}. \quad (31)$$

This value will enter explicitly the computation of the equality point between radiation and nonrelativistic matter and will be used in the evaluation of the transfer function in Sect. IV C.

Finally, let us stress that the DVMs have a background cosmology similar to that of the  $\Lambda$ CDM. The main differences appear at the cosmic perturbations level, which will be discussed in the next section. But at the moment let us mention that all of them have a transition point from braking (deceleration) to acceleration. This is clear since they all describe some dynamical behavior around a dominant (nonvanishing) constant term. The deceleration parameter  $q = -\ddot{a}a/\dot{a}^2$  can be comfortably

computed from

$$q(a) = -1 - \frac{a}{2E^2(a)} \frac{dE^2(a)}{da}, \quad (32)$$

where  $E = H/H_0$  is the normalized Hubble function. This function is available for the three DVMs under study, see Eqs. (21)-(23). Obviously we can neglect the radiation terms in these expressions for this kind of calculation. The transition point is the scale factor value  $a_t$  (or redshift value  $z_t = 1/a_t - 1$ ) where  $q(a_t) = 0$ . For instance, for the RVM one finds

$$\text{RVM : } a_t = \left[ \frac{(1-3\nu)\Omega_m}{2(\Omega_\Lambda - \nu)} \right]^{1/(3(1-\nu))}. \quad (33)$$

From this expression we see that if the constant term in Eq. (11) would be  $c_0 = 0$ , then  $\Omega_\Lambda = \nu$  and  $a_t = \infty$ , i.e. in the absence of  $c_0$  there would be no transition. One can reason similarly in the case of models  $Q_{dm}$  and  $Q_\Lambda$ .

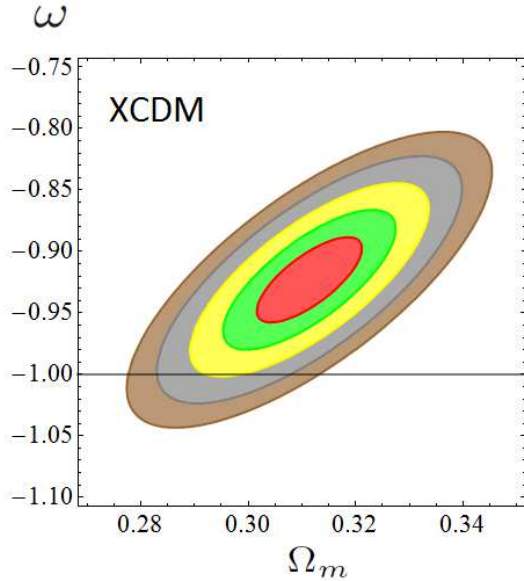


FIG. 3: As in Fig. 1, but for model XCDM. The  $\Lambda$ CDM is excluded in this case at  $\sim 3\sigma$  c.l. Marginalization over  $\Omega_m$  increases the c.l. up to  $3.35\sigma$  (cf. Table I).

However, for model  $Q_{dm}$  it turns out that an explicit formula for  $a_t$  is not possible since different powers of the scale factor appear mixed up with an additive term. As a result the equation  $q(a_t) = 0$  cannot be solved analytically. For model  $Q_\Lambda$ , however, an explicit result can be obtained:

$$Q_\Lambda : \quad a_t = \left[ \frac{\Omega_m - \nu_\Lambda}{\Omega_\Lambda(2 - 3\nu_\Lambda)} \right]^{1/(3(1-\nu_\Lambda))}. \quad (34)$$

For  $\nu_i = 0$  the above formulas boil down to the  $\Lambda$ CDM expression, as they should. Let us quote the values for the transition redshift, which we have obtain using the posterior distribution of the analysis in Table I. For the  $\Lambda$ CDM we obtain  $z_t^{\Lambda\text{CDM}} = 0.681 \pm 0.012$ , whereas from (33) and (34) we find:

$$z_t^{RVM} = 0.667 \pm 0.013, \quad z_t^{Q_\Lambda} = 0.687 \pm 0.012. \quad (35)$$

The value, obtained numerically, for  $Q_{dm}$  is:

$$z_t^{Q_{dm}} = 0.668 \pm 0.013. \quad (36)$$

Clearly, for both the RVM and  $Q_{dm}$  the transition occurs essentially at the same point, and such a point is closer to our time than in the  $\Lambda$ CDM case. In contrast, for model  $Q_\Lambda$  the transition occurs slightly earlier. Unfortunately, owing to the errors these differences are too small and cannot be disentangled; in fact they are compatible with the  $\Lambda$ CDM at  $1\sigma$  c.l. We conclude that the transition redshift is not, at the moment, sufficiently accurate to be used as a tool for distinguishing among these models. The measurable differences will appear, instead, when we move from the background cosmology to the perturbed one. We prepare the ground for it in the next section.

#### IV. STRUCTURE FORMATION WITH DYNAMICAL VACUUM

The analysis of the linear structure formation data deserves some remarks. It hinges on the theory of cosmological perturbations, which has been discussed at length in several specialized textbooks, see e.g. [50] and [132–134]. Notwithstanding, the analysis of new types of models may introduce novel features that must be carefully taken into account. At deep subhorizon scales and in the presence of dynamical vacuum energy one can show that the matter density contrast  $\delta_m = \delta\rho_m/\rho_m$  obeys the following differential equation (cf. [59, 60] for details):

$$\ddot{\delta}_m + (2H + \Psi) \dot{\delta}_m - \left( 4\pi G\rho_m - 2H\Psi - \dot{\Psi} \right) \delta_m = 0, \quad (37)$$

where  $\Psi \equiv -\dot{\rho}_\Lambda/\rho_m = Q/\rho_m$ , and the (vacuum-matter) interaction source  $Q$  for each DVM is given by Eqs. (12)–(14). For  $\rho_\Lambda = \text{const.}$  and for the XCDM and CPL there is no such an interaction, therefore  $Q = 0$ , and Eq. (37) reduces to the  $\Lambda$ CDM form [50]:

$$\ddot{\delta}_m + 2H \dot{\delta}_m - 4\pi G\rho_m \delta_m = 0. \quad (38)$$

We note that at the scales under consideration we are neglecting the perturbations of the vacuum energy density in front of the perturbations of the matter field.

Let us briefly justify by two alternative methods the modified form (37), in which the variation of  $\rho_\Lambda$  enters only through the Hubble function and the background quantity  $\Psi$ , but not through any perturbed quantity. We shall conveniently argue in the context of two well-known gauges, the synchronous gauge and the Newtonian conformal gauge, thus providing a twofold justification. In the synchronous gauge, vacuum perturbations  $\delta\rho_\Lambda$  modify the momentum conservation equation for the matter particles in a way that we can easily get e.g. from the general formulae of [135], with the result

$$\dot{v}_m + Hv_m = \frac{1}{a} \frac{\delta\rho_\Lambda}{\rho_m} - \Psi v_m, \quad (39)$$

where  $\vec{v} = \vec{\nabla}v_m$  is the associated peculiar velocity, with potential  $v_m$  (notice that this quantity has dimension of inverse energy in natural units). By setting  $\delta\rho_\Lambda = aQ v_m = a\rho_m \Psi v_m$  the two terms on the r.h.s. of (39) cancel each other and we recover the corresponding equation of the  $\Lambda$ CDM. On the other hand, in the Newtonian or conformal gauge [136] we find a similar situation. The analog of the previous equation is the modified Euler's equation in the presence of dynamical vacuum energy. It reads as follows:

$$\frac{d}{d\eta} (\rho_m v_m) + 4\mathcal{H}\rho_m v_m + \rho_m \phi - \delta\rho_\Lambda = 0, \quad (40)$$

where  $\phi$  is the gravitational potential that appears explicitly in the Newtonian conformal gauge, and  $\eta$  is the conformal time. Let an overhead circle denote a derivative with respect to the conformal time,  $\dot{f} = df/d\eta$  for

any  $f$ . We define the quantities  $\mathcal{H} = \dot{a}/a = aH$  and  $\bar{\Psi} = -\dot{\rho}_\Lambda/\rho_m = a\Psi$ , which are the analogues of  $H$  and  $\Psi$  in conformal time. Using the background local conservation equation (5) for the current epoch (neglecting therefore radiation) and rephrasing it in conformal time, i.e.  $\dot{\rho}_\Lambda + \dot{\rho}_m + 3\mathcal{H}\rho_m = 0$ , we can bring (40) to the simpler form

$$\dot{v}_m + \mathcal{H}v_m + \phi = \frac{\delta\rho_\Lambda}{\rho_m} - \bar{\Psi}v_m. \quad (41)$$

Once more the usual fluid equation (in this case Euler's equation) is retrieved if we arrange that  $\delta\rho_\Lambda = \rho_m \bar{\Psi} v_m = a \rho_m \Psi v_m$ , as then the two terms on the r.h.s. of (41) cancel each other. Alternatively, one can use the covariant form  $\nabla^\mu T_{\mu\nu} = Q_\nu$  for the local conservation law, with the source 4-vector  $Q_\nu = QU_\nu$ , where  $U_\nu = (a, \vec{0})$  is the background matter 4-velocity in conformal time [72]. By perturbing the covariant conservation equation one finds

$$\delta(\nabla^\mu T_{\mu\nu}) = \delta Q_\nu = \delta Q U_\nu + Q \delta U_\nu, \quad (42)$$

where  $\delta Q$  and  $\delta U_\nu = a(\phi, -\vec{v})$  are the perturbations of the source function and the 4-velocity, respectively. Thus, we obtain

$$\delta(\nabla^\mu T_{\mu\nu}) = a(\delta Q + Q\phi, -Q\vec{v}). \quad (43)$$

From the  $\nu = j$  component of the above equation, we derive anew the usual Euler equation  $\dot{v}_m + \mathcal{H}v_m + \phi = 0$ , which means that the relation  $\delta\rho_\Lambda = aQ v_m = a \rho_m \Psi v_m$  is automatically fulfilled. So the analyses in the two gauges converge to the same final result for  $\delta\rho_\Lambda$ .

After we have found the condition that  $\delta\rho_\Lambda$  must satisfy in each gauge so as to prevent that the vacuum modifies basic conservation laws of the matter fluid, one can readily show that any of the above equations (39) or (41) for each gauge (now with their r.h.s. set to zero), in combination with the corresponding perturbed continuity equation and the perturbed 00-component of Einstein's equations (giving Poisson's equation in the Newtonian approximation), leads to the desired matter perturbations equation (37), in accordance with the result previously derived by other means in Refs. [59, 60]. While our discussion holds good in a rigorous relativistic context, a derivation was first possible in the Newtonian formalism [45]. Altogether, the above considerations formulated in the context of different gauges allow us to consistently neglect the DE perturbations at scales down the horizon. This justifies the use of Eq. (37) for the effective matter perturbation equation in our study of linear structure formation in the framework of the DVMs. We refer the reader to [63, 135] for additional discussions on the suppression of the DE perturbations at subhorizon scales.

It will be convenient for further use to rewrite Eq. (37) in terms of the scale factor variable rather than the cos-

mic time. A straightforward calculation leads to the following expression

$$\delta''_m + \frac{A(a)}{a} \delta'_m + \frac{B(a)}{a^2} \delta_m = 0, \quad (44)$$

where primes denote differentiation  $d/da$ , and the functions  $A$  and  $B$  of the scale factor are given by

$$A(a) = 3 + a \frac{H'(a)}{H(a)} + \frac{\Psi(a)}{H(a)}, \quad (45)$$

$$B(a) = -\frac{4\pi G \rho_m(a)}{H^2(a)} + \frac{2\Psi(a)}{H(a)} + a \frac{\Psi'(a)}{H(a)}. \quad (46)$$

### A. Initial conditions

To solve (44) we have to fix the initial conditions for  $\delta_m(a)$  and  $\delta'_m(a)$  for each model at high redshift, say at  $z_i \sim 100$  ( $a_i \sim 10^{-2}$ ), when nonrelativistic matter dominates both over the vacuum and the radiation contributions. We have to calculate the limit of the functions (45)-(46) for small values of the scale factor. In this limit, the leading form of the normalized Hubble rate (squared) for each model, see equations (21)-(23), can be written to within very good approximation as follows:

$$\text{RVM : } E^2(a) = \frac{\Omega_m}{1-\nu} a^{-3(1-\nu)} \quad (47)$$

$$\text{Q}_\text{dm} : E^2(a) = \frac{\Omega_m}{1-\nu_{dm}} a^{-3(1-\nu_{dm})} \quad (48)$$

$$\text{Q}_\Lambda : E^2(a) = \frac{\Omega_m - \nu_\Lambda}{1-\nu_\Lambda} a^{-3}. \quad (49)$$

These equalities are to be understood in an approximate sense, that is to say, as the leading expressions at the point where we take the initial conditions. As it is clear from them, each model remains close to the  $\Lambda$ CDM behavior, given by  $E^2(a) \simeq \Omega_m a^{-3}$  in the same limit, and perfectly reduces to it for  $\nu_i \rightarrow 0$ , as expected. The small departure, however, must be duly taken into account when fixing the initial conditions. Below we explain how this is done.

A key ingredient in the structure formation equation for the DVMs is  $\Psi(a)$ , since it encodes the dynamical character of the vacuum energy at the background level. It can be easily computed for each model and yields:

$$\text{RVM : } \Psi(a) = 3\nu H(a) \quad (50)$$

$$\text{Q}_\text{dm} : \Psi(a) = 3\nu_{dm} \frac{\Omega_{dm}}{\Omega_m} H(a) + \mathcal{O}(\nu_{dm}^2) \quad (51)$$

$$\text{Q}_\Lambda : \Psi(a) = 3\nu_\Lambda \frac{\rho_\Lambda(a)}{\rho_m(a)} H(a), \quad (52)$$

where the first and third expressions are exact in  $\nu_i$  since we disregard the radiation terms proportional to  $\Omega_r$ , whereas the second expression involves subleading contributions of  $\mathcal{O}(\nu_{dm}^2)$ , which will be neglected. With the

above estimates we can assess the value of the correction terms  $\Psi/H$  and  $a\Psi'/H$  in (45)-(46). They represent the extra terms in the matter perturbations equation with respect to the  $\Lambda$ CDM. We immediately see that both for the RVM and  $Q_{dm}$  we have  $\Psi/H = \text{const.}$  and such a constant is proportional to  $\nu_i$ , whereby  $\Psi/H$  is small but not necessary negligible. In contrast, for model  $Q_\Lambda$  the ratio  $\Psi/H \sim \nu_\Lambda a^{3(1-\nu_\Lambda)}$  becomes smaller and smaller in the past, and therefore its value at  $a \sim 10^{-2}$  is strongly suppressed as compared to the other DVMs. Thus, in leading order, there are no corrections to the matter perturbations equation for model  $Q_\Lambda$  other than the background effect associated to the modified Hubble function. Similar considerations apply to the term  $a\Psi'/H$  for each model.

From the above formulas we can straightforwardly obtain the leading form of the functions (45)-(46) for the different DVMs:

$$\text{RVM} : A = \frac{3}{2}(1+3\nu) \quad (53)$$

$$Q_{dm} : A = \frac{3}{2}(1+\nu_{dm}) + 3\frac{\Omega_{dm}}{\Omega_m}\nu_{dm} + \mathcal{O}(\nu_{dm}^2) \quad (54)$$

$$Q_\Lambda : A = \frac{3}{2}, \quad (55)$$

and

$$\text{RVM} : B = -\frac{3}{2} + 3\nu + \frac{9}{2}\nu^2 \quad (56)$$

$$Q_{dm} : B = -\frac{3}{2}\left(1 - \nu_{dm} - \frac{\Omega_{dm}}{\Omega_m}\nu_{dm}\right) + \mathcal{O}(\nu_{dm}^2) \quad (57)$$

$$Q_\Lambda : B = -\frac{3}{2}. \quad (58)$$

For  $\nu_i \rightarrow 0$ , we recover the  $\Lambda$ CDM behavior  $A \rightarrow \frac{3}{2}$  and  $B \rightarrow -\frac{3}{2}$ , as it should. This is already true for the  $Q_\Lambda$  without imposing  $\nu_\Lambda \rightarrow 0$ , therefore its initial conditions are precisely the same as for the concordance model. Once the functions (45)-(46) take constant values (as it is the case here at the high redshifts where we fix the initial conditions), the differential equation (44) admits power-like solutions of the form  $\delta_m(a_i) = a_i^s$ . Of the two solutions, we are interested only in the growing mode solution, as this is the only one relevant for structure formation. For example, using (53) and (56) for the case of the RVM, the perturbations equation (44) becomes

$$\delta_m'' + \frac{3}{2a}(1+3\nu)\delta_m' - \left(\frac{3}{2} - 3\nu - \frac{9}{2}\nu^2\right)\frac{\delta_m}{a^2} = 0. \quad (59)$$

The power-law solution for the growing mode gives the result  $\delta_m = a^{1-3\nu}$ , which is exact even keeping the  $\mathcal{O}(\nu^2)$  term. Nevertheless, as warned previously, in practice we can neglect all  $\mathcal{O}(\nu_i^2)$  contributions despite we indicate their presence. Repeating the same procedure for the

other models, the final outcome for the growing mode solution  $\delta_m \sim a^s$  is the following:

$$\text{RVM} : s = 1 - 3\nu \quad (60)$$

$$Q_{dm} : s = 1 - \nu_{dm} \left( \frac{6\Omega_m + 9\Omega_{dm}}{5\Omega_m} \right) + \mathcal{O}(\nu_{dm}^2) \quad (61)$$

$$Q_\Lambda : s = 1. \quad (62)$$

As expected the deviations with respect to  $\Lambda$ CDM are small (and for  $Q_\Lambda$  there is no deviation at all). For the RVM and  $Q_{dm}$  the departures from the  $\Lambda$ CDM are proportional to  $\nu_i$ , and therefore the dynamical vacuum energy induces small changes in the initial conditions. Imposing the above analytical results to fix the initial conditions, we are then able to solve numerically the full differential equation (44) from a high redshift  $z_i \sim 100$  ( $a_i \sim 10^{-2}$ ) up to our days. The result does not significantly depend on the precise value of  $z_i$ , provided it is large enough but still well below the decoupling time ( $z \sim 10^3$ ), where the radiation component starts to be nonnegligible.

## B. Linear growth and growth index

The linear growth rate of clustering is an important (dimensionless) indicator of structure formation [50]. It is defined as the logarithmic derivative of the linear growth factor  $\delta_m(a)$  with respect to the log of the scale factor,  $\ln a$ . Therefore,

$$f(a) \equiv \frac{a}{\delta_m} \frac{d\delta_m}{da} = \frac{d\ln\delta_m}{d\ln a}, \quad (63)$$

where  $\delta_m(a)$  is obtained from solving the differential equation (44) for each model. Since  $f(a)$  is equal to  $(\dot{\delta}_m/\delta_m)/(\dot{a}/a)$  (the ratio of the peculiar flow rate to the Hubble rate), the physical significance of  $f(a)$  is that it determines the peculiar velocity flows [50]. In terms of the redshift variable, we have  $f(z) = -(1+z)\ln\delta_m/dz$ , and thus the linear growth can also be used to determine the amplitude of the redshift distortions. This quantity has been analytically computed for the RVM in [137]. Here we shall take it into account for the study of the LSS data in our overall fit to the cosmological observations.

One usually expresses the linear growth rate of clustering in terms of  $\Omega_m(z) = \rho_m(z)/\rho_c(z)$ , where  $\rho_c(z) = 3H^2(z)/(8\pi G)$  is the evolving critical density, as follows [50]:

$$f(z) \simeq [\Omega_m(z)]^{\gamma(z)}, \quad (64)$$

where  $\gamma$  is the so-called linear growth rate index. For the usual  $\Lambda$ CDM model, such an index is approximately given by  $\gamma_\Lambda \simeq 6/11 \simeq 0.545$ . For models with a slowly

varying equation of state  $w_D$  (i.e. approximately behaving as the XCDM, with  $w_D \simeq w_0$ ) one finds the approximate formula  $\gamma_D \simeq 3(w_D - 1)/(6w_D - 5)$  [138] for the asymptotic value when  $\Omega_m \rightarrow 1$ . Setting  $w_D = -1 + \epsilon$ , it can be rewritten

$$\gamma_D \simeq \frac{6 - 3\epsilon}{11 - 6\epsilon} \simeq \frac{6}{11} \left(1 + \frac{1}{22} \epsilon\right). \quad (65)$$

Obviously, for  $\epsilon \rightarrow 0$  (equivalently,  $\omega_D \rightarrow -1$ ) one retrieves the  $\Lambda$ CDM case. Since the current experimental error on the  $\gamma$ -index is of order 10%, it opens the possibility to discriminate cosmological models using such an index, see e.g. [139, 140]. In the case of the RVM and related models, the function  $\gamma(z)$  has been computed numerically in [60]. Under certain approximations, an analytical result can also be obtained for the asymptotic value [137]:

$$\gamma_{\text{RVM}} \simeq \frac{6 + 3\nu}{11 - 12\nu} \simeq \frac{6}{11} \left(1 + \frac{35}{22} \nu\right). \quad (66)$$

This expression for the RVM is similar to (65) for an approximate XCDM parametrization, and it reduces to the  $\Lambda$ CDM value for  $\nu = 0$ , as it should. It is interesting to note that for  $\epsilon > 0$  and  $\nu > 0$  (which correspond to quintessence-like behavior in both pictures, XCDM and RVM) one consistently finds  $\gamma$  slightly bigger than the  $\Lambda$ CDM value.

One hopes that models might be resolvable by this method in the future when more accurate data will be available [139]. However, in the present analysis we will not concentrate on  $f(z)$  nor on  $\gamma(z)$ , but on a related quantity on which we focus in the next section,  $f(z)\sigma_8(z)$ . This important quantity defines the LSS data used in our analysis.

### C. Weighted linear growth and power spectrum

A most suitable observable to assess the performance of our vacuum models in regard to structure formation is the combined quantity  $f(z)\sigma_8(z)$ , viz. the ordinary growth rate weighted with  $\sigma_8$ , the rms total matter fluctuation (baryons + CDM) on  $R_8 = 8h^{-1}$  Mpc spheres at the given redshift  $z$ , computed in linear theory. It has long been recognized that this estimator is almost a model-independent way of expressing the observed growth history of the universe, most noticeably it is found to be independent of the galaxy density bias [103].

Equipped with the above generalized matter perturbations equation (44) and the appropriate initial conditions, the analysis of the linear LSS regime is implemented with the help of the weighted linear growth  $f(z)\sigma_8(z)$ , in which the variance of the smoothed linear density field on  $R_8 = 8h^{-1}$  Mpc spheres at redshift  $z$  is computed from

$$\sigma_8^2(z) = \delta_m^2(z) \int \frac{d^3k}{(2\pi)^3} P(k, \vec{p}) W^2(kR_8). \quad (67)$$

Here  $P(k, \vec{p}) = P_0 k^{n_s} T^2(k)$  is the ordinary linear matter power spectrum (i.e. the coefficient of the two-point correlator of the linear perturbations), with  $P_0$  a normalization factor,  $n_s$  the spectral index and  $T(k)$  the transfer function. Furthermore,  $W(kR_8)$  in the above formula is a top-hat smoothing function (see e.g. [60] for details), which can be expressed in terms of the spherical Bessel function of order 1, as follows:

$$W(kR_8) = 3 \frac{j_1(kR_8)}{kR_8} = \frac{3}{k^2 R_8^2} \left( \frac{\sin(kR_8)}{kR_8} - \cos(kR_8) \right). \quad (68)$$

Moreover,

$$\vec{p} = (h, \omega_b, n_s, \Omega_m, \nu_i) \quad (69)$$

is the 5-dimensional fitting vector of free parameters for the vacuum models we are analyzing. The concordance  $\Lambda$ CDM model can be viewed as the particular case  $\nu_i = 0$ . It is understood that for the XCDM and CPL parametrizations the fitting parameter  $\nu_i$  is replaced by  $w_0$  and  $(w_0, w_1)$ , respectively.

The power spectrum depends on all the components of the fitting vector (69). The dependence on the spectral index  $n_s$  is power-like, whereas the transfer function  $T(k, \vec{q})$  depends in a more complicated way on the rest of the fitting parameters (see below), and thus for convenience we collect them in the reduced 4-dimensional vector

$$\vec{q} = (h, \omega_b, \Omega_m, \nu_i). \quad (70)$$

In the expression (67) both  $P(k)$  and  $W(k)$  are functions of  $k \equiv |\vec{k}|$ . Therefore, it is possible to integrate  $d^3k P(k)/(2\pi)^3$  (i.e. the elementary bin power centered at  $k$ ) over all orientations of  $\vec{k}$ . Writing

$$\int \frac{d^3k}{(2\pi)^3} P(k, \vec{p}) = \int_0^\infty \frac{dk}{k} \mathcal{P}(k, \vec{p}), \quad (71)$$

where we have introduced the dimensionless linear matter power spectrum,  $\mathcal{P}(k, \vec{p}) = (k^3/2\pi^2) P(k, \vec{p})$ , the variance (67) can finally be written as

$$\sigma_8^2(z) = \delta_m^2(z) \int_0^\infty \frac{dk}{k} \mathcal{P}(k, \vec{p}) W^2(kR_8), \quad (72)$$

with

$$\mathcal{P}(k, \vec{p}) = \mathcal{P}_0 k^{n_s+3} T^2(k, \vec{q}). \quad (73)$$

The normalization factor  $\mathcal{P}_0 = P_0/2\pi^2$  will be determined in the next section in view of defining a fiducial model.

For the transfer function, we have adopted the usual BBKS form [141] (see, however, below):

$$T(x) = \frac{\ln(1+0.171x)}{0.171x} \left[ 1 + 0.284x + (1.18x)^2 + (0.399x)^3 + (0.490x)^4 \right]^{-1/4}. \quad (74)$$

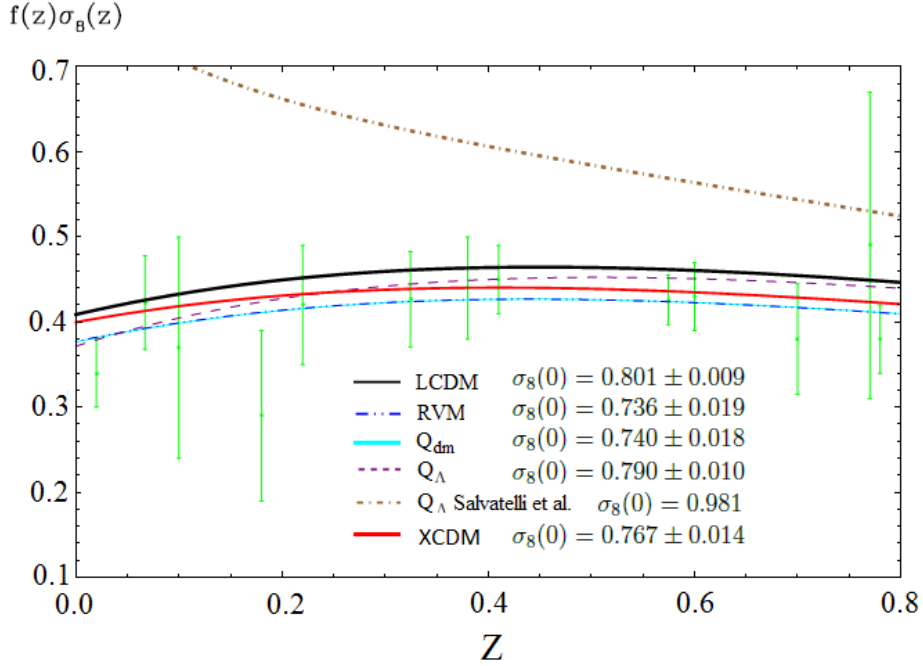


FIG. 4: The  $f(z)\sigma_8(z)$  data (Table III) and the predicted curves by the DVMs, XCDM and the  $\Lambda$ CDM, for the best-fit values in Table I. The highest curve (in brown) corresponds to model  $Q_\Lambda$  for the same best-fit values as [82] and assuming (as they do) that the dark sector interaction begins at  $z = 0.9$ . Such a strayed curve is unable to explain the LSS data (see the text for discussion) and corresponds to  $Q_\Lambda < 0$ . As explained in the text, this sign of the interaction source violates the SLT. This is in stark contrast to the well-behaved results of all the DVMs and XCDM when we use the fitting results of our own analysis, all of them plotted in the figure. Shown are also the central values and uncertainties of  $\sigma_8(0)$  that we have obtained for all the models.

Originally,  $x = k/k_{eq}$ , with

$$k_{eq} = a_{eq}H(a_{eq}), \quad (75)$$

being the value of the comoving wavenumber at the equality scale  $a_{eq}$  between matter and radiation densities:  $\rho_r(a_{eq}) = \rho_m(a_{eq})$ . It is well-known that (74) does not incorporate the effects produced by the tightly coupled photo-baryon plasma before the decoupling time. The fight between pressure and gravity in this coupled system generates the baryon acoustic oscillations in the matter power spectrum at “small” scales, i.e. for  $k > k_{eq}$ . The baryon density effects can be introduced in (74) through the modified shape parameter  $\tilde{\Gamma}$  [142, 143] in  $x = k/(k_{eq}\tilde{\Gamma})$ , with

$$\tilde{\Gamma} = e^{-\Omega_b - \sqrt{2h}\frac{\Omega_b}{\Omega_m}}. \quad (76)$$

Here it is understood that  $\Omega_b = \omega_b/h^2$  since we have to express the remaining parameters in terms of the components of the basic free set in (69).

We remark that  $k_{eq}$  is a model-dependent quantity, which departs from the  $\Lambda$ CDM expression in those models in which matter and/or radiation are governed by an anomalous continuity equation, as e.g. in the DVMs. In point of fact  $k_{eq}$  depends on all the parameters of the reduced fitting vector (70) since for a given model beyond the  $\Lambda$ CDM  $a_{eq}$  and/or  $H(a_{eq})$  depend on  $\vec{q}$ , as it will be clear below.

For the concordance model,  $k_{eq}$  has the simplest expression, which depends on  $h$  and  $\Omega_m$  only:

$$k_{eq}^\Lambda = H_0 \Omega_m \sqrt{\frac{2}{\Omega_r}}, \quad (77)$$

where we recall that  $\Omega_r = \omega_r/h^2$ , with  $\omega_r$  fixed from Eq. (31). The above expression for the wavenumber at equality can also be written as follows:

$$k_{eq}^\Lambda = \frac{\Omega_m h^2}{2997.9} \sqrt{\frac{2}{\omega_r}} \text{ Mpc}^{-1}, \quad (78)$$

where we have used the relation  $H_0^{-1} = 2997.9h^{-1}$  Mpc. For the DVMs is not possible to find a formula as compact as (78), since either the corresponding expression for  $a_{eq}$  is quite involved, as in the RVM case:

$$\text{RVM : } a_{eq} = \left[ \frac{\Omega_r(1+7\nu)}{\Omega_m(1+3\nu) + 4\nu\Omega_r} \right]^{\frac{1}{1+3\nu}}, \quad (79)$$

or because  $a_{eq}$  must be computed numerically, as for the models  $Q_{dm}$  and  $Q_\Lambda$ . In all cases, for  $\nu_i = 0$  we retrieve the value of  $a_{eq}$  in the  $\Lambda$ CDM. This is pretty obvious for the RVM from (79), where  $a_{eq} \rightarrow \Omega_r/\Omega_m$  for  $\nu \rightarrow 0$ . After obtaining  $a_{eq}$  for the various models, it is straightforward to calculate the corresponding value of  $k_{eq}$  from (75). Needless to say, for  $\nu_i = 0$  the  $\Lambda$ CDM value of  $k_{eq}$  is recovered too, since  $H(a)$  in Eq. (75) also

adopts the  $\Lambda$ CDM form for  $\nu_i = 0$ , as we know from Sect. II C. Similar comments apply for the XCDM and CPL parametrizations. For these two parametrizations,  $a_{eq}$  is exactly the same as in the  $\Lambda$ CDM, and  $k_{eq}$  presents only a negligible difference with respect to the  $\Lambda$ CDM. This is because the effect of the DE on the value of  $H(a_{eq})$  is very small. The main correction on  $k_{eq}$  indeed comes from the situations in which the modification impinges on the value of  $a_{eq}$  itself – see (75) – such as in the case of the DVMs.

Let us stress the importance of correctly computing the characteristic comoving wavenumber  $k_{eq}$  for all models, as we have done above, since it determines the borderline between small and large modes that entered the horizon in the radiation-matter equality time. Finally, let us mention that, for the sake of completeness, we have checked that the use of the alternative matter transfer function furnished by Eisenstein and Hu [144] does not produce any significant change in our results.

#### D. Fiducial model

Inserting the dimensionless power spectrum (73) into the variance (72) at  $z = 0$  allows us to write  $\sigma_8(0)$  in terms of the power spectrum normalization factor  $\mathcal{P}_0$  and the primary parameters that enter our fit for each model. This is tantamount to saying that  $\mathcal{P}_0$  can be fixed as follows:

$$\mathcal{P}_0 = \frac{\sigma_{8,\Lambda}^2}{\delta_{m,\Lambda}^2} \left[ \int_0^\infty k^{n_{s,\Lambda}+3} T^2(k, \vec{q}_\Lambda) W^2(k R_{8,\Lambda}) (dk/k) \right]^{-1}, \quad (80)$$

where the chosen values of the parameters in this expression define our fiducial model. Specifically, we have set  $\sigma_{8,\Lambda} \equiv \sigma_{8,\Lambda}(0)$  and  $\delta_{m,\Lambda} \equiv \delta_{m,\Lambda}(0)$ , and at the same time we define the vector of fiducial parameters

$$\vec{p}_\Lambda = (h_\Lambda, \omega_{b,\Lambda}, n_{s,\Lambda}, \Omega_{m,\Lambda}, 0) \quad (81)$$

and the corresponding reduced one

$$\vec{q}_\Lambda = (h_\Lambda, \omega_{b,\Lambda}, \Omega_{m,\Lambda}, 0), \quad (82)$$

which enters Eq. (80). These vectors are defined in analogy with the fitting vectors introduced before, see equations (69)-(70), but all their parameters are taken to be equal to those from the Planck 2015 TT,TE,EE+lowP+lensing analysis [5] with  $\nu_i = 0$ . The subindex  $\Lambda$  in all these parameters denotes such a setting. In particular,  $\sigma_{8,\Lambda}$  in (80) is also taken from the aforementioned Planck 2015 data. However,  $\delta_{m,\Lambda}$  in the same formula is computable: it is the value of  $\delta_m(z = 0)$  obtained from solving the perturbation equation of the  $\Lambda$ CDM, Eq. (38), using the mentioned fiducial values of the other parameters. Finally, plugging the normaliza-

tion factor (80) in (72) one finds:

$$\sigma_8(z) = \sigma_{8,\Lambda} \frac{\delta_m(z)}{\delta_{m,\Lambda}} \sqrt{\frac{\int_0^\infty k^{n_s+2} T^2(k, \vec{q}) W^2(k R_8) dk}{\int_0^\infty k^{n_{s,\Lambda}+2} T^2(k, \vec{q}_\Lambda) W^2(k R_{8,\Lambda}) dk}}. \quad (83)$$

For the fiducial  $\Lambda$ CDM, this expression just gives the scaling of  $\sigma_{8,\Lambda}(z)$  with the redshift in the linear theory, that is to say,  $\sigma_{8,\Lambda}(z)/\sigma_{8,\Lambda} = \delta_{m,\Lambda}(z)/\delta_{m,\Lambda}$ . But for an arbitrary model, Eq. (83) normalizes the corresponding  $\sigma_8(z)$  with respect to the fiducial value,  $\sigma_{8,\Lambda}$ . This includes, of course, our fitted  $\Lambda$ CDM, which is not the same as the fiducial  $\Lambda$ CDM. So all fitted models are compared to the same fiducial model, and this should be the fairest procedure. If, in contrast, we would let the normalization factor (80) free for each model, we could not secure the Planck 2015 results and the corresponding normalization of the power spectrum. Similarly, upon computing with this method the weighted linear growth rate  $f(z)\sigma_8(z)$  for each model under consideration, (including the  $\Lambda$ CDM) the functions  $f(z)\sigma_8(z)$  for all models become normalized to the same fiducial model. It is important to emphasize that one cannot adjust the power spectrum and the  $f(z)\sigma_8(z)$  values independently. Therefore, we first normalize with Planck 2015 results, as above described, and from here we fit the models to the data, in which the LSS component takes an essential part.

In Fig. 4 we display the theoretical results for  $f(z)\sigma_8(z)$  from the various models, side by side with the LSS data measurements (cf. Table III), using the fitted values of Table I. We indicate also in the figure the values that we find for  $\sigma_8(0)$  for each model, with the corresponding uncertainties. In addition, we include the curve for model  $Q_\Lambda$  under the conditions of Ref. [82]. We disagree both in magnitude and sign concerning their fitted parameter  $q_V$  ( $\equiv 3\nu_\Lambda$  in our notation). We find  $q_V > 0$  whereas they find  $q_V < 0$ , and our  $q_V$  is roughly one order of magnitude smaller in absolute value. The curve with  $q_V < 0$  clearly has a wrong behavior in the face of the data points, and therefore we exclude such a possibility.

#### E. DVMs and the second law of thermodynamics

For fixed values of the present-day energy densities, if  $q_V > 0$  (equivalently  $\nu_\Lambda > 0$ ) implies that the vacuum transfers energy to the matter sector and hence there will be more vacuum energy (and less dark matter) in the past than what is predicted by the  $\Lambda$ CDM. If, on the contrary,  $q_V < 0$  (equivalently  $\nu_\Lambda < 0$ ), there will be less vacuum energy (and more dark matter) in the past than predicted by the  $\Lambda$ CDM. This last situation generally entails a violation of the second law of thermodynamics (SLT) since it implies the decay of matter into vacuum energy, and thus the disappearance of particles. The SLT can only be preserved when it is the vacuum that decays into matter rather than the other way around, as particle creation from vacuum introduces the only genuine source of irreversibility here. DM particles are created out of the va-

uum at a rate given by  $\Gamma_{dm} \sim \Psi_i \propto \nu_i H$ , see (50)-(52), the rate being positive only if  $\nu_i > 0$ . Therefore, in ordinary conditions, namely in the absence of a significant asymmetry between the number of particles and antiparticles in the universe (implying the chemical potential of the particles being vanishing or very small), the decaying of vacuum into matter is the only thermodynamically safe option [145–147]. In the concrete case of model  $Q_\Lambda$  the situation is particularly odd when  $\nu_\Lambda < 0$ , as the corresponding DM mass density eventually becomes more and more negative:

$$\rho_{dm}(a) \longrightarrow \frac{\nu_\Lambda}{1 - \nu_\Lambda} \rho_{\Lambda 0} a^{3|\nu_\Lambda|} < 0, \quad (84)$$

as can be easily checked from Eq. (17). This is, of course, rather ugly as it leads to a highly unstable model of the universe, whose matter content would cascade down into increasingly negative energy states. Both matter and vacuum energy densities would increase without end as  $\rho_{m,\Lambda} \sim a^{3|\nu_\Lambda|}$  (in absolute value), but in the asymptotic limit (i.e. for  $a \rightarrow \infty$ ) the ratio between the two stays constant and can be computed exactly:  $\rho_\Lambda/\rho_m = (1 - \nu_\Lambda)/\nu_\Lambda$ . This is a large, but bounded, ratio since  $\nu_\Lambda$  has to be small in absolute value. The ratio is positive for  $\nu_\Lambda > 0$  and negative for  $\nu_\Lambda < 0$ . In the last case the universe would accumulate an arbitrarily large amount of vacuum energy at the expense of acquiring an arbitrarily large negative mass density!

The asymptotic state of such a universe can be compared to that of the “big rip” in the phantom scalar field case [38]. In the latter case,  $\rho_m \rightarrow 0$ , whereas the DE density  $\rho_D \rightarrow \infty$ , so that  $\rho_D/\rho_m \rightarrow \infty$ . It is this unbounded ratio that is responsible for the final big rip. In the  $Q_\Lambda$  case with  $\nu_\Lambda < 0$ , the ratio  $\rho_\Lambda/\rho_m$  stays bounded, but the universe is left with an evermore increasing amount of vacuum energy and negative mass density. A planet bounded in an orbit of radius  $R$  (or, for that matter, any bounded state of any sort) has a net negative energy density associated to the binding energy. However, in the  $Q_\Lambda$  model with negative  $\nu_\Lambda$ , the universe is bound to acquire an unlimited amount of extra energy density of cosmological origin, given by

$$\begin{aligned} -\frac{4\pi}{3} \sum_{i=m,\Lambda} (\rho_i + 3p_i) R^3 &= -\frac{4\pi}{3} (\rho_m - 2\rho_\Lambda) R^3 \rightarrow \\ +\frac{4\pi}{3} \frac{2 - 3\nu_\Lambda}{1 - \nu_\Lambda} \rho_{\Lambda 0} a^{-3\nu_\Lambda} R^3 &\rightarrow +\infty \quad (\nu_\Lambda < 0), \end{aligned} \quad (85)$$

and therefore any bounded system eventually becomes dissociated. Such a universe is in fact driven into a crazy new form of big rip final state, akin to that of usual phantom fields, but with negative mass. A rather weird universe too! For  $\nu_\Lambda > 0$  the problem disappears altogether since the extra energy that such a universe acquires tends to zero with the expansion, as it is clear from (85).

The  $\nu_\Lambda < 0$  version of the  $Q_\Lambda$  universe is not only at odds with the SLT and leads to a catastrophic end point in its evolution (which, in itself, is of course not

forbidden a priori); its truly inadmissible behavior lies, however, on the fact that it does not fit the structure formation data at all. The highest curve in our Fig. 4 neatly shows that the instance  $\nu_\Lambda < 0$  is an outlier and is plainly ruled out. That curve is computed from the fit value of  $q_V \equiv 3\nu_\Lambda < 0$  given in Ref. [82], and in contrast to these authors we find that such a value is unacceptable. Moreover, using our own fit value  $\nu_\Lambda$  (quoted in Table I), which is positive, the  $Q_\Lambda$  model does no longer exhibit such an anomalous departure from the LSS data, see Fig. 4. For the other dynamical vacuum models under consideration (RVM and  $Q_{dm}$ ) we definitely favor again the option  $\nu_i > 0$ , which perfectly fits in with the expectations of the SLT. For these two models, the asymptotic values of the DM densities never become negative, irrespective of the sign of  $\nu_i$ , see Eqs. (15)-(16). Thus, while the SLT would still be violated if the sign of the corresponding vacuum parameters were negative, there is no analogous doomsday for these models.

Even if one would put in doubt the SLT on the grounds that it is applied here to an unusual global system (the universe as a whole) the bare fact is that the sign occurrence in  $\nu_i$  that violates the SLT does bluntly contradict the observational data, as we have shown. For models  $Q_\Lambda$  and  $Q_{dm}$ , our fitting results on  $\nu_i > 0$  in Table I are compatible with those of [83, 84, 86], but in our case we were able to attain much higher accuracy, allowing us to claim significant hints of physics beyond the  $\Lambda$ CDM (see below).

It is worth mentioning that one can extend these considerations in terms of the so-called generalized second law of thermodynamics (GSLT), in which the effect of the area entropy associated to the horizon is also added to the matter entropy contained inside the horizon [148]. For a detailed discussion of the GSLT in the context of this kind of models and related ones, see [149].

Let us finally mention that there are other model variants in which matter decays into vacuum [150] under special conditions. We have not analyzed these variants here since they involve *ad hoc* massive neutrinos. In these cases, in order to preserve the thermodynamic standards, the chemical potential of the massive neutrino species should be significant, thereby implying a large neutrino-antineutrino asymmetry associated to a net lepton number of the universe. As shown in our analysis, we can perfectly dispense with this kind of exotic frameworks since we can substantially improve the  $\Lambda$ CDM fit under perfectly reasonable conditions for the DVMs which are in full accordance with the GSLT.

## V. MAIN NUMERICAL RESULTS

For the statistical analysis, we define the joint likelihood function as the product of the likelihoods for all the data sets. Correspondingly, for Gaussian errors the total  $\chi^2$  to be minimized reads:

$$\chi_{tot}^2 = \chi_{SNIA}^2 + \chi_{BAO}^2 + \chi_H^2 + \chi_{LSS}^2 + \chi_{CMB}^2. \quad (86)$$

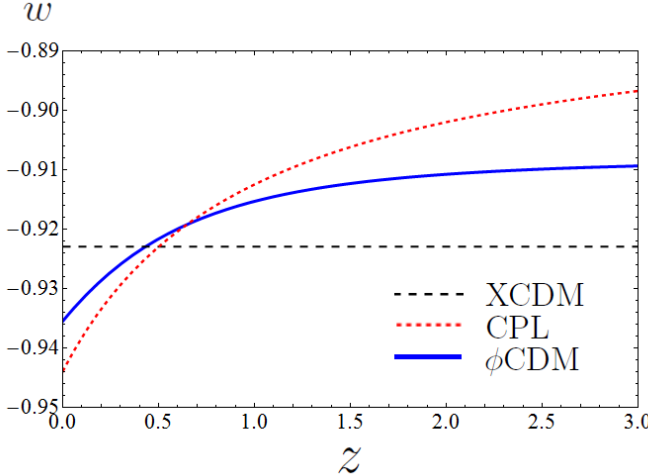


FIG. 5: The EoS  $w = w(z)$  for the XCDM and CPL parametrizations, as compared to that of a typical  $\phi$ CDM model. The first two are obtained using the central values of the fitting parameters in Table I. While for the XCDM the EoS is of course “flat” (constant), for the CPL presents some evolution with the redshift, and in both cases the quintessence region  $w \gtrsim -1$  is singled out. The value  $w_0 = -0.923 \pm 0.023$  for the XCDM in Table I points indeed to effective quintessence at  $3.35\sigma$  c.l. As for the EoS of the  $\phi$ CDM model, we have used the original Peebles & Ratra potential (see Sect. VI F for details) and fitted it to the same cosmological data (cf. Table XII in that section). The current value of the EoS can be determined and reads  $w_\phi(z=0) = -0.936 \pm 0.019$ , which favors once more the quintessence region at  $3.37\sigma$  c.l. These results are compatible with the fitted values for the DVMs in Table I, which signal an effective quintessence behavior ( $\nu_1 > 0$ ) of vacuum dynamics. For the RVM,  $\nu = 0.00158 \pm 0.00042$ , and thus the significance is at  $3.76\sigma$  c.l. In all cases the signal of dynamical DE is favored at a remarkable confidence level.

Each one of these terms is defined in the standard way and they include the corresponding covariance matrices (see Appendix B for a detailed explanation).

Table I and Figs. 1-4 contain the essentials of our analysis. In particular, Fig. 2 displays in a nutshell our main results in all possible planes of the fitting parameter space. Among the other figures, let us stand out here Figs. 7-9, which reveal the very clue to the final results. We will further comment on them in the next sections. We observe from Figs. 1-2 that the vacuum parameters,  $\nu$  and  $\nu_{dm}$ , are neatly projected non null and positive for the RVM and the  $Q_{dm}$ . Remarkably enough, the significance of this dynamical vacuum effect reaches, in our analysis, up to about  $\sim 4\sigma$  c.l. after marginalizing over the remaining parameters.

### A. Fitting the data with the XCDM and CPL parametrizations

Here we further elaborate on the results we have found by exploring now the possible time evolution of the DE in terms of the well-known XCDM and CPL parametrizations (introduced in Sect. II D), in which the DE is mimicked through the density  $\rho_X(a) = \rho_{X0}a^{-3(1+w)}$  associated to some generic (unspecified) entity X, which acts

as an ersatz for the  $\Lambda$  term. Being  $\rho_{X0}$  the current energy density value of X, its value must be identified with the measured  $\rho_{\Lambda0}$ . For the XCDM,  $w = w_0$  is the (constant) equation of state (EoS) parameter for X, whereas for the CPL there is also a dynamical component introduced by  $w_1$ , see Eq. (25). The XCDM trivially boils down to the rigid  $\Lambda$ -term for  $w_0 = -1$ , but by leaving  $w_0$  free it proves a useful approach to roughly mimic a (non-interactive) DE scalar field with constant EoS. Similarly for the CPL, in which some EoS evolution is allowed; we have, however, in this case two free parameters,  $w_0$  and  $w_1$ , to be determined by the data. The corresponding fitting results for the XCDM parametrization is included in all our tables, along with those for the DVMs and the  $\Lambda$ CDM. For the main Table I, and also for Table II, we also include the CPL fitting results. For example, reading off Table I we can see that the best-fit value for  $w_0$  in the XCDM is

$$w_0 = -0.923 \pm 0.023. \quad (87)$$

It is notorious that this EoS value is far from being compatible with a rigid  $\Lambda$ -term. It actually departs from  $-1$  by precisely  $3.35\sigma$  c.l. In Fig. 3 we depict the contour plot for the XCDM in the  $(\Omega_m, w_0)$  plane. Practically all of the  $3\sigma$ -region lies above the horizontal line at  $w_0 = -1$ . Subsequent marginalization over  $\Omega_m$  renders the result (87). Concerning the CPL, we can see from Table I that the errors on the fitting parameters are larger, specially on  $w_1$ , but it concurs with the XCDM that vacuum dynamics is also preferred (see also Sect. V C). The errors are larger in this case simply because the CPL has one more parameter than the XCDM. The plot of the CPL (dynamical) EoS (25), using the central values of the fitting parameters  $w_0$  and  $w_1$  in Table I, is shown in Fig. 5, together with the “flat” EoS (87) for the XCDM. Both parametrizations point to the quintessence region ( $w \gtrsim -1$ ) as the preferred one. To ease future comparison with a more realistic quintessence model, in Fig. 5 we have also included the evolving EoS,  $w = w_\phi(z)$ , of a concrete scalar field model ( $\phi$ CDM) with the Peebles & Ratra potential for  $\phi$ . This model will be studied in more detail in Sect. VI F.

The following observation is in order. For the first time, even the simplest XCDM parametrization has been able to capture nontrivial signs of dynamical DE, in the form of effective quintessence behavior ( $w_0 \gtrsim -1$ ), at more than  $3\sigma$  c.l. This is unprecedented, that is to say, nonexisting in any of the analyses in the literature that we are aware of (previous to our studies). Obviously, given the significance of this fact, it is highly convenient to compare it with well-known previous fitting analyses of the XCDM parametrization, such as the ones performed by the Planck and BOSS collaborations 2-3 years ago. The Planck 2015 value for the EoS parameter of the XCDM reads  $w_0 = -1.019^{+0.075}_{-0.080}$  [5] and the BOSS one is  $w_0 = -0.97 \pm 0.05$  [94]. These results are perfectly compatible with our own fitting value for  $w_0$  given in (87), but in stark contrast to it their errors are big enough as to

be also fully compatible with the  $\Lambda$ CDM value  $w_0 = -1$ . This is not too surprising if we bear in mind that none of these analyses included LSS data in their fits, as explicitly recognized in the text of their papers. Furthermore, at the time when these analyses appeared they could not have used the important LSS and BAO results from [92] – which we have, of course, incorporated as part of our current data set – not even the previous ones from [151]. In Sect. VI B, we discuss the alternate result of our fit if we would use precisely the data by Planck 2015 [5, 6].

In the absence of the modern LSS data we would indeed find a very different situation to that in Table I. As our Table VI clearly shows, the removal of the LSS data set in our fit induces a significant increase in the magnitude of the central value of the EoS parameter for the XCDM, as well as of the corresponding error. This happens because the higher is  $|w|$  the higher is the structure formation power predicted by the XCDM, and therefore the closer is such a prediction with that of the  $\Lambda$ CDM (which is seen to predict too much power as compared to the data, see Fig. 4). Under these conditions our analysis renders  $w = -0.992 \pm 0.040$  (cf. Table VI), which is manifestly closer to (in fact consistent with) the aforementioned central values (and errors) obtained by Planck and BOSS teams. In addition, this result is now fully compatible with the  $\Lambda$ CDM, as in the Planck 2015 and BOSS cases, and all of them are unfavored by the LSS observations. This also agrees with the fact that both information criteria,  $\Delta$ AIC and  $\Delta$ BIC, become now slightly negative in Table VI, which reconfirms that if the LSS data are not used the  $\Lambda$ CDM performance is slightly superior to that of the dynamical DE models.

From the foregoing observations it becomes clear that in order to improve the fit to the observed values of  $f(z)\sigma_8(z)$ , which generally appear lower-powered with respect to those predicted by the  $\Lambda$ CDM (cf. Fig. 4),  $|w|$  should decrease. This is just what happens in our fit for the XCDM, see Eq. (87). At the level of the DVMs this translates into positive values of  $\nu_i$ , as these values cause the vacuum energy to be larger in our past; and, consequently, it introduces a time modulation of the growth suppression of matter. Such an advantage of the vacuum dynamics was mentioned in the Introduction as a potential source of improvement with respect to the  $\Lambda$ CDM. It is apparent from Fig. 4 that the  $f(z)\sigma_8(z)$  curves for the vacuum models are shifted downwards (they have less power than the  $\Lambda$ CDM) and hence adapt significantly better to the LSS data points. Correspondingly, the quality of the fits increases dramatically for the XCDM, RVM and  $Q_{dm}$ , and this is also borne out by the large and positive values of  $\Delta$ AIC and  $\Delta$ BIC (as can be checked in Table I). The upshot is a net enhancement of the observational account by the dynamical DE models versus the  $\Lambda$ CDM.

It is worth realizing that the fit improvement obtained with the XCDM parametrization of the DE concurs with the prediction of the dynamical vacuum models using exactly the same data. This was not evident a priori,

since for the DVMs there is an interaction between vacuum and matter that triggers an anomalous conservation law, whereas for the XCDM we do not have such an interaction (meaning that matter is conserved in them, thereby following the standard decay laws for relativistic and nonrelativistic components). The interaction, however, is proportional to  $\nu_i$  and, thus, is small. This probably explains why the XCDM can also succeed in nailing down the dynamical nature of the DE.

Overall the results are consistent: in the XCDM case the departure from the  $\Lambda$ CDM takes on the fashion of “effective quintessence”, whereas for the DVMs (in which  $\nu_i > 0$ ) it appears as vacuum energy decreasing with time; and in all cases, except for the  $Q_\Lambda$  (where the effect is lesser), we find compelling signs of DE physics beyond the  $\Lambda$ CDM (cf. Table I).

## B. On the purported tension between the measured values of the Hubble parameter

Recently, a significant tension between the local and nonlocal measurements of the Hubble parameter  $H_0$  obtained from different types of observations has generated some perplexity in the literature. There is a kind of bipolarization into two groups of values. Most conspicuously, Riess et al. reported  $H_0 = 73.24 \pm 1.74$  Km/s/Mpc [152], based on Hubble Space Telescope data. This value is  $\sim 3.3\sigma$  higher than the Planck result  $H_0 = 67.51 \pm 0.64$  Km/s/Mpc [5] inferred from the CMB. For other measurements and discussions, see e.g. [3], [94], [153], [154], [155], and [156]. This situation has stimulated a number of discussions and possible solutions in the literature, see e.g. [157–159] and references therein.

As indicated before, owing to the lack of consensus on the experimental value of  $H_0 = 100h$  Km/s/Mpc, in this work we have fitted  $h$  using an uninformative flat prior. This should be fairer in these circumstances, rather than making a subjective choice among the different measurements of  $h$  put forward in the aforementioned papers. One can see from Table I that our fitted value of the local Hubble parameter within the  $\Lambda$ CDM is  $H_0 = 69.2 \pm 0.4$  Km/s/Mpc. Compared to  $H_0 = 73.24 \pm 1.74$  Km/s/Mpc from Riess et al. it is only  $2.3\sigma$ , i.e. one standard deviation less than the discrepancy with the Planck 2015 measurement. This result clearly helps to alleviate the discrepancy, which is now not so severe. Let us recall that in our fit we use not only the CMB data from Planck 2015 but a rich variety of observational sources, which were not considered (and some of them not even available) in the fit analysis performed by Planck in 2015. We are mainly referring to the wealth of BAO+LSS data that we have used in our own analysis, see items DS2, DS3 and DS5 of Sect. III A. Our fitting result for the  $\Lambda$ CDM is by the way perfectly in accordance with the WMAP+ACT+SPT+BAO result  $H_0 = 69.3 \pm 0.7$  Km/s/Mpc [152] and is in between the bipolarized local and nonlocal values mentioned above.

It is not obvious to us that the purported tension is suggesting some systematic uncertainties in CMB measurements, as has been claimed. Our  $\Lambda$ CDM fit involving the full set of SNIa+BAO+ $H(z)$ +LSS+CMB data is actually in good agreement with Planck and WMAP, and it suggests that once a richer set of observations (specifically on LSS) are included the tension will loosen up substantially. As far as our favorite dynamical vacuum model RVM is concerned, which gives a significantly better fit than the  $\Lambda$ CDM, we can see from Table I that we tend to favor lower values of the local Hubble parameter:  $H_0 = 67.7 \pm 0.5$  Km/s/Mpc. This has been the main trend of the cosmological observations for years, see the summary of [154] and the more recent analysis [115].

### C. Comparing the competing vacuum models through Akaike and Bayesian information criteria

We may judge the fit quality obtained for the different vacuum models in this work from a different perspective. Although the  $\chi^2_{\min}$  value of the overall fits for the main DVMs (RVM and  $Q_{dm}$ ) and XCDM appear to be definitely smaller than the  $\Lambda$ CDM one, it proves extremely useful to reassess the degree of success of each competing model by invoking the time-honored Akaike and Bayesian information criteria, denoted as AIC and BIC. See [160–162] for the original papers, and [163] for a textbook exposition. The Akaike information criterion is defined as follows:

$$AIC = \chi^2_{\min} + \frac{2nN}{N - n - 1}, \quad (88)$$

whereas the Bayesian information criterion reads

$$BIC = \chi^2_{\min} + n \ln N. \quad (89)$$

In these formulas,  $n$  is the number of independent fitting parameters and  $N$  the number of data points. The added terms on  $\chi^2_{\min}$  represent the penalty assigned by these information criteria to the models owing to the presence of additional parameters.

To test, with the help of AIC and BIC, the degree of success of a dynamical DE model (versus the  $\Lambda$ CDM) for describing a set of cosmological data, we have to evaluate the pairwise differences  $\Delta AIC$  ( $\Delta BIC$ ) between the AIC and BIC values of the  $\Lambda$ CDM with respect to the corresponding values of the models having a smaller value of these criteria – in our case the DVMs, XCDM and CPL. The larger these (positive) differences are the higher is the evidence against the model with larger value of AIC (BIC) – i.e. the  $\Lambda$ CDM in the present case.

Notice that when the number of points is much larger than the number of parameters the AIC criterion behaves approximately as  $AIC = \chi^2_{\min} + 2n$ . Comparing with (89) we see that, for large  $N$ , the penalty applied by BIC is bigger than the one applied by AIC. As a result,  $\Delta BIC < \Delta AIC$ , as can be seen in our tables.

According to the standard usage of these criteria, for  $\Delta AIC$  and/or  $\Delta BIC$  below 2 one judges that there is “consistency” between the two models under comparison; in the range 2–6 there exists a “positive evidence”; for values within 6–10 one may claim “strong evidence” against such a model; finally, above 10, one speaks of “very strong evidence” [160, 163]. The evidence ratio associated to rejection of the unfavored model is given by the ratio of Akaike weights,  $e^{\Delta AIC/2}$ . Similarly,  $e^{\Delta BIC/2}$  estimates the so-called Bayes factor, which gives the ratio of marginal likelihoods between the two models [72, 88].

Table I reveals conspicuously that the  $\Lambda$ CDM appears very strongly disfavored (according to the above statistical standards) when confronted to some of the dynamical DE models. More precisely, for the RVM and the  $Q_{dm}$  the  $\Delta AIC$  and  $\Delta BIC$  are in the range 12–13 and 9–11, respectively. These results are fully consistent and outstanding; and since both  $\Delta AIC$  and  $\Delta BIC$  are above 9–10 the verdict of the information criteria is conclusive. For instance, the Bayes factor in favor of the RVM relative to the  $\Lambda$ CDM is larger than  $e^{5.3} \sim 200$ . The situation with model  $Q_{dm}$  is comparable.

It goes without saying that not all dynamical vacuum models describe the data with the same efficiency. In the case of the  $Q_\Lambda$  model the improvement is so mild that Occam’s razor criterion (“among equally competing models describing the same observations, choose the simplest one”) would probably not recommend its choice. However, since the other dynamical DE models are able to describe the current observations significantly better than the  $\Lambda$ CDM, and not just alike, Occam’s razor should definitely bet in their favor. The AIC and BIC criteria can be thought of as a modern quantitative formulation of Occam’s razor, in which the presence of extra parameters in a given model is conveniently penalized so as to achieve a fairer comparison with the model having less parameters.

Thus, e.g. model  $Q_\Lambda$  despite being also better than the traditional  $\Lambda$ -picture, the values of  $\Delta AIC$  and  $\Delta BIC$  are sitting in the much more moderate range 1–3 (cf. Table I), and hence that model is certainly not comparable in efficiency to the main DVMs. Model  $Q_\Lambda$  is also left behind in comparison to the output of the simple XCDM and CPL parametrizations. The corresponding XCDM values of  $\Delta AIC$  and  $\Delta BIC$  are in the range 6–9 (reconfirming the ability of the XCDM to substantially improve the  $\Lambda$ CDM fit). Similarly for the CPL parametrization, where  $\Delta AIC$  and  $\Delta BIC$  stay in the approximate range 2–6. This also confirms a superior performance of the CPL versus the  $\Lambda$ CDM and the  $Q_\Lambda$  model in their different abilities for describing the data. The lesser quality fit of the CPL with respect to the XCDM, though, is obviously caused by the presence of an extra fitting parameter in the first, as previously pointed out.

It is remarkable the amount of evidence on dynamical DE that can be presently gathered with the simple XCDM parametrization. As formerly noted, to the best of our knowledge it is unprecedented in the literature. It

is even more remarkable, if we realize that it equals the level of evidence that we will be able to pick up from the analysis of a full-fledged quintessence model with a given potential, see Sect. VI F. Nonetheless the difference of roughly 4 (positive) points in the value of  $\Delta\text{AIC}$  and  $\Delta\text{BIC}$  in favor of the main DVMs with respect to the XCDM is considered significant from the point of view of the information criteria. Therefore, the simple XCDM approach lags behind the main dynamical vacuum models under consideration. The RVM and  $Q_{dm}$  stand out here as superior competing candidates as compared to the XCDM (and in fact compared to all the other models under scrutiny in this work) in their capacity to fit the overall cosmological data.

## VI. DISCUSSION

### A. Anomalous matter conservation law

As we have discussed in Section II, for the DVMs there is an interaction between vacuum and matter. Such an interaction is, of course, small because the fitted values of  $\nu_i$  are small, see Table I. The obtained values are in the ballpark of  $\nu_i \sim \mathcal{O}(10^{-3})$  and therefore this is also the order of magnitude associated to the anomalous conservation law of matter. For example, for the nonrelativistic component in the RVM we have

$$\rho_m(a) = \rho_{dm}(a) + \rho_b(a) = \rho_{m0}a^{-3(1-\nu)} . \quad (90)$$

Here  $\rho_{m0} = \rho_{dmo} + \rho_{b0}$ , and use has been made of the conservation law of baryons, Eq. (8), as well as of the DM density in the RVM, Eq. (15). As previously mentioned, the possible anomalous behavior of matter conservation has been exploited in devoted works such as [79–81]. These are essentially based on the RVM as a possible explanation for the various hints on the time variation of the fundamental constants, such as coupling constants and particle masses, frequently considered in the literature. See e.g. [126, 127] and [164] for reviews.

Let us note that the time variation of the mass density can be interpreted either as an anomalous change in the number density of particles during the expansion or as a change in their mass values [79]. It is interesting that the current observational limits for such a time variation are compatible with the fitted values we have found here [81]. The possibility that the baryon masses can also change slowly with the cosmic evolution has also been tested, and could be connected with the possible time variation of the fine structure constant [81], but the limits are rather strict, much more than the possible time variation of the DM masses. This is the reason why we have assumed from the beginning that the exchange between matter and vacuum energy is strictly confined to the DM sector. If there is some exchange with baryons, it must be so small that it cannot influence significantly the main cosmological considerations that are under study here.

The potential time variation of the fundamental constants is a very active field of research and is therefore nowadays of high interest and can have a variety of implications, see e.g. [164, 165] and references therein. As we can see, there are different phenomenological possibilities that can be used to test the RVM and other DVMs from various points of view. A positive measurement of that kind of effects could be interpreted as strong support to the ‘micro and macro connection’ hypothesis, viz. the dynamical feedback between the evolution of the cosmological parameters and the time variation of the fundamental constants of the microscopic world [80].

### B. Testing the impact of the different data sets in our analysis and comparing with Planck 2015

The current work is the natural extension of [68]. It follows the track of [67] and is also firmly aligned with [66]. Although the models analyzed in [66, 67] have some differences with respect to the ones treated here, the outcome of the analysis points to the very same direction, to wit: some DVMs and the XCDM do fit considerably better the available data than the  $\Lambda$ CDM. But we want to emphasize some important aspects of the analysis carried out in this paper as compared to other analyses:

- We have used a large and fully updated set of cosmological SNIa+BAO+ $H(z)$ +LSS+CMB observations. To our knowledge, this is one of the most complete and consistent data sets used in the literature. The current data set has been well tested in [66] and [69], but differs from the one used in these analyses in that we have now used the updated BAO and LSS analysis from Ref. [92], see more details in Sect. VI E.
- The selected string SNIa+BAO+ $H(z)$ +LSS+CMB of observational data has been obtained from independent analyses in the literature, see the detailed description of the data sets DS1-DS6) in Sect. III A and references therein.
- We have duly taken into account all the known covariance matrices in the total  $\chi^2$  function (86), which means that we have accounted for all the known correlations among the data. See Appendix B for a detailed explanation. Not all data sets existing in the literature are fully consistent, sometimes they are affected from important correlations that have not been evaluated. We refer the reader to our discussion on correlated data sets in items DS3, DS4 and DS5 of Sect. III A, including the comparison example made there of our fitting results in Tables I and II.
- We have removed from our analysis all data that are manifestly correlated. As an example, we have avoided to use Hubble parameter data extracted

| Model               | $h$               | $\omega_b = \Omega_b h^2$ | $n_s$             | $\Omega_m$        | $\nu_i$               | $w$                | $\chi^2_{\min}/dof$ | $\Delta\text{AIC}$ | $\Delta\text{BIC}$ |
|---------------------|-------------------|---------------------------|-------------------|-------------------|-----------------------|--------------------|---------------------|--------------------|--------------------|
| $\Lambda\text{CDM}$ | $0.679 \pm 0.005$ | $0.02241 \pm 0.00017$     | $0.968 \pm 0.005$ | $0.291 \pm 0.005$ | -                     | -1                 | $67.86/83$          | -                  | -                  |
| $\text{XCDM}$       | $0.674 \pm 0.007$ | $0.02241 \pm 0.00017$     | $0.968 \pm 0.005$ | $0.298 \pm 0.009$ | -                     | $-0.960 \pm 0.038$ | $66.79/82$          | -1.18              | -3.40              |
| $\text{RVM}$        | $0.679 \pm 0.008$ | $0.02241 \pm 0.00017$     | $0.968 \pm 0.005$ | $0.296 \pm 0.015$ | $0.00061 \pm 0.00158$ | -1                 | $67.71/82$          | -2.10              | -4.32              |
| $Q_{dm}$            | $0.677 \pm 0.008$ | $0.02241 \pm 0.00017$     | $0.968 \pm 0.005$ | $0.296 \pm 0.015$ | $0.00086 \pm 0.00228$ | -1                 | $67.71/82$          | -2.10              | -4.32              |
| $Q_\Lambda$         | $0.679 \pm 0.005$ | $0.02241 \pm 0.00017$     | $0.968 \pm 0.005$ | $0.297 \pm 0.013$ | $0.00463 \pm 0.00922$ | -1                 | $67.59/82$          | -1.98              | -4.20              |

TABLE V: Same as in Table I, but removing both the  $R$ -shift parameter and the acoustic length  $l_a$  from our fitting analysis.

| Model               | $h$               | $\omega_b = \Omega_b h^2$ | $n_s$             | $\Omega_m$        | $\nu_i$               | $w$                | $\chi^2_{\min}/dof$ | $\Delta\text{AIC}$ | $\Delta\text{BIC}$ |
|---------------------|-------------------|---------------------------|-------------------|-------------------|-----------------------|--------------------|---------------------|--------------------|--------------------|
| $\Lambda\text{CDM}$ | $0.685 \pm 0.004$ | $0.02243 \pm 0.00014$     | $0.969 \pm 0.004$ | $0.304 \pm 0.005$ | -                     | -1                 | $61.45/72$          | -                  | -                  |
| $\text{XCDM}$       | $0.684 \pm 0.009$ | $0.02244 \pm 0.00015$     | $0.969 \pm 0.004$ | $0.305 \pm 0.007$ | -                     | $-0.992 \pm 0.040$ | $61.41/71$          | -2.25              | -4.29              |
| $\text{RVM}$        | $0.684 \pm 0.008$ | $0.02242 \pm 0.00016$     | $0.969 \pm 0.005$ | $0.304 \pm 0.005$ | $0.00014 \pm 0.00103$ | -1                 | $61.43/71$          | -2.27              | -4.31              |
| $Q_{dm}$            | $0.685 \pm 0.007$ | $0.02242 \pm 0.00016$     | $0.969 \pm 0.005$ | $0.304 \pm 0.005$ | $0.00019 \pm 0.00126$ | -1                 | $61.43/71$          | -2.27              | -4.31              |
| $Q_\Lambda$         | $0.686 \pm 0.004$ | $0.02240 \pm 0.00017$     | $0.968 \pm 0.005$ | $0.304 \pm 0.005$ | $0.00090 \pm 0.00330$ | -1                 | $61.37/71$          | -2.21              | -4.25              |

TABLE VI: Same as in Table I, but removing the LSS data set from our fitting analysis.

from BAO measurements, see DS4. Similarly, we have avoided to perform double counting using “different” data releases that are fully or partially overlapping; in particular, we have carefully averted using subsets of data that are part of a bigger set and then treat them all as independent data sets. We have carefully assessed these situations. From our data set list in Sect. III A and the attached explanations there the reader can check that we have thoroughly complied with these important requirements.

All in all, this explains the reliable accuracy obtained in the current fitted values of the vacuum parameters  $\nu_i$  (and the EoS parameter  $w_0$  of the XCDM), as well as the significant reduction in the error bars with respect to the ones we had previously obtained in, e.g. [67], where the first hints of dynamical DE were reported.

We have actually conducted a series of practical tests in order to check what would be the impact on the fitting quality of our main analysis (cf. Table I) if we would remove some of the data points or even a particular data source. For instance, removing from our analysis crucial ingredients of the CMB data, such as the acoustic length  $l_a$  and at the same time replace the current BAO data points by those of [166] relying on the BAO  $A(z)$ -estimator. Notice that the CMB part is now left essentially with the  $R$ -shift parameter only. This is precisely the old situation that we considered in [67] with other models. In doing this we obtain indeed results perfectly consistent with that reference: namely, the error bars’ size become  $\sim 4 - 5$  times larger than the current ones, i.e. of order  $\mathcal{O}(10^{-3})$  rather than  $\mathcal{O}(10^{-4})$ .

We have also checked what would be the effect on our fit if we would remove both the data on the shift parameter and on the acoustic length; or if we would remove only the data points on LSS. In the first case it means to essentially dispense with the CMB data, and in the second case to ignore altogether the information on structure formation. The results are presented in Tables V and VI, respectively. We observe that in both cases the va-

cuum parameters are compatible with zero at one  $\sigma$  c.l., and the  $\Delta\text{AIC}$  and  $\Delta\text{BIC}$  values become  $\sim 2 - 4$  points negative. This means that under any of these two conditions the  $\Lambda\text{CDM}$  does better than the XCDM and the DVMs. The obvious conclusion is that the full CMB and LSS data are individually very important for the quality of the fit and that without a single one of these data sources the dynamical DE signal gets completely lost.

With the same testing spirit we have refitted the models excluding the BAO data only, and the result is shown in Table VII. It is noticeable that in this case the dynamical DE signal, despite it gets weakened and in fact disappears altogether from the XCDM parametrization, it still survives at  $\lesssim 3\sigma$  c.l. for the three DVMs, with both information criteria  $\Delta\text{AIC}$  and  $\Delta\text{BIC}$  rendering 4 – 6 (positive) points significantly in favor of the signal. This tells us that the bulk of the signal is probably encoded in the CMB and LSS data, and that the BAO data helps to make it crisper (finally attaining  $\sim 4\sigma$  c.l. in the main Table I). However, this requires further confirmation since we have to separate the rest of the data sources. We will do it in Sect. VID.

We conclude this section by answering a most natural question. Why the dynamical DE signal that we are glimpsing here escaped undetected from the fitting analyses of Planck 2015? The answer can be obtained by repeating our fitting procedure and restricting ourselves to the much more limited data sets used by the Planck 2015 collaboration, more precisely in the papers [5] and [6]. In contrast to [5], where no LSS (RSD) data were used at all, in the case of [6] they used only some BAO and LSS data, but their fit is rather limited in scope. Specifically, they used only 4 BAO data points, 1 AP (Alcock-Paczynski parameter) data point, and one single LSS point, namely the value of  $f(z)\sigma_8(z)$  at  $z = 0.57$  – see details in that paper. Using this same data we obtain the fitting results presented in our Table VIII. They are perfectly compatible with the fitting results mentioned in Sect. VA obtained by Planck 2015 and BOSS [94], i.e. none of them carries evidence of dynamical DE, with only the data used by these collaborations two-three years ago.

| Model               | $h$               | $\omega_b = \Omega_b h^2$ | $n_s$             | $\Omega_m$        | $\nu_i$               | $\omega$           | $\chi^2_{\min}/dof$ | $\Delta\text{AIC}$ | $\Delta\text{BIC}$ |
|---------------------|-------------------|---------------------------|-------------------|-------------------|-----------------------|--------------------|---------------------|--------------------|--------------------|
| $\Lambda\text{CDM}$ | $0.698 \pm 0.005$ | $0.02263 \pm 0.00015$     | $0.977 \pm 0.004$ | $0.288 \pm 0.006$ | -                     | -1                 | $61.25/74$          | -                  | -                  |
| $\text{XCDM}$       | $0.681 \pm 0.015$ | $0.02262 \pm 0.00015$     | $0.976 \pm 0.004$ | $0.303 \pm 0.014$ | -                     | $-0.949 \pm 0.042$ | $59.72/73$          | -0.75              | -2.83              |
| $\text{RVM}$        | $0.683 \pm 0.007$ | $0.02242 \pm 0.00016$     | $0.969 \pm 0.005$ | $0.296 \pm 0.007$ | $0.00138 \pm 0.00049$ | -1                 | $52.95/73$          | 6.02               | 3.94               |
| $Q_{dm}$            | $0.685 \pm 0.007$ | $0.02241 \pm 0.00016$     | $0.968 \pm 0.005$ | $0.295 \pm 0.007$ | $0.00192 \pm 0.00069$ | -1                 | $52.91/73$          | 6.06               | 3.98               |
| $Q_\Lambda$         | $0.701 \pm 0.005$ | $0.02240 \pm 0.00017$     | $0.968 \pm 0.005$ | $0.287 \pm 0.006$ | $0.00733 \pm 0.00257$ | -1                 | $53.36/73$          | 5.61               | 3.53               |

TABLE VII: Same as in Table I, but removing the BAO data set from our fitting analysis.

| Model               | $h$               | $\omega_b = \Omega_b h^2$ | $n_s$             | $\Omega_m$        | $\nu_i$               | $w$                | $\chi^2_{\min}/dof$ | $\Delta\text{AIC}$ | $\Delta\text{BIC}$ |
|---------------------|-------------------|---------------------------|-------------------|-------------------|-----------------------|--------------------|---------------------|--------------------|--------------------|
| $\Lambda\text{CDM}$ | $0.694 \pm 0.005$ | $0.02265 \pm 0.00022$     | $0.976 \pm 0.004$ | $0.293 \pm 0.007$ | -                     | -1                 | $38.98/39$          | -                  | -                  |
| $\text{XCDM}$       | $0.684 \pm 0.010$ | $0.02272 \pm 0.00023$     | $0.977 \pm 0.005$ | $0.299 \pm 0.009$ | -                     | $-0.961 \pm 0.033$ | $37.61/38$          | -1.20              | -2.39              |
| $\text{RVM}$        | $0.685 \pm 0.009$ | $0.02252 \pm 0.00024$     | $0.971 \pm 0.006$ | $0.297 \pm 0.008$ | $0.00080 \pm 0.00062$ | -1                 | $37.29/38$          | -0.88              | -2.07              |
| $Q_{dm}$            | $0.686 \pm 0.008$ | $0.02251 \pm 0.00025$     | $0.971 \pm 0.006$ | $0.297 \pm 0.008$ | $0.00108 \pm 0.00088$ | -1                 | $37.43/38$          | -1.02              | -2.21              |
| $Q_\Lambda$         | $0.694 \pm 0.006$ | $0.02258 \pm 0.00029$     | $0.974 \pm 0.007$ | $0.293 \pm 0.007$ | $0.00167 \pm 0.00471$ | -1                 | $38.86/38$          | -2.45              | -3.64              |

TABLE VIII: As in Table I, but using the same data set as the Planck Collaboration [6]. See the text for further details.

In contradistinction to them, in our full analysis presented in Table I we used 11 BAO and 13 LSS data points, some of them available only from the recent literature and of high precision [92]. From Table VIII it is apparent that with only the data used in [6] the fitting results for the RVM are poor enough and cannot still detect clear traces of the vacuum dynamics. In fact, the vacuum parameters are compatible with zero at one  $\sigma$  c.l. and the values of  $\Delta\text{AIC}$  and  $\Delta\text{BIC}$  in that table are moderately negative, showing that the DVMs do not fit better the data than the  $\Lambda\text{CDM}$  model with only such a limited input. The obtained result is reasonably compatible with what we saw in Tables V-VII since the full CMB data, but only a limited part of the BAO and LSS data, participate in the Planck 2015 analysis; but such an analysis cannot yet reach the threshold of visibility of the signal. In fact, not even the XCDM parametrization is capable of detecting any trace of dynamical DE with that limited data set, as the effective EoS is compatible with  $w_0 = -1$  at roughly  $1\sigma$  c.l. ( $w_0 = -0.961 \pm 0.033$ ). Compare with the EoS result using our full data set, see Eq. (87), where  $w_0$  was pinned down to lie above  $-1$  at  $\gtrsim 3.3\sigma$  c.l.

This should explain why the features that we are reporting here have remained hitherto unnoticed in the literature, except in our recent papers [66–69], and also by the very recent analysis [73]. These authors have been able to find a significant  $3.5\sigma$  c.l. effect on dynamical DE, presumably in a model-independent way. The result is well along the lines of the present work and its recent predecessors, in all of which we have been able to collect evidence, even at a slightly stronger level that these authors, using different models and parametrizations.

### C. Results with and without including the bispectrum

The following question is now in order: why is it important to include the BOSS data from [92]? Recently, the cosmological results from the final galaxy clustering data set of BOSS (SDSS-III) were made public [167]. This

analysis is even fresher than the one presented in [92], so again, which is the reason to stick to the particular data analysis from [92] rather than using the more recent one presented in [167]? Both actually emerge from the same DR12 galaxy sample of BOSS, but the treatment of the data in each case is different. What is the difference? The important answer to this question is provided explicitly by the authors of [167] themselves, and we just quote it: *one can attribute the improvement in [92] when compared to our measurements to the use of the bispectrum, which has not been used in our analysis [167]*. It is somehow natural that this is so, since the bispectrum is a higher-order statistics, which involves the three-point correlation function instead of the two-point correlation function (the inverse Fourier transform of the power spectrum). It represents the next-to-leading contribution in the analysis of cosmic fluctuations in perturbation theory.

In what follows we check explicitly the implications of using or not using the bispectrum in our analysis. The results presented in [92] are grounded on the RSD measurements of the power spectrum combined with the bispectrum, and the BAO post-reconstruction analysis of the power spectrum. In contrast, the authors of [167] do not make use of the bispectrum. Nonetheless, its use is of great importance since it leads to a significant decrease of the error bars of the data inferred from the corresponding study; and this, of course, has a direct bearing on our own results, for the smaller the error bars of the data, the smaller are the error bars of the cosmological parameters (including, of course, those sensitive to the dynamical DE) obtained from our fitting analysis.

While the spectrum  $P(\mathbf{k})$  is connected with the two-point correlator of the density field  $D(\mathbf{k})$  in Fourier space, namely  $\langle D(\mathbf{k}) D(\mathbf{k}') \rangle = \delta(\mathbf{k} - \mathbf{k}') P(\mathbf{k})$ , in which  $\delta$  is a Dirac delta, the bispectrum  $B(\mathbf{k}_1, \mathbf{k}_2, \mathbf{k}_3)$  is formally connected with the three-point correlator

$$\langle D(\mathbf{k}_1) D(\mathbf{k}_2) D(\mathbf{k}_3) \rangle = \delta(\mathbf{k}_1 + \mathbf{k}_2 + \mathbf{k}_3) B(\mathbf{k}_1, \mathbf{k}_2, \mathbf{k}_3), \quad (91)$$

where the Dirac  $\delta$  selects the triangular configurations.

| Model               | $h$               | $\omega_b = \Omega_b h^2$ | $n_s$             | $\Omega_m$        | $\nu_i$               | $w$                | $\chi^2_{\min}/dof$ | $\Delta\text{AIC}$ | $\Delta\text{BIC}$ |
|---------------------|-------------------|---------------------------|-------------------|-------------------|-----------------------|--------------------|---------------------|--------------------|--------------------|
| $\Lambda\text{CDM}$ | $0.691 \pm 0.004$ | $0.02251 \pm 0.00014$     | $0.973 \pm 0.004$ | $0.297 \pm 0.005$ | -                     | -1                 | 79.67/88            | -                  | -                  |
| $\text{XCDM}$       | $0.676 \pm 0.008$ | $0.02257 \pm 0.00014$     | $0.974 \pm 0.004$ | $0.309 \pm 0.008$ | -                     | $-0.945 \pm 0.029$ | 76.14/87            | 1.29               | -0.99              |
| RVM                 | $0.680 \pm 0.006$ | $0.02235 \pm 0.00015$     | $0.966 \pm 0.005$ | $0.302 \pm 0.006$ | $0.00120 \pm 0.00047$ | -1                 | 72.74/87            | 4.69               | 2.41               |
| $Q_{dm}$            | $0.680 \pm 0.006$ | $0.02235 \pm 0.00015$     | $0.966 \pm 0.005$ | $0.302 \pm 0.006$ | $0.00162 \pm 0.00065$ | -1                 | 73.11/87            | 4.32               | 2.04               |
| $Q_\Lambda$         | $0.691 \pm 0.004$ | $0.02234 \pm 0.00017$     | $0.967 \pm 0.005$ | $0.298 \pm 0.005$ | $0.00502 \pm 0.00261$ | -1                 | 76.01/87            | 1.42               | -0.86              |

TABLE IX: Same as Table I, but using the BOSS data from [167] instead of [92]. In contradistinction to the latter, the former does not include the bispectrum effects in their results. See the discussion.

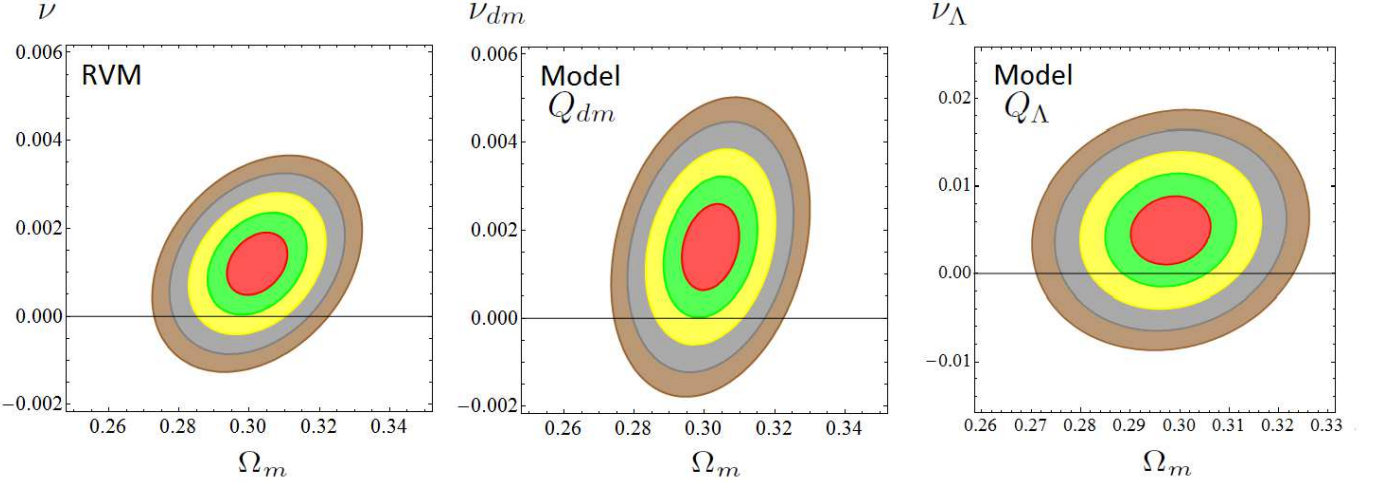


FIG. 6: As in Fig. 1, but using the BOSS data of [167], which does not include the bispectrum, in contrast to the BOSS data of [92], which does include it. The fitting results associated to this figure are provided in Table IX.

The bispectrum has been described in many places in the literature, see e.g.[50, 72, 133] and references therein. Now, while the above definition is the formal one, operationally (in other words, at the practical level of galaxy counting) a bispectrum estimator  $\langle F_3(\mathbf{k}_1)F_3(\mathbf{k}_2)F_3(\mathbf{k}_3) \rangle$  can be defined from the angle-average of closed triangles defined by the  $\mathbf{k}$ -modes,  $\mathbf{k}_1, \mathbf{k}_2, \mathbf{k}_3$ , where  $F_3(\mathbf{q})$  is the Fourier transform of an appropriately defined weighted field of density fluctuations, that is to say, one formulated in terms of the number density of galaxies [92]. It can be conveniently written as

$$\langle F_3(\mathbf{k}_1)F_3(\mathbf{k}_2)F_3(\mathbf{k}_3) \rangle = \frac{k_f^3}{V_{123}} \int d^3\mathbf{r} \mathcal{D}_{\mathcal{S}_1}(\mathbf{r}) \mathcal{D}_{\mathcal{S}_2}(\mathbf{r}) \mathcal{D}_{\mathcal{S}_3}(\mathbf{r}), \quad (92)$$

i.e. through an expression involving a separate product of Fourier integrals

$$\mathcal{D}_{\mathcal{S}_j}(\mathbf{r}) \equiv \int_{\mathcal{S}_j} d\mathbf{q}_j F_3(\mathbf{q}_j) e^{i\mathbf{q}_j \cdot \mathbf{r}}. \quad (93)$$

Here  $k_f$  is the fundamental frequency,  $k_f = 2\pi/L_{\text{box}}$ ,  $L_{\text{box}}$  the size of the box in which the galaxies are embedded and

$$V_{123} \equiv \int_{\mathcal{S}_1} d\mathbf{q}_1 \int_{\mathcal{S}_2} d\mathbf{q}_2 \int_{\mathcal{S}_3} d\mathbf{q}_3 \delta(\mathbf{q}_1 + \mathbf{q}_2 + \mathbf{q}_3), \quad (94)$$

is the number of fundamental triangles inside the shell defined by  $\mathcal{S}_1, \mathcal{S}_2$  and  $\mathcal{S}_3$ , with  $\mathcal{S}_i$  the region of the  $k$ -modes contained in a  $k$ -bin,  $\Delta k$ , around  $k_i$ . The Dirac  $\delta$

insures that only closed triangles are included – see [92] for more details.

The physical importance of including the bispectrum cannot be overemphasized. The bispectrum furnishes important complementary information that goes beyond the spectrum. If fluctuations in the structure formation were strictly Gaussian, their full statistical description would be contained in the two-point correlation function, or equivalently the power spectrum estimator  $\langle F_2(\mathbf{k}_1)F_2(\mathbf{k}_2) \rangle$ . In such a case the formal bispectrum defined above would identically vanish. Therefore, its inclusion is essential to be sensitive to possible higher order effects associated to non-Gaussianities in the distribution of galaxies. Even if one starts from Gaussian initial conditions, gravity makes fluctuations evolve non-Gaussian. Therefore, such deviations with respect to a normal distribution may be due both to the evolution of gravitational instabilities that are amplified from the initial perturbations, or even from some intrinsic non-Gaussianity of the primordial spectrum.

In order to study the effect of the bispectrum on our analysis of dynamical DE in a quantitative way we have completely refitted our models using now the data from [167] concerning BAO and LSS, not carrying any information on the bispectrum component, leaving of course the remaining data exactly as before. The numerical results corresponding to this new setup are collected in Table IX. We may now compare the results of Table I (in

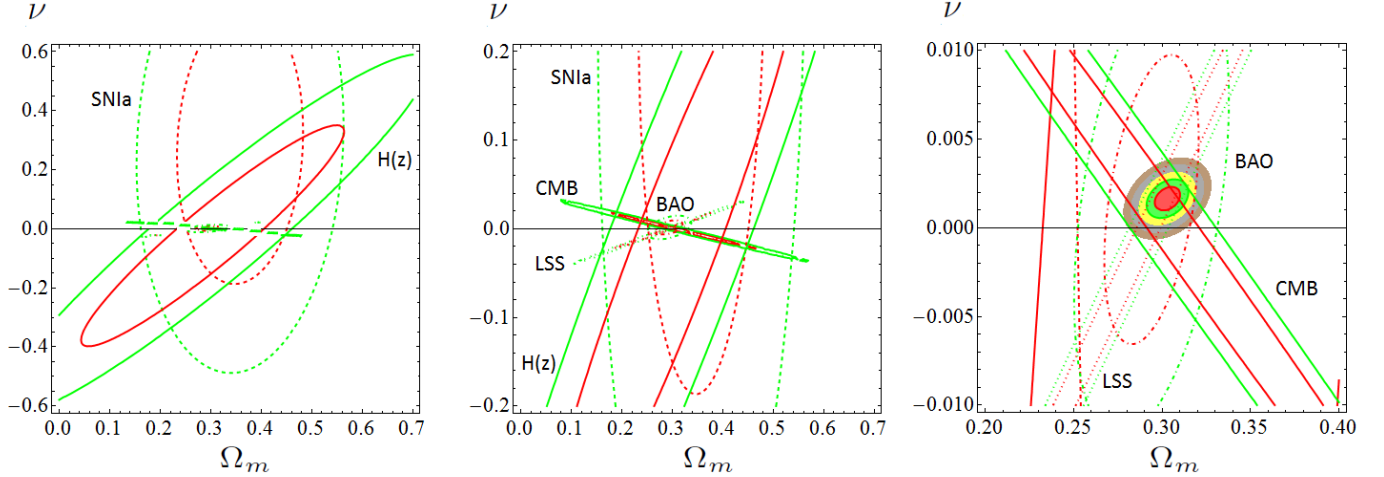


FIG. 7: Reconstruction of the contour lines for the RVM, from the partial contour plots of the different SNIa+BAO+ $H(z)$ +LSS+CMB data sources. The  $1\sigma$  c.l. and  $2\sigma$  c.l. contours are shown in all cases. For the reconstructed final contour lines we also plot the  $3\sigma$ ,  $4\sigma$  and  $5\sigma$  confidence level regions.

which the bispectrum was included) with those produced in Table IX (where the bispectrum is missing). In addition, we may compare the contour plots of Fig. 1 with those of Fig. 6, associated to Table IX.

The upshot of such a comparison is quite enlightening, as the inclusion of the bispectrum turns out to be very relevant. It significantly enhances the signal of dynamical DE. The bispectrum emerges as a key element to produce the  $3.76\sigma$  c.l. signal (resp.  $3.60\sigma$  c.l.) in favor of the RVM (resp.  $Q_{dm}$ ). Without the inclusion of the bispectrum, the signal gets reduced down to  $2.55\sigma$  c.l. (resp.  $2.49\sigma$  c.l.). A similar decrease is found for the XCDM (from  $3.35\sigma \rightarrow 1.90\sigma$  c.l.) and for  $Q_\Lambda$  ( $2.38\sigma \rightarrow 1.92\sigma$  c.l.).

We could of course invert the argument in a positive way, and say that even without including the bispectrum the dynamical DE signal remains fair enough – it pops up at a level near or above  $2.5\sigma$  c.l. for the favorite models – specially for the RVM model, i.e. the one best motivated from the QFT point of view. It is reassuring to learn, after this very practical and enlightening exercise of numerical cosmology, that the quantitative signs of dynamical vacuum energy are sufficiently robust in our data as to be fairly detectable with the power spectrum alone, only to be subsequently reinforced with the help of the bispectrum.

The main practical conclusion that we can draw from this section is quite remarkable: the potential of the bispectrum for being sensitive to DE effects is perhaps more important than it was suspected until now. As it turns out, its more conventional application as a tool to estimate the bias between the observed galaxy spectrum and the underlying matter power spectrum may now be significantly enlarged, for the bispectrum (as the leading higher-order correction to the power spectrum) might finally reveal itself as an excellent tracer of dynamical DE effects, and ultimately of the fine structure of the DE.

#### D. Deconstruction and reconstruction of the final contour plots

We further complement our analysis by displaying in a graphical way the deconstructed contributions from the different data sets to our final contour plots in Fig. 1, for the specific case of the RVM. One can do similarly for any of the models under consideration. The result is depicted in Fig. 7, where we can assess the detailed deconstruction of the final contours in terms of the partial contours from the different SNIa+BAO+ $H(z)$ +LSS+CMB data sources. A similar deconstruction plot for the XCDM is shown in Fig. 8.

The deconstruction plot for the RVM case is dealt with in Fig. 7, through a series of three plots made at different magnifications. In the third plot of the sequence we can immediately appraise that the BAO+LSS+CMB data subset plays a fundamental role in narrowing down the final physical region of the  $(\Omega_m, \nu)$  parameter space, in which all the remaining parameters have been marginalized over. This deconstruction process also explains in very transparent visual terms why the conclusions that we are presenting here hinge to a large extent on some particularly sensitive components of the data. While there is no doubt that the CMB is a high precision component in the fit, our study demonstrates (both numerically and graphically) that the maximum power of the fit is achieved when it is combined with the wealth of BAO and LSS data points currently available.

To gauge the importance of the BAO+LSS+CMB combination more deeply, in Fig. 9 we try to reconstruct the final RVM plot in Fig. 1 (left) from only these three data sources. First we consider the overlapping regions obtained when we cross the pairs of data sources BAO+LSS, BAO+CMB, LSS+CMB and finally the trio BAO+LSS+CMB (in all cases excluding the SNIa and

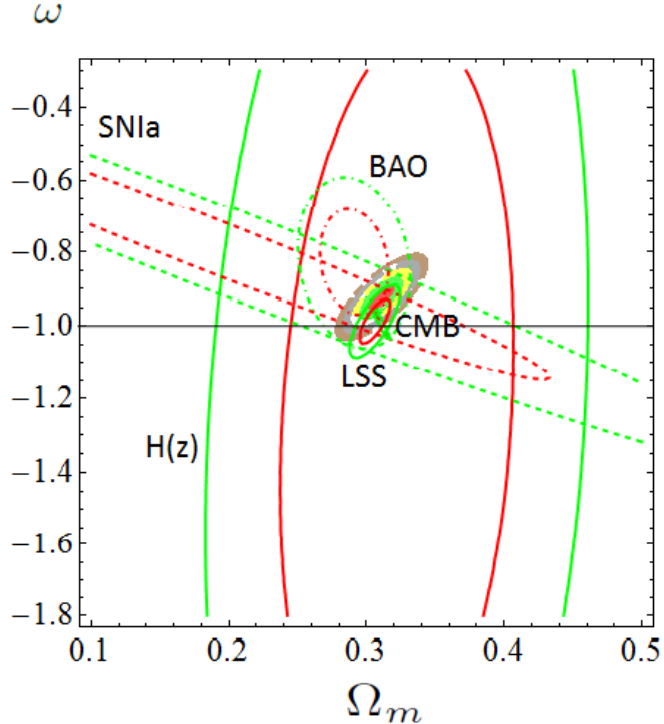


FIG. 8: As in the previous figure, reconstruction of the contour lines for the XCDM from the partial contour plots of the different SNIa+BAO+ $H(z)$ +LSS+CMB data sources.

$H(z)$  data). One can see that neither the BAO+LSS nor the BAO+CMB crossings yield a definite sign for  $\nu$ , despite the obtained regions are very narrow and small as compared to the scale used in Fig. 7 (in which all the data are used). This can also be confirmed numerically from Tables V and VI, where the removal of either the CMB data or the LSS data renders rather poor fits with negative values of  $\Delta\text{AIC}$  and  $\Delta\text{BIC}$ . Remarkably, it is the LSS+CMB combination the one that carries a well-defined, positive, sign for  $\nu$ , as it is seen from the lower-left plot in Fig. 9 and also reconfirmed numerically in Table VII, where  $\Delta\text{AIC}$  and  $\Delta\text{BIC}$  are now both positive and above 6 for the main DVMs (RVM and  $Q_{dm}$ ). As pointed out, the XCDM yields in contrast a bad fit when BAO is not included. Also noticeable is the fact that, in the lower-left plot in Fig. 9, the significance of  $\nu > 0$  (and hence of the dynamical vacuum signature) is “only” at  $2.8\sigma$  c.l. It is precisely when we next intersect the pair LSS+CMB with the BAO data that the signal rockets from  $2.8\sigma$  c.l to  $3.8\sigma$  c.l., the final contours being now those shown in the lower-right plot of Fig. 9. Thus, the crossing with BAO further drags the intersection region upwards in that plane and intensifies the signal of dynamical vacuum by one full additional  $\sigma$ . At the same time the XCDM also improves dramatically since the combined BAO+LSS+CMB data produces essentially the same output as in Table I with all the data.

The outcome of this exercise is clear. For the RVM case, we have checked that the final BAO+LSS+CMB

plot in Fig. 9 is essentially the same as the original RVM plot in Fig. 1 (the leftmost one). In other words, the final RVM contour plot containing the information from all our five data sources can essentially be reconstructed with only the triad BAO+LSS+CMB.

#### E. Testing the influence of alternative data sets

We deem interesting to test the impact of the new BAO measurement extracted from the analysis of the auto-correlation function of the Ly $\alpha$  flux-transmission field using the Sloan Digital Sky Survey Data Release 12 (SDSS-DR12) [168]. It corresponds to the BAO auto-correlation data provided in [93], in which the authors made use of the SDSS-DR11 sample. Apart from an increase of the 15% in the volume sample, in [168] they apply some technical improvements in the methodology over the study of [93]. After all, the differences in the BAO measurements are fully consistent with those found in [93], so we should not expect that the change in the BAO data set is to induce significant differences in our fitting results. But of course putting it to the test is the best way to verify it. The output for this test can be read off Table X, where we can see how the results shown in Table I are modified when we replace the BAO data from [93] with those from the very recent analysis of [168]. But before continuing our comparison of the fitting results in the main analysis shown in Table

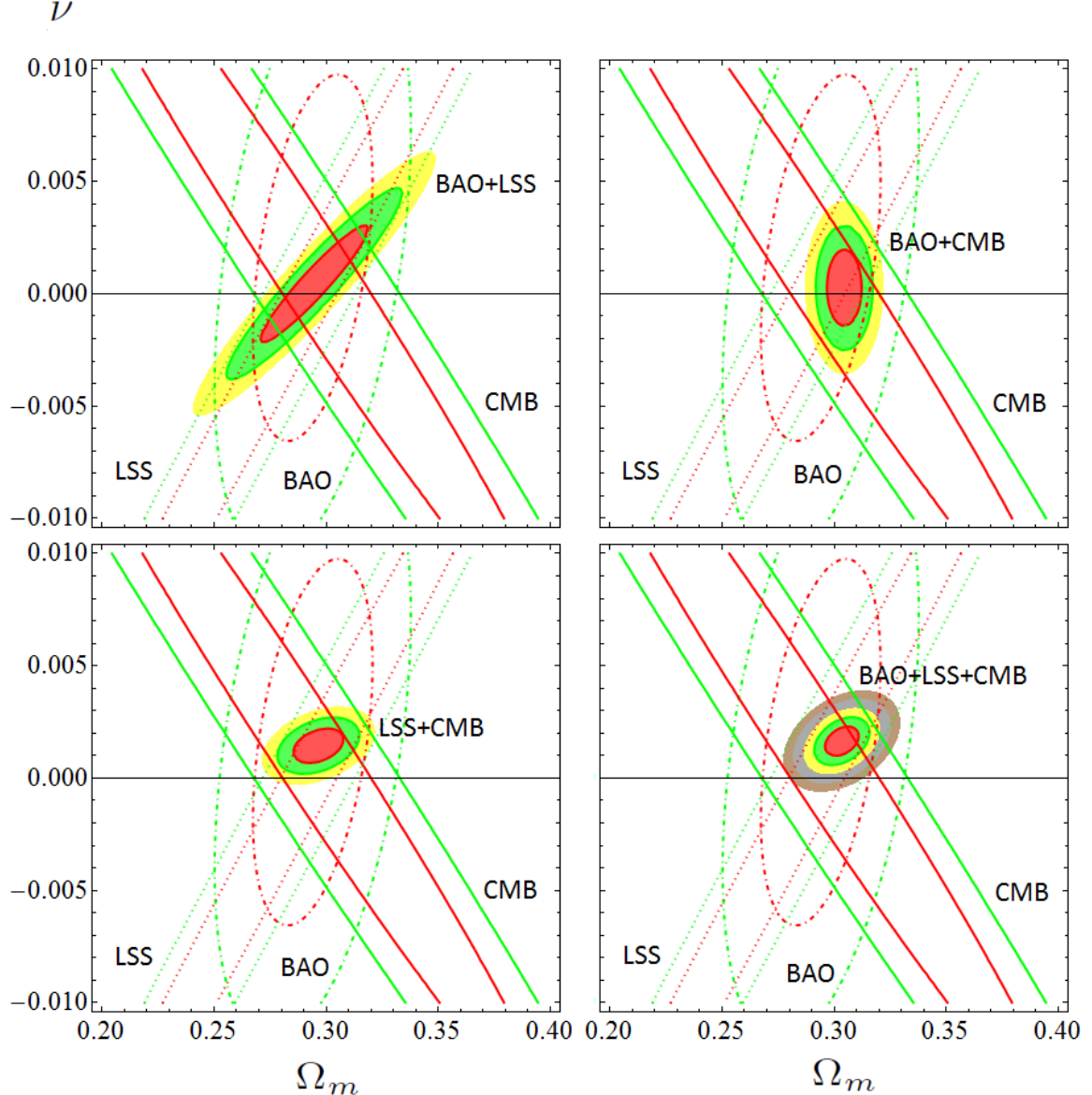


FIG. 9: As in Fig. 7, but considering the effect of only the BAO, LSS and CMB in all the possible combinations: BAO+LSS, BAO+CMB, LSS+CMB and BAO+LSS+CMB. As discussed in the text, it is only when such a triad of observables is combined that we can see a clear  $\sim 4\sigma$  c.l. effect, which is comparable to intersecting the whole set of SNIa+BAO+ $H(z)$ +LSS+CMB data.

I with those in the new Table X, let us make some technical comments concerning the implementation of this change in our data set. In Table I we used the BAO auto-correlation data [93] and the cross-correlation data [169] obtained from the SDSS-DR11. In fact, we used the “combined” (auto+cross-correlation) Ly $\alpha$ F data at the effective redshift  $z = 2.34$  (see data set DS3 for details). In Table X, however, we use 2 data points for the anisotropic BAO estimators,  $D_A/r_s(z_d)$  and  $D_H/r_s(z_d)$  (cf. Appendix B) at  $z = 2.36$  from [169] together with the best-determined combination  $D_H^{0.3}D_M^{0.7}/r_s(r_d)$  from [168] at  $z = 2.33$ , assuming no correlation between the two analyses. Notice that although the data from [169]

and [168] are obtained from overlapping SDSS samples, and they correspond to very close redshifts ( $z = 2.36$  and  $z = 2.33$ , respectively), the cross covariance between the auto and cross-correlation measurements proves to be small for the SDSS-DR11 sample, as explicitly stated in [93, 94]. Thus one may judiciously assume that it is also the case for the SDSS-DR12 sample.

Furthermore, we find reasonable to proceed in this way for the following two reasons: i) the analogous of the cross-correlation analysis of the DR12 sample is not available, and therefore the analysis of the “combined” data for the SDSS-DR12 sample is not possible; ii) we do not have the correlation coefficient between the  $D_A/r_s(z_d)$

| Model               | $h$               | $\omega_b = \Omega_b h^2$ | $n_s$             | $\Omega_m$        | $\nu_i$               | $w$                | $\chi^2_{\min}/dof$ | $\Delta\text{AIC}$ | $\Delta\text{BIC}$ |
|---------------------|-------------------|---------------------------|-------------------|-------------------|-----------------------|--------------------|---------------------|--------------------|--------------------|
| $\Lambda\text{CDM}$ | $0.692 \pm 0.004$ | $0.02252 \pm 0.00013$     | $0.974 \pm 0.004$ | $0.296 \pm 0.004$ | -                     | -1                 | 83.14/85            | -                  | -                  |
| $\text{XCDM}$       | $0.671 \pm 0.007$ | $0.02262 \pm 0.00014$     | $0.976 \pm 0.004$ | $0.312 \pm 0.007$ | -                     | $-0.922 \pm 0.023$ | 71.98/84            | 8.92               | 6.66               |
| $\text{RVM}$        | $0.677 \pm 0.005$ | $0.02231 \pm 0.00014$     | $0.965 \pm 0.004$ | $0.303 \pm 0.005$ | $0.00159 \pm 0.00042$ | -1                 | 67.72/84            | 13.18              | 10.92              |
| $Q_{dm}$            | $0.678 \pm 0.005$ | $0.02229 \pm 0.00015$     | $0.965 \pm 0.004$ | $0.303 \pm 0.005$ | $0.00218 \pm 0.00059$ | -1                 | 68.47/84            | 12.43              | 10.17              |
| $Q_\Lambda$         | $0.691 \pm 0.004$ | $0.02230 \pm 0.00016$     | $0.966 \pm 0.005$ | $0.298 \pm 0.005$ | $0.00602 \pm 0.00253$ | -1                 | 77.46/84            | 3.45               | 1.18               |

TABLE X: As in Table I, but replacing the BAO data of [93] with the BAO data from [168] and [169].

| Model               | $h$               | $\omega_b = \Omega_b h^2$ | $n_s$             | $\Omega_m$        | $\nu_i$               | $w$                | $\chi^2_{\min}/dof$ | $\Delta\text{AIC}$ | $\Delta\text{BIC}$ |
|---------------------|-------------------|---------------------------|-------------------|-------------------|-----------------------|--------------------|---------------------|--------------------|--------------------|
| $\Lambda\text{CDM}$ | $0.693 \pm 0.003$ | $0.02255 \pm 0.00013$     | $0.976 \pm 0.003$ | $0.294 \pm 0.004$ | -                     | -1                 | 90.44/84            | -                  | -                  |
| $\text{XCDM}$       | $0.670 \pm 0.007$ | $0.02264 \pm 0.00014$     | $0.977 \pm 0.004$ | $0.312 \pm 0.007$ | -                     | $-0.916 \pm 0.021$ | 74.91/83            | 13.23              | 11.04              |
| $\text{RVM}$        | $0.676 \pm 0.005$ | $0.02231 \pm 0.00014$     | $0.965 \pm 0.004$ | $0.303 \pm 0.005$ | $0.00165 \pm 0.00038$ | -1                 | 70.32/83            | 17.82              | 15.63              |
| $Q_{dm}$            | $0.677 \pm 0.005$ | $0.02229 \pm 0.00015$     | $0.964 \pm 0.004$ | $0.303 \pm 0.005$ | $0.00228 \pm 0.00054$ | -1                 | 71.19/83            | 16.95              | 14.76              |
| $Q_\Lambda$         | $0.692 \pm 0.004$ | $0.02229 \pm 0.00016$     | $0.966 \pm 0.005$ | $0.297 \pm 0.004$ | $0.00671 \pm 0.00246$ | -1                 | 83.08/83            | 5.06               | 2.87               |

TABLE XI: As in Table I, but making use of the original LSS data of [170], instead of that from the revised version [92] (cf. Tables 5 of these two references). In the latter, the uncertainty of the  $f(z = 0.32)\sigma_8(z = 0.32)$  (resp.  $f(z = 0.57)\sigma_8(z = 0.57)$ ) increases  $\sim 8\%$  (resp.  $\sim 26\%$ ) with respect to the former. See the discussion in the text.

and  $D_H/r_s(z_d)$  data points of [168], so we have considered more appropriate to follow these authors in using the aforementioned combination  $D_H^{0.3}D_M^{0.7}/r_s(r_d)$ , in which the powers 0.3 and 0.7 have been optimized in order to minimize the variance of the product (see [168] for details). We have also checked that if in the above implemented change we would only use the data from [168], but not that from [169], the results stand essentially the same. For example, for the RVM we find  $\nu = 0.00160 \pm 0.00042$  and  $(\Delta\text{AIC}, \Delta\text{BIC}) = (13.33, 11.10)$ , which favour slightly more the RVM against the  $\Lambda\text{CDM}$  in comparison to the result in Table X.

Notwithstanding the above alternative approach, we have opted from the very beginning for presenting our main results as they appear in our Table I, which is based on the “combined” LyaF DR11 data mentioned before. In this way we fully incorporate the small correlations between the auto and cross-correlation data, which is the most advisable option. Moreover, as we have mentioned before, the changes in the auto-correlation measurements extracted from the DR12 with respect to the DR11 ones are not significant, so no big difference should be expected between Tables I and X. What we have done here is to check it explicitly. The fitting results from Table X appear to favor all the dynamical vacuum models slightly more than those in Table I, so the latter (our main table) is actually a bit conservative. This feature also applies to the XCDM and CPL parametrizations. The differences, however, are not very significant in any of the cases. If we should quote them here for, say, the RVM (resp.  $Q_{dm}$ ), we find that the confidence level of the dynamical DE signature has increased now from  $3.76\sigma$  (resp.  $3.60\sigma$ ) to  $3.78\sigma$  (resp.  $3.69\sigma$ ); and the respective differences in the values of the Akaike and Bayesian information criteria with respect to the  $\Lambda\text{CDM}$ ,  $(\Delta\text{AIC}, \Delta\text{BIC})$ , have also correspondingly increased, viz. from  $(12.91, 10.67)$  to  $(13.18, 10.92)$  in the RVM case, and from  $(12.13, 9.89)$  to  $(12.43, 10.17)$  in the  $Q_{dm}$  case. The fact that the differences with respect to our main table are small, and the

confirmation that the new results remain well anchored to the high significance levels already attained in Table I, already speaks up both of the robustness of the current analysis and of the significance of the reported results.

We finish this section with some comments on the differences between the current results and the ones advanced in an earlier version of the Letter-type presentation of them in [68], specifically in version v2 of it. In Table XI of this section we exhibit the fitting outputs obtained in that previous version. The differences with respect to the updated ones, i.e. those recorded in the current Table I, are basically caused by the change in the uncertainties of the LSS data presented in [170] as compared to the more recent ones in [92]. While the central values of the LSS observations quoted in [92] are the same as those in the previous version of their work [170], the errors in the new version are slightly larger than those in the older. It is not clear to us the reason for it, we were unable to trace a justification for that change in [92]. We nevertheless find a valuable numerical exercise to check the impact of such a difference on our results, as this can be used to test the reaction of our analysis to a change in the errors on these significant data sources.

In Ref. [92], the uncertainties affecting the two LSS data points  $f(z_i)\sigma_8(z_i)$  at  $z_i = 0.32$  and  $z_i = 0.57$  increased about  $\sim 8\%$  and  $\sim 26\%$ , respectively, with respect to the old version [170]. The change is not such a trifle, at least a priori, as it induces a non-negligible increase of the uncertainties for the various cosmological parameters. For example, the comparison of the results for the RVM in Tables I and XI tells us that by using the LSS data from [92], instead of that from [170], the  $\nu$  parameter departs from 0 at  $3.76\sigma$  c.l. whereas in the former case the departure is at  $4.34\sigma$  c.l. In both cases, a  $\sim 4\sigma$  c.l. signal seems to be secured, but of course there is some difference, which we have been able to quantify. A similar conclusion applies to the other models under study, as we have checked.

At the end of the day the main conclusion is rewarding:

in spite of some changes in the uncertainties of the BOSS LSS+BAO data in the above mentioned two versions of the same work, the signature on dynamical DE stands upright. We devote the next subsection to check if such a signature can also be grasped to some extent by using one of the most well-known quintessence models in the market: the Peebles & Ratra model [31].

#### F. Dynamical dark energy and the $\phi$ CDM

A natural question that can be formulated is whether the traditional class of  $\phi$ CDM models, which have a well-defined local Lagrangian description and in which the DE is described in terms of a scalar field  $\phi$  with some standard form for its potential  $V(\phi)$ , are also capable of capturing clear signs of dynamical DE using the same set of cosmological observations used for fitting the DVMs. The traditional quintessence and phantom scalar fields [31–38] mentioned in the introduction are included in the  $\phi$ CDM class. If we take the scalar field  $\phi$  dimensionless, its energy density and pressure are given by

$$\rho_\phi = \frac{M_P^2}{16\pi} \left[ \frac{\dot{\phi}^2}{2} + V(\phi) \right], \quad p_\phi = \frac{M_P^2}{16\pi} \left[ \frac{\dot{\phi}^2}{2} - V(\phi) \right]. \quad (95)$$

We cannot advance an universal solution to the above question, as the result depends, of course, on the particular structure of the potential. Needless to say, not all potentials are equally suitable. As a representative potential we borrow the original Peebles & Ratra (PR) form [31]:

$$V(\phi) = \frac{1}{2} \kappa M_P^2 \phi^{-\alpha}, \quad (96)$$

in which  $\kappa$  and  $\alpha$  are dimensionless parameters and  $M_P = 1/\sqrt{G} = 1.2211 \times 10^{19}$  GeV is the Planck mass (in natural units). The parameters  $\kappa$  and  $\alpha$  are to be determined in our fit to the overall cosmological data. A recent analysis of this model was performed by us in [69]. However, we have to repeat the fitting analysis here since we are now using more updated observations, as explained in the data set items DS1-DS6 listed in Sect. III A, and of course we wish to compare all models to the same set of observations. The new fitting results for the PR model are presented in Table XII. These are most conveniently expressed by means of the following 5-dimensional fitting vector (see [69] for details):

$$\vec{p}_{\phi\text{CDM}} = (\omega_m, \omega_b, n_s, \alpha, \bar{\kappa}), \quad (97)$$

in which we have traded the original parameter  $\kappa$  in the PR potential for  $\bar{\kappa} \equiv \kappa M_P^2 / \zeta^2$ . Recall the previously defined parameter  $\zeta \equiv 1 \text{ Km/s/Mpc} = 2.1332 \times 10^{-44} \text{ GeV}$  (in natural units). Note that the fitting vector (97) has also 5 parameters (one more than the  $\Lambda$ CDM) but equal number to any of the DVMs, see Eq. (69), and the XCDM. Therefore the number of parameters is equalized

for all the DE models under consideration, except for the CPL parametrization, which has one more parameter and as a result the fitting errors are larger.

The motivation for the PR potential is well described in the original paper [31]. First of all let us recall that it admits tracker solutions of the field equations for  $\alpha > 0$ , which is of course very convenient. We can see from Table XII that we have determined  $\alpha$  as being indeed positive at more than  $3\sigma$  c.l.

Both in the radiation-dominated (RD) and matter-dominated (MD) epochs the equation of state (EoS) of the scalar field remains stationary since the Hubble function in these epochs is dominated by the usual behavior  $\rho \propto a^{-n}$  of the matter component, with  $n = 4$  and  $n = 3$  in the respective periods. As a result it is possible to find power-law solutions  $\phi \propto t^p$  ( $t$  being the cosmic time) of the Klein-Gordon equation with PR potential (96) in the FLRW metric,  $\ddot{\phi} + 3H\dot{\phi} + dV/d\phi = 0$ . This allows to establish the initial conditions for the integration of such an equation [69]. Finally, with the help of (95) we can derive after some calculations a very compact form for the EoS [69]:

$$w_\phi = \frac{p_\phi}{\rho_\phi} = -1 + \frac{\alpha n}{3(2 + \alpha)}. \quad (98)$$

This stationary form, valid only in the pure RD and MD regimes, was expected and it perfectly adapts to the well-known result that holds for general tracking solutions [36]. The more complicated behavior of the EoS, namely the time-evolving  $w_\phi(a)$  that interpolates between the RD and MD epochs, and accounts for the transition from the MD to the DE epoch, obviously requires a numerical integration of the Klein-Gordon equation with the PR potential. We have performed such an integration following the method of Ref. [69] and using the fitting values of Table XII. The plot of  $w_\phi(z)$  in terms of the redshift near our time is shown in Fig. 5, side by side with the (constant) EoS value of the XCDM parametrization and the evolving one of the CPL parametrization, see Sect. II D. The behavior of the curves in Fig. 5 shows that the quintessence-like behavior is sustained until the present epoch. The numerically computed EoS value reads:

$$w_\phi(z = 0) = -0.936 \pm 0.019. \quad (99)$$

This result deviates from  $-1$  by  $3.37\sigma$  c.l. and therefore points to quintessence behavior at such a confidence level. Comparing with the EoS of the XCDM parametrization in Table I, whose departure from  $-1$  is at  $3.35\sigma$  c.l. we discover that the agreement with the  $\phi$ CDM prediction is surprisingly very good: the current EoS values in each case are very close and both resonate in predicting quintessence-like behavior at  $\gtrsim 3.3\sigma$  c.l.

We point out that in the present case the parameter  $h$  is not a fitting parameter, as the Hubble function can be computed only after first numerically solving the Klein-Gordon equation in the FLRW metric. Thus, for the

| Model            | $\omega_m = \Omega_m h^2$ | $\omega_b = \Omega_b h^2$ | $n_s$             | $\alpha$          | $\bar{\kappa}$               | $\chi^2_{\min}/dof$ | $\Delta\text{AIC}$ | $\Delta\text{BIC}$ |
|------------------|---------------------------|---------------------------|-------------------|-------------------|------------------------------|---------------------|--------------------|--------------------|
| $\phi\text{CDM}$ | $0.1405 \pm 0.0008$       | $0.02263 \pm 0.00014$     | $0.976 \pm 0.004$ | $0.202 \pm 0.065$ | $(32.7 \pm 1.2) \times 10^3$ | 74.08/84            | 8.55               | 6.31               |

TABLE XII: The best-fit values for the parameter fitting vector (97) of the  $\phi$ CDM model with Peebles & Ratra potential (96). We use the same cosmological data set as in Table I. The specific fitting parameters for  $\phi$ CDM are  $\bar{\kappa}$  and  $\alpha$ . The total number of independent parameters is 5, see Eq. (97) – one more than in the  $\Lambda$ CDM, as in the DVMs and XCDM. Using the best-fit values of this table and the overall covariance matrix derived from our fit, we obtain:  $h = 0.671 \pm 0.006$  and  $\Omega_m = 0.312 \pm 0.006$ , which allows direct comparison with Table I. We find  $\gtrsim 3\sigma$  c.l. evidence in favor of  $\alpha > 0$ . In terms of the EoS of  $\phi$  at present, the DE behavior appears quintessence-like at  $\sim 3.3\sigma$  c.l. since  $w_\phi(z=0) = -0.936 \pm 0.019$ , see Eq. (99).

$\phi$ CDM it proves more convenient to fit the parameter  $\omega_m = \Omega_m h^2$  rather than  $\Omega_m$  and  $h$  separately. Recall that  $3H^2 = 8\pi G(\rho_\phi + \rho_m)$ , where  $\rho_\phi$  is given in Eq. (95) and  $\rho_m = \rho_{c0}\Omega_m a^{-3} = (3 \times 10^4/8\pi G)\zeta^2 \omega_m a^{-3}$  is the conserved matter component. In the matter-dominated epoch, one can show that [69]

$$\bar{H}^2(a) = \frac{\bar{\kappa} \phi^{-\alpha}(a) + 1.2 \times 10^5 \omega_m a^{-3}}{12 - a^2 \phi'^2(a)}, \quad (100)$$

where we have defined  $\bar{H} = H/\zeta$ , and used  $\dot{\phi} = aH\phi'(a)$ . It is clear that Eq. (100) is a numerical expression since  $\phi(a)$  and  $\phi'(a)$  are known only after solving by numerical methods the Klein-Gordon equation in the FLRW metric with Peebles & Ratra potential. In terms of the scale factor variable, the Klein-Gordon equation with that potential takes on the form

$$\phi'' + \phi' \left( \frac{\bar{H}'}{\bar{H}} + \frac{4}{a} \right) - \frac{\alpha}{2} \frac{\bar{\kappa} \phi^{-(\alpha+1)}}{(a\bar{H})^2} = 0. \quad (101)$$

The initial conditions for  $\phi(a)$  and  $\phi'(a)$  are fixed as explained above, see [69] for details. Finally, we can determine  $h \equiv \bar{H}(a=1)/100$  and  $\Omega_m = \omega_m/h^2$ . Using the posterior distribution of the analysis in Table XII we find (as quoted in the table caption itself):

$$h = 0.671 \pm 0.006, \quad \Omega_m = \frac{\omega_m}{h^2} = 0.312 \pm 0.006. \quad (102)$$

They are very close to those for the XCDM in Table I.

The likelihood contours for the PR model in the  $(\Omega_m, \alpha)$ -plane are depicted in Fig. 10. They clearly point to a nonvanishing and positive value of  $\alpha$  at  $\sim 3\sigma$  c.l. Bearing also in mind the EoS value (99), the two quantities consistently signal quintessence behavior at more than  $3\sigma$  c.l. The numerical details are furnished in Table XII. These results, along with those from our previous paper [69] (based on a slightly different data set), apparently are unprecedented in the literature. Other studies had previously considered the PR-potential in the light of older or more limited cosmological data sets, see e.g. [171–173], but they did not find comparable signs of dynamical DE as the ones presented here.

If we compare the above results for the PR model with the DVMs we see that they are compatible and all of them pointing towards the same direction. For the DVMs, being vacuum models, the EoS is of course identically  $-1$ , but since the vacuum is dynamical the

quintessence or phantom-like effective behavior shows up here through the sign of the  $\nu_i$  parameters. Take e.g. the RVM, for which  $\nu = 0.00158 \pm 0.00042$ . This value is positive at  $3.76\sigma$  c.l. and therefore the vacuum energy is larger in the past ( $a \rightarrow 0$ ) and decreases towards the future (increasing  $a$ ), see Eq. (18). It means that the RVM behaves effectively as quintessence. The same occurs with models  $Q_{dm}$  and  $Q_\Lambda$  with different levels of significance. We point out, however, that in contrast to true quintessence the vacuum density of the RVM while is evolving from a large value in the past (always well below that of the matter density) it does not asymptote to zero in the remote future. The limiting value for  $a \rightarrow \infty$  reads

$$\rho_\Lambda \rightarrow \rho_{\Lambda 0} - \frac{\nu \rho_{m0}}{1 - \nu}. \quad (103)$$

A similar result holds for model  $Q_{dm}$ . In contrast, for model  $Q_\Lambda$  we have  $\rho_\Lambda \rightarrow 0$  in the future (for  $\nu_\Lambda > 0$ ). All these results ensue immediately from Eqs. (18)–(20).

Other  $\phi$ CDM models can be tested, of course, but shall not be addressed here. It suffices to say that the required consistency of any scalar field model with BBN bounds and the existence of the attractor solution is a crucial condition that further motivates the Peebles & Ratra potential (96). Compared, say to the exponential potential,  $V(\phi) = V_0 e^{-\lambda \phi/\bar{M}_P}$ , the problem is that the latter is incompatible with BBN (if  $\lambda$  is too small) or cannot become sizeable enough to cause accelerated expansion at present (if  $\lambda$  is too large) [32, 174]. This situation can be amended with a sum of two exponentials with different values of  $\lambda$  [175], but is not so well motivated since involves more parameters, and of course the fitting results would then worsen in statistical significance. For other interesting possibilities involving exponential potential with additional features, see [176–178].

All in all the signs of dynamical DE conspicuously perceived with the use of different models and parametrizations are quite evident. But we should make clear once more that they are only at reach when the crucial triplet of BAO+LSS+CMB data are included in the fitting analysis of these models. Let us stay alert to the evolution of the future cosmological observations. Other possibilities qualitatively very different (e.g. scale invariant theories [179]) are, in principle, also compatible with observations, but need more phenomenological test. In such a context the traditional CC appears as related to the properties of scale invariance of the empty space and as a

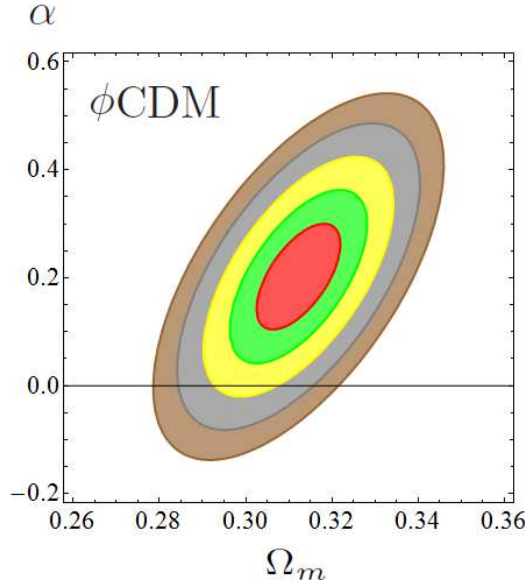


FIG. 10: Likelihood contours for the  $\phi$ CDM model in the  $(\Omega_m, \alpha)$ -plane after marginalizing over the remaining parameters (cf. Table XII). The various contours correspond to  $1\sigma$ ,  $2\sigma$ ,  $3\sigma$ ,  $4\sigma$  and  $5\sigma$  c.l. The central value  $(0.312, 0.202)$  is  $\sim 3\sigma$  away from the  $\Lambda$ CDM result  $(\alpha = 0)$ . Compare with the XCDM contour plots in Fig. 3. Upon marginalizing also with respect to  $\Omega_m$ , both for the  $\phi$ CDM and XCDM we find evidence of dynamical DE at  $> 3\sigma$  c.l. Confronting also with the DVMs contours, specially with the RVM one in Fig. 1, we find that all of them signal dynamical DE with quintessence-like behavior. For the RVM, however, the level of evidence is closer to  $\sim 4\sigma$ .

result a new dynamical contribution appears that mimics the DE and replaces the role of the rigid  $\Lambda$  in Einstein's equations. Or, in a very different vein, dynamical vacuum energy could be the result of a nonperturbative approach to strong field interactions relying on quasiparticles, which results in a variable vacuum energy that depends on the state of the system [180].

In one way or another, the dynamical DE germ that seems to be imprinted in the data appears at play and can possibly be unveiled using a variety of independent frameworks. We are, of course, not yet claiming incontestable evidence of dynamical vacuum energy or, in general, of dynamical DE, but the improvement of the overall fit to the cosmological data under this hypothesis starts to be rampant. We are eager to hear of new observational data, see for instance [73]. At the moment, the best fit of the data implying dynamical DE signature is fulfilled by means of the RVM and reaches  $\sim 4\sigma$  c.l. Ongoing work will soon clarify if the most successful DVMs being considered here can further improve the description of the cosmological data by allowing a small departure of its equation of state from the strict vacuum setting [181].

## VII. CONCLUSIONS

To conclude, in this work we aimed at testing cosmological physics beyond the standard or concordance

$\Lambda$ CDM model, built upon a rigid cosmological constant. We have presented a comprehensive study on the possibility that the global cosmological observations can be better described in terms of vacuum models equipped with a dynamical component that evolves with the cosmic expansion. This should be considered a natural possibility in the context of quantum field theory (QFT) in a curved background. Our task focused on three dynamical vacuum models (DVMs): the running vacuum model (RVM) along with two more phenomenological models, denoted  $Q_{dm}$  and  $Q_\Lambda$ —see equations (11)–(14). At the same time, we have compared the performance of these models with the general XCDM and CPL parametrizations as well as with concrete scalar field models ( $\phi$ CDM), such as the original Peebles & Ratra model. We have fitted all these models and parametrizations to the same set of cosmological data based on the observables SNIa+BAO+ $H(z)$ +LSS+CMB. Needless to say, we have fitted the  $\Lambda$ CDM to the same data too. The remarkable outcome of this investigation is that in all the considered cases we find an improvement of the description of the cosmological data in comparison to the  $\Lambda$ CDM. Our conclusion is that there are significant signs of dynamical DE in the current data, which we have been able to capture at different intensities with the various analyzed models and parametrizations.

The model that renders the best fit to the overall SNIa+BAO+ $H(z)$ +LSS+CMB data is the RVM, which emerges as a serious alternative candidate for the description of the current state of the universe in accelerated expansion. The RVM is the only DVM among those that we have analyzed here that has a close connection with the possible quantum effects on the effective action of QFT in curved spacetime, see [12, 51, 52] and references therein. There were previous phenomenological studies that hinted in different degrees at the possibility that the RVM could fit the data similarly as the  $\Lambda$ CDM, see e.g. the relatively recent papers [55–58], as well as the more recent ones [59–65], including the closely related series [66–69].

Previous analyses by other authors on the more phenomenological DVMs, i.e. models  $Q_{dm}$  and  $Q_\Lambda$ , are available in the literature, see e.g. [82–84]. We have discussed the comparison of our results with theirs and have pointed out some differences with [82] concerning model  $Q_\Lambda$ . We find that this model is far less competitive as compared to the RVM and  $Q_{dm}$ .

As indicated in the introduction, the main results of this paper have been advanced in the companion Letter [68]. In the current work we have presented some of the bulk details of the analysis and we have updated the results. To our knowledge there is no devoted work comparable in scope to the one presented here. The significantly enhanced level of evidence on dynamical DE achieved with the DVMs, the XCDM and CPL parametrizations, as well with specific scalar field models ( $\phi$ CDM), is unprecedented in the literature (to the best of our knowledge), all the more if we

bear in mind the diversified amount of data used. Our study employed the largest, updated and self-consistent SNIa+BAO+ $H(z)$ +LSS+CMB data set of cosmological observations currently available. The “deconstruction analysis” of the contour plots in Sect. VID has revealed with pristine clarity which are the most decisive data ingredients responsible for the dynamical vacuum signal. We have identified that the BAO+LSS+CMB components play a momentous role in the overall fit, as they are responsible for the main effects uncovered here. The impact of the SNIa and  $H(z)$  observables appears to be more moderate. While the SNIa data were of course essential for the detection of a nonvanishing value of  $\Lambda$ , these data do not seem to have sufficient sensitivity (at present) for the next-to-leading step, which is to unveil the possible dynamics of  $\Lambda$ . The sensitivity for that seems to be reserved for the LSS, BAO and CMB data.

The crossing of the LSS and CMB data seems to be most sensitive to the dynamical vacuum signature, and the simultaneous concurrence of the BAO part enhances even more the effect. Recently the BAO+LSS components have been enriched by more accurate contributions, which have helped to augment the signs of vacuum dynamics. As we have proven here, in their absence (or with insufficient data of this sort) the signal appears blurred or invisible, as it was until very recently. In addition, we have demonstrated that including the leading higher-order correlator data in the spectral analysis, namely the bispectrum data, is instrumental for distilling the maximum strength of the dynamical DE signal.

At the end of the day it has been possible to improve the significance of the hints of dynamical vacuum energy, which were first harvested at a confidence level of “only”  $\gtrsim 2\sigma$  in a previous work [67], reaching up to about  $\sim 4\sigma$  here. Our results are consistent with those found in [66] for other type of dynamical models. Overall, the signature of vacuum dynamics seems to be considerably supported by the current cosmological observations. Interestingly enough, we have shown that is also attainable through a well-known example of  $\phi$ CDM model endowed of realistic ingredients, the Peebles & Ratra (PR) model, recently revisited in [69]. With the updated data we find now that it still renders a dynamical signature comparable to the XCDM parametrization. The upshot is that either with the XCDM or the PR model we are able to exclude the absence of vacuum dynamics ( $\Lambda$ CDM) at  $> 3.3\sigma$  c.l. Noteworthy, this result can be surpassed with the main DVMs (RVM and  $Q_{dm}$ ), with which we are able to find a c.l. of up to  $3.8\sigma$  and  $3.6\sigma$ , respectively. Taking, however, into account that the details of the fit depend on small variations caused by the use of different data sources and computational codes, we can assert that the DE dynamics for the main DVMs is secured at a confidence level in between  $3.6-4.3\sigma$  throughout our analysis. These results are, in addition, backed up with compelling  $\Delta$ AIC and  $\Delta$ BIC values of the Akaike and Bayesian information criteria, both being firmly anchored in the high ranges 12–18 and 10–15 respectively, thereby ensuring

very strong evidence (according to the conventional usage of these criteria [163]) of the claimed dynamical effects.

We have also found that the signs of dynamical DE correspond to an effective quintessence behavior, in which the vacuum energy decreases with the expansion. Whether or not the ultimate reason for such a signal stems from the properties of the quantum vacuum or from some particular quintessence model, it is difficult to say at this point. Once more we can only say that, quantitatively, the best description is granted in terms of the RVM and the  $Q_{dm}$ , and that the results are consistent with the traces of dynamical DE that can be found with the help of the XCDM and CPL parametrizations, as well as with a true quintessence model [31]. In all five cases we find unmistakable signs of DE physics beyond the  $\Lambda$ CDM.

In our work we have also clarified why previous fitting analyses based e.g. on the simple XCDM parametrization, such as the ones by the Planck 2015 [5] and BOSS collaborations [94], did entirely miss any hint of dynamical vacuum signature. Basically, the reason stems from not using a sufficiently rich sample of the most crucial data, namely BAO and LSS, some of which were unavailable a few years ago, and could not be subsequently combined with the CMB data. The situation has now changed, as we have shown, because a wide span of sensitive data is presently at disposal. It is timely to mention at this point that a significant level of evidence on dynamical DE at  $\sim 3.5\sigma$  c.l. has recently been reported from non-parametric studies of the observational data on the DE, which aim at a model-independent result [73]. The findings of their analysis are compatible with the ones we have disclosed here and in our recent papers. Finally, it may prove interesting to note that according to a forecast of the Dark Energy Spectroscopic Instrument (DESI) survey [182] the dynamics of the dark energy could eventually be detected at  $7\sigma$  c.l. [183]. It is thus encouraging to see that we are on the way to have at disposal the necessary technological instruments that will enable to test the dynamics of the DE with a high level of precision, certainly sufficient for unraveling the kind of effects that we are reporting here, if they are finally reconfirmed.

Needless to say, statistical evidence conventionally starts at  $5\sigma$  c.l. and we will have to wait for updated observations to see if such a level of significance can be achieved in the future. In the meantime, the possible dynamical character of the cosmic vacuum, as suggested by the present study, is pretty high. It should be welcome since a dynamical vacuum gives more hope for an eventual solution of the old cosmological constant problem, perhaps the toughest problem of fundamental physics [7].

Let us close this work by noting that if the results presented here would be consolidated in future investigations, the longstanding – hundred years hitherto! – rigid status of the “cosmological constant” in Einstein’s equations, in its traditionally accepted role for the optimal description of the cosmological data, would be seriously disputable.

## Acknowledgments

JS acknowledges the hospitality and support received from the Institute for Advanced Study at the Nanyang Technological University in Singapore while part of this work was being accomplished. We thank Gil-Marín for useful observations on BAO estimators. JS and AGV are specially grateful to S. Basilakos for the recent collaboration on previous related works and for valuable comments and discussions. JS has been supported by FPA2013-46570 (MICINN), Consolider grant CSD2007-00042 (CPAN) and by 2014-SGR-104 (Generalitat de Catalunya); AGV acknowledges the support of an APIF grant of the U. Barcelona. We are also partially supported by MDM-2014-0369 (ICCUB).

## Appendix A: Cosmological constant problem and running vacuum

It is well-known that the usual calculations of the zero-point energy (ZPE) in quantum field theory (QFT) and those from spontaneous symmetry breaking (SSB) lead to large contributions to the vacuum energy density of the order of the fourth power of the particle masses, see the Introduction and references therein. For example, at one loop the renormalized value of the ZPE for a scalar field of mass  $m$  is (see e.g. [12])

$$\rho_{\text{vac}}^{(1)} = \rho_{\Lambda}(\mu) + \frac{m^4}{64\pi^2} \left( \ln \frac{m^2}{\mu^2} + C_{\text{vac}} \right). \quad (\text{A1})$$

It is a pure quantum effect, and since it is a one-loop contribution it would be proportional to  $\hbar$ , if it were to be expressed in conventional units. At higher orders it would contain more terms, each one with a power of  $\hbar$  given by the number of loops at that order. The constant  $C_{\text{vac}}$  is finite. Usually the calculation is carried out in dimensional regularization and one splits the bare cosmological constant (CC) term sitting in the original Einstein-Hilbert action as  $\rho_{\Lambda}^{(\text{b})} = \rho_{\Lambda}(\mu) + \delta\rho_{\Lambda}$ , i.e. into a renormalized part plus a counterterm. The latter is chosen to cancel the pole of the unrenormalized effective action and carries an arbitrary finite part that depends on the renormalization prescription. The above result is not only valid in flat spacetime but also in curved spacetime [12], although in this case it is accompanied with a pleiad of purely geometric terms given by a linear combination of the curvature  $R$  and the higher derivative contributions  $R^2$ ,  $R_{\mu\nu}^2$  etc [184].

The SSB part of the vacuum energy density, associated to the Higgs mechanism [15] in the standard model (SM) of particle physics, is also as big as the ZPE one. Even at a purely classical level such a contribution, written in terms of two measurable quantities,  $M_H \simeq 125$  GeV (the physically measured Higgs mass [185]) and  $G_F \simeq 1.166 \times 10^{-5}$  GeV $^{-2}$  (Fermi's constant), is incommensurably large for the cosmological standards of our

(post-inflationary) universe[12]:

$$\langle V \rangle = -\frac{1}{8\sqrt{2}} \frac{M_H^2}{G_F} \simeq -1.2 \times 10^8 \text{ GeV}^4. \quad (\text{A2})$$

To this effect one still has to add, of course, the quantum corrections to the effective potential, which again would be proportional to powers of  $\hbar$  in accordance to the number of loops. The Higgs field would also contribute to the one-loop ZPE value an amount of order  $M_H^4 \sim 10^9$  GeV $^4$ . Moreover, one has to sum over the contributions from all the particles. The problem with Eq. (A1) is that the component  $\propto m^4$  is very large (against the measured value of  $\rho_{\Lambda} \sim 10^{-47}$  GeV $^4$  in cosmology) for virtually any particle of the SM (except perhaps for a very light neutrino of order of a milli eV), and this enforces a preposterous fine tuning of all the contributions with the renormalized part. Whether the effects (A1) and (A2) are formal or "real" is not clear at present. It is generally acknowledged that the solution of the cosmological constant problem (CCP) is not presently known. In any case these terms are not phenomenologically admissible unless there is a large cancellation among them (the aforementioned fine tuning), which is deemed impossible. This conundrum ultimately lies at the root of the old CCP [7].

Actually, since none of the terms on the r.h.s. of (A1) is physically meaningful by itself, it suggests that the problem might be formal and its interpretation could be different from the usual one, see [12, 76]. If the offending terms could be renormalized away within a consistent framework, the genuinely physical vacuum contributions related to the cosmological expanding background should also be purely geometric and of quantum nature, for only in this way could they be as small as are currently observed. This should be possible if the common contributions with flat, Minkowskian, spacetime could be subtracted from the curved spacetime result, since they are actually responsible for the large  $\sim m^4$  contributions. This idea has been expressed in different ways in the literature [12, 53, 76], see also [54, 186, 187].

Although a general action formulation is not available at present, one expects that the leading effects for the FLRW cosmological background, free from the above mentioned contributions, can be extracted from a generic renormalization group (RG) equation of the form

$$\frac{d\rho_{\Lambda}}{d\ln\mu^2} = \frac{1}{(4\pi)^2} \sum_i \left[ a_i M_i^2 \mu^2 + b_i \mu^4 + c_i \frac{\mu^6}{M_i^2} + \dots \right]. \quad (\text{A3})$$

This equation describes the rate of change of  $\rho_{\Lambda}$  with the running scale  $\mu$  – see [12] for a review and a comprehensive list of references. To make contact with physics, the running scale  $\mu$  is put in correspondence with a characteristic energy or momentum. This is the standard practice in particle physics, but in cosmology it is not so straightforward. It is however natural to associate it with a cosmic variable  $\zeta(t)$  closely connected to the

FLRW metric. A most reasonable ansatz is the Hubble rate,  $\zeta = H$ , which has natural dimension of energy-momentum. Thus we set  $\mu = H$ , and this setting characterizes the RVM framework, in contrast to other DVMs in which the dynamics of  $\rho_\Lambda(\zeta)$  enters only through the scale factor ( $\zeta = a$ ) or the cosmic time ( $\zeta = t$ ) in a way that is unrelated to the RG, cf. Sect. II.

The r.h.s. of (A3) represents the  $\beta$ -function of  $\rho_\Lambda$ . It can involve even powers of the Hubble rate  $H$  *only* (because of the covariance of the effective action). The coefficients  $a_i, b_i, c_i, \dots$  are dimensionless, and the  $M_i$  are the masses of the particles in the loops within a typical Grand Unified Theory (GUT) [53]. Notice that there are no  $M_i^4$  contributions on the r.h.s. of Eq. (A3). These terms would produce a too fast running of the CC and moreover they are forbidden within the RG approach since  $H$  plays the role of the running scale and its value is of course smaller than the mass of any known particle in QFT. Let us remark that the  $\sim M_i^4$  contributions would also be present in the vacuum energy in flat space-time [12]; but, as noted before, here we take the point of view that these effects must be subtracted since they are the primary cause of trouble.

Lacking of a more fundamental knowledge of the CCP, we have to adopt this setting as an educated ansatz, which is inspired in the kind of subtraction procedure employed in the calculation of the Casimir effect, see [76]. Concrete scenarios of this kind can be found within the context of anomaly-induced inflation, see [53], and also within dynamically broken Supergravity [188].

Integrating the above equation and keeping, for the sake of illustration, only one of the higher powers  $H^{n+2}$ , we can express the result as follows:

$$\rho_\Lambda(H) = \frac{3M_P^2}{8\pi} \left[ c_0 + \nu H^2 + 3\alpha_{n+2} \frac{H^{n+2}}{H_I^n} \right] \quad (n \geq 2), \quad (\text{A4})$$

with  $c_0$  an integration constant and  $H_I$  a parameter, both dimensionful. For the early universe,  $H_I$  is connected with the Hubble parameter at the inflationary epoch since this model indeed admits inflationary solutions, see [74]. For a generic GUT, the dimensionless parameter

$$\nu = \frac{1}{6\pi} \sum_{i=f,b} a_i \frac{M_i^2}{M_P^2} \quad (\text{A5})$$

is feeded by the heavy masses  $M_i$  of boson and fermions of the given GUT relative to the Planck mass,  $M_P$ . Typically one can estimate  $|\nu| = 10^{-6} - 10^{-3}$  [53]. The minimal case,  $n = 2$ , corresponding to adding the power  $H^4$  to the low energy term  $H^2$ , was mentioned in Eq. (10) of Sect. II A.

The dynamical vacuum option has extensively been used to attempt an unified model of vacuum dynamics. As mentioned, it offers an alternative description of inflation in the early universe (where the  $\sim H^{n+2}$  terms dominate) as well as of the current universe (where the

dynamical behavior is sustained by the milder  $\sim H^2$  term with small coefficient  $|\nu|$ ), see [51, 74–78]. Of course, in the current universe the expression (A4) boils down to the simpler form (11) for the RVM quoted in the main text.

Let us mention that at present we do not possess a general Lagrangian description of the RVM nor of any of the DVMs considered here. Still, in certain cases the RVM can be associated to an action, the anomaly-induced action. It is in these cases when one can estimate the value of  $|\nu|$  from the one-loop contributions of the matter particles [53]. This is in contrast to the usual scalar field models of the DE [10, 11], where a general and simple action formulation is available from the very beginning. Notwithstanding, let us make clear that the severity of the old CCP impinges on every formulation in the same way and in this sense it is convenient to explore all possibilities, especially from the point of view of their successfulness in the phenomenological arena. This is ultimately the way to recognize the physically promising theories, all the more given the outstanding richness of the current cosmological observations.

## Appendix B: Cosmological observables and statistical analysis

In this Appendix we explicitly define and discuss the various observables used in the current phenomenological analysis, and also collect some basic (essentially technical) information about the fitting procedure that has been followed, which we omitted in the main text of the paper, such as e.g. the correlation matrices entering the complete  $\chi^2$  function (86) or the precise values (with the corresponding uncertainties) of the BAO and CMB data sets.

Each of the  $\chi_s^2$  functions in the total  $\chi^2$  to be minimized can be written as follows,

$$\chi_s^2(\vec{p}) = [\vec{x}_s(\vec{p}) - \vec{d}_s]^T C_s^{-1} [\vec{x}_s(\vec{p}) - \vec{d}_s], \quad (\text{B1})$$

where the data set vector  $\vec{d}_s$  runs over all the data sets DS1-DS6 described in detail in Sect. III A. They are labeled here in a compact way as  $s = (\text{SNIa}, \text{BAO}, \text{LSS}, \text{BAO\&LSS}, \text{H}, \text{CMB})$ . In the particular case of DS3, part of the data are from [92] and in this case BAO and LSS are correlated. We have denoted this situation with BAO\&LSS: it reflects the contribution from the combined BAO+LSS covariance matrices for the LOWZ and CMASS data samples from that reference, see (B31) and (B32) below. Similarly  $\vec{x}_s$  are the vectors containing the theoretically computed values from the different models; and  $C_s$  is the covariance matrix for each data set  $s$ , which can be constructed from the correlation matrix  $\rho_s$  and the  $1\sigma$  uncertainties according to  $C_{s,ij} = \rho_{s,ij} \sigma_{s,i} \sigma_{s,j}$ .

## 1. SNIa

For the SNIa sector, we have used the binned distance modulus fitted to the JLA sample shown in Table F.1 of [87], together with the  $31 \times 31$  covariance matrix presented in Table F.2 of the same paper. The fitted quantity is the distance modulus, defined as

$$\mu(z, \vec{p}) = 5 \log D_L(z, \vec{p}) + M, \quad (\text{B2})$$

where  $M$  is a free normalization parameter (see [87] for details) and  $D_L(z, \vec{p})$  is the luminosity distance:

$$D_L(z, \vec{p}) = c(1+z) \int_0^z \frac{dz'}{H(z')}, \quad (\text{B3})$$

with  $c$  the speed of light (now included explicitly in this formula for better clarity). The previous formula (B3) for the luminosity distance applies only for spatially flat universes, which we are assuming throughout.

Parameter  $M$  is treated as a nuisance parameter and, therefore, it can be integrated out through the corresponding marginalization of the SNIa likelihood. It can be done analytically, as this helps to improve the computational efficiency by reducing in one dimension the fitting parameter space. After this marginalization, the resulting effective  $\chi^2$ -function for this data set reads:

$$\chi_{SNIa}^2(\vec{p}) = \vec{y}(\vec{p})^T J \vec{y}(\vec{p}) - \frac{[\sum_{i,j=1}^{31} J_{ij} y_i(\vec{p})]^2}{\sum_{i,j=1}^{31} J_{ij}}, \quad (\text{B4})$$

where  $J \equiv C_{SNIa}^{-1}$  and  $y_i(\vec{p}) \equiv 5 \log D_L(z_i, \vec{p}) - \mu_{\text{obs},i}$ . (B4) is the direct generalization of formula (13.16) of [72], since we are now considering a non-diagonal covariance matrix, instead of a diagonal one. Let us prove (B4). The original SNIa likelihood can be written as follows,

$$\mathcal{L}_{SNIa}(\vec{p}, M) = \mathcal{L}_0 e^{-\frac{1}{2} [y_i(\vec{p}) + M] J_{ij} [y_j(\vec{p}) + M]}, \quad (\text{B5})$$

where we have assumed the Einstein summation convention in order to write the result more concisely, and  $\mathcal{L}_0$  is the normalization constant. Let us now marginalize this distribution over the parameter  $M$ ,

$$\tilde{\mathcal{L}}(\vec{p}) \equiv \int_{-\infty}^{+\infty} \mathcal{L}_{SNIa}(\vec{p}, M) dM. \quad (\text{B6})$$

This can be expressed as

$$\tilde{\mathcal{L}}(\vec{p}) = \mathcal{L}_0 e^{-\frac{1}{2} B_0(\vec{p})} F(\vec{p}), \quad (\text{B7})$$

where

$$F(\vec{p}) \equiv \int_{-\infty}^{+\infty} e^{-\frac{B_1}{2} M^2 - M B_2(\vec{p})} dM, \quad (\text{B8})$$

with the definitions

$$\begin{aligned} B_0(\vec{p}) &\equiv \sum_{i,j=1}^{31} y_i(\vec{p}) J_{ij} y_j(\vec{p}), \\ B_1 &\equiv \sum_{i,j=1}^{31} J_{ij}, \\ B_2(\vec{p}) &\equiv \sum_{i,j=1}^{31} J_{ij} y_i(\vec{p}). \end{aligned} \quad (\text{B9})$$

The problem is basically reduced to compute the function  $F(\vec{p})$  appearing in (B7). Let us perform the derivative of the latter with respect to  $M$  and the  $i$ th-component of the fitting vector  $\vec{p}$ ,

$$\frac{\partial F}{\partial M} = 0 = - \int_{-\infty}^{+\infty} [M B_1 + B_2(\vec{p})] e^{-\frac{B_1}{2} M^2 - M B_2(\vec{p})} dM, \quad (\text{B10})$$

$$\frac{\partial F}{\partial p_i} = - \frac{\partial B_2(\vec{p})}{\partial p_i} \int_{-\infty}^{+\infty} M e^{-\frac{B_1}{2} M^2 - M B_2(\vec{p})} dM. \quad (\text{B11})$$

Combining these two expressions, we obtain a differential equation for  $F(\vec{p})$ ,

$$\frac{1}{F(\vec{p})} \frac{\partial F}{\partial p_i} = \frac{\partial B_2}{\partial p_i} \frac{B_2(\vec{p})}{B_1},$$

whose solution is very simple:

$$F(\vec{p}) \propto e^{\frac{B_2^2(\vec{p})}{2B_1}}. \quad (\text{B12})$$

The integration constant is irrelevant since it can be absorbed by the normalization factor  $\mathcal{L}_0$  in (B7), giving rise to a new one,  $\tilde{\mathcal{L}}_0$ . Thus, the marginalized likelihood reads,

$$\tilde{\mathcal{L}}(\vec{p}) = \tilde{\mathcal{L}}_0 e^{-\frac{\chi_{SNIa}^2(\vec{p})}{2}}, \quad (\text{B13})$$

with  $\chi_{SNIa}^2(\vec{p})$  given by (B4).

## 2. BAO and LSS

Galaxy surveys measure angular and redshift distributions of galaxies. Using these data, they are able to obtain the matter power spectrum  $P(\vec{k}, z)$  in redshift space upon modeling the bias factor and transforming these angles and redshifts into distances. However, the distance of two sources along the line of sight, being given by the difference of redshift  $\Delta z$ , depends on the cosmological model. Similarly, the distance of two sources in the direction perpendicular to the line of sight is given by the angular separation,  $\Delta\theta$ , which also depends on the cosmological model. Therefore, it is convenient to first define a fiducial model to which one refers the predictions of the new models being studied. Usually such a model is the  $\Lambda$ CDM with appropriately chosen values of the free parameters. We have already used a fiducial model in our analysis, cf. Sect. IV D, but different papers may use slightly different fiducial parameters and one has to take this feature carefully into account. If that is not enough, one has to disentangle the effect of the redshift space distortions that are due to the peculiar velocities of galaxies falling into the gravitational potential wells. The comoving wavevector  $\vec{k}$  is usually decomposed in a parallel to the line of sight component,  $k_{\parallel}$ , and another one which is perpendicular to it,  $k_{\perp}$ . These two directions determine the two-dimensional (2D) space in which

the distribution of galaxies is studied. The analysis of the BAO signal in the 2D power spectrum carries precious information about the angular and longitudinal size of the BAO standard ruler at the measured redshift  $z$ , namely

$$\Delta\theta_s(z) = \frac{ar_s(a_d)}{D_A(a)} = \frac{r_s(z_d)}{(1+z)D_A(z)}, \quad (\text{B14})$$

where  $a = 1/(1+z)$  is the scale factor, and

$$\Delta z_s(z) = \frac{r_s(z_d)H(z)}{c}, \quad (\text{B15})$$

$r_s(z_d)$  being the sound horizon at the redshift of the drag epoch (see below), with  $D_A$  the proper diameter angular distance,

$$D_A(z, \vec{p}) \equiv \frac{c}{(1+z)} \int_0^z \frac{dz'}{H(z')} \cdot \quad (\text{B16})$$

In principle, the various galaxy surveys are able to extract anisotropic BAO information from their analyses. That is to say, they can afford constraints on the quantities  $r_s(z_d)/D_A(z)$  and  $H(z)r_s(z_d)$  through the perpendicular and parallel dilation scale factors [92–94],

$$\begin{aligned} \alpha_{\perp} &\equiv \frac{r_s^{fid}(z_d)/D_A^{fid}(z)}{r_s(z_d)/D_A(z)} = \frac{D_A(z)r_s^{fid}(z_d)}{D_A^{fid}(z)r_s(z_d)} \\ \alpha_{\parallel} &\equiv \frac{H^{fid}(z)r_s^{fid}(z_d)}{H(z)r_s(z_d)}, \end{aligned} \quad (\text{B17})$$

where  $r_s^{fid}(z_d)$ ,  $D_A^{fid}(z)$  and  $H^{fid}(z)$  are obtained in the fiducial cosmology that the survey has used to convert redshift and angles into distances. The quantity  $r_s(z_d)/D_A(z)$  is the sound horizon at the drag epoch measured in units of the angular diameter distance at redshift  $z$ , and similarly  $r_s^{fid}(z_d)/D_A^{fid}(z)$  is the corresponding value in the fiducial model. These ratios are just the comoving angular sizes (B14), i.e. the angular sizes divided by the scale factor. Similarly,  $H(z)r_s(z_d)$  and  $H^{fid}(z)r_s^{fid}(z_d)$  are, respectively, the sound horizon in units of the Hubble horizon in the given model and in the fiducial model.

Sometimes the surveys are not equipped with enough BAO data to obtain (B14) and (B15) separately. In this case they limit themselves to compute the volume-averaged spectrum in a conveniently defined volume  $V$  and obtain a constraint which is usually encapsulated in the isotropic BAO estimator  $r_s(z_d)/D_V(z)$  (sometimes denoted  $d_z$  [166]). Here  $D_V(z)$  is an effective distance or dilation scale [189] obtained from the cubic root of the volume  $V$  (whose value is defined from the square of the transverse dilation scale times the radial dilation scale):

$$D_V(z, \vec{p}) = [zD_H(z, \vec{p})D_M^2(z, \vec{p})]^{1/3}. \quad (\text{B18})$$

In this expression,  $D_M = (1+z)D_A$  is the comoving angular diameter distance (playing the role of the transverse dilation scale at redshift  $z$ ) and  $D_H$  is the Hubble

| Model               | $r_s(z_d)_{ff}$   | $r_s(z_d)_{\text{Boltz}}$ |
|---------------------|-------------------|---------------------------|
| $\Lambda\text{CDM}$ | $150.85 \pm 0.24$ | $147.32 \pm 0.22$         |
| $\text{XCDM}$       | $151.02 \pm 0.23$ | $147.48 \pm 0.22$         |
| $\text{RVM}$        | $153.34 \pm 0.74$ | $148.25 \pm 0.33$         |
| $Q_{dm}$            | $153.34 \pm 0.72$ | $148.25 \pm 0.34$         |
| $Q_{\Lambda}$       | $151.39 \pm 0.32$ | $147.32 \pm 0.21$         |

TABLE XIII: The obtained values of the sound horizon distance at the drag epoch for the different models,  $r_s(z_d)$  (in Mpc), using (B22)–(B25) in the first column and (B26) in the second. We show the central values and associated uncertainties of  $r_s(z_d)$  for each model, which have been obtained using the posterior distribution of the analysis in Table I.

radius

$$D_H(z, \vec{p}) \equiv \frac{c}{H(z)}, \quad (\text{B19})$$

with  $zD_H$  acting as the radial dilation scale at redshift  $z$ . Therefore, the distilled BAO estimator  $d_z$  measures the sound horizon distance at the drag epoch in units of the effective dilation scale (B18).

Again a comparison with a fiducial value is necessary. The isotropic BAO parameter relating the fiducial model value of  $D_V$  with the actual value of a given model is defined in [89] as

$$\alpha \equiv \frac{D_V(z)}{D_V^{fid}(z)}. \quad (\text{B20})$$

In other cases  $\alpha$  is defined in terms of  $d_z$ ,

$$\alpha \equiv \frac{r_s^{fid}(z_d)/D_V^{fid}(z)}{r_s(z_d)/D_V(z)} = \frac{D_V(z)r_s^{fid}(z_d)}{D_V^{fid}(z)r_s(z_d)}, \quad (\text{B21})$$

as in [90, 91]. These isotropic BAO estimators (B20 and B21) are akin to the Alcock-Paczynski (AP) test [190], in which the ratio of the observed radial/redshift to the angular size at different redshifts,  $\Delta z_s/\Delta\theta_s$ , is used to obtain cosmological constraints on the product  $H(z)D_M(z)$  and hence of  $H(z)D_A(z)$ . Both for the AP test and the isotropic BAO measurement, the value of the Hubble parameter  $H(z)$  cannot be disentangled from  $D_A(z)$ , there is a degeneracy. This is in contradistinction to the situation with the anisotropic BAO parameters (B17), in which a measurement of both  $\alpha_{\perp}$  and  $\alpha_{\parallel}$  permits to extract the individual values of  $H(z)$  and  $D_A(z)$ .

In our fitting analysis, we use data of both types of BAO estimators: isotropic and anisotropic ones, see the data set items DS2 and DS3 in Sect. III A. The anisotropic BAO data contains more information than the isotropic one because the aforementioned degeneracy between  $H(z)$  and  $D_A(z)$  has been broken. Thus, anisotropic BAO is richer and yields stronger cosmological constraints [191, 192].

To compute the theoretical predictions for the above BAO estimators, we need some extra formulas. For instance, the sound horizon at redshift  $z$ , i.e.  $r_s(z)$ , is given

| Model               | $h$               | $\omega_b = \Omega_b h^2$ | $n_s$             | $\Omega_m$        | $\nu_i$               | $w_0$              | $w_1$             | $\chi^2_{\min}/dof$ | $\Delta \text{AIC}$ | $\Delta \text{BIC}$ |
|---------------------|-------------------|---------------------------|-------------------|-------------------|-----------------------|--------------------|-------------------|---------------------|---------------------|---------------------|
| $\Lambda\text{CDM}$ | $0.692 \pm 0.004$ | $0.02253 \pm 0.00013$     | $0.974 \pm 0.004$ | $0.296 \pm 0.004$ | -                     | -1                 | -                 | 84.83/85            | -                   | -                   |
| $\text{XCDM}$       | $0.672 \pm 0.007$ | $0.02262 \pm 0.00014$     | $0.976 \pm 0.004$ | $0.311 \pm 0.007$ | -                     | $-0.923 \pm 0.023$ | -                 | 74.15/84            | 8.54                | 6.19                |
| $\text{CPL}$        | $0.674 \pm 0.009$ | $0.02263 \pm 0.00014$     | $0.976 \pm 0.004$ | $0.310 \pm 0.009$ | -                     | $-0.946 \pm 0.085$ | $0.070 \pm 0.250$ | 74.08/83            | 6.31                | 1.77                |
| $\text{RVM}$        | $0.682 \pm 0.004$ | $0.02240 \pm 0.00014$     | $0.968 \pm 0.004$ | $0.296 \pm 0.004$ | $0.00152 \pm 0.00038$ | -1                 | -                 | 66.95/84            | 15.74               | 13.39               |
| $Q_{dm}$            | $0.683 \pm 0.004$ | $0.02238 \pm 0.00014$     | $0.967 \pm 0.004$ | $0.296 \pm 0.004$ | $0.00217 \pm 0.00055$ | -1                 | -                 | 66.99/84            | 15.70               | 13.35               |
| $Q_\Lambda$         | $0.693 \pm 0.004$ | $0.02226 \pm 0.00016$     | $0.964 \pm 0.005$ | $0.296 \pm 0.004$ | $0.00785 \pm 0.00256$ | -1                 | -                 | 75.56/84            | 7.13                | 4.78                |

TABLE XIV: Fitting results for the different models using (B26), instead of (B22)-(B25), in the computation of the comoving sound horizon at the drag epoch. It is noteworthy that in the RVM case we find  $\nu > 0$  at exactly  $4\sigma$  c.l. Compare with Table I, where  $\nu > 0$  at  $3.76\sigma$  c.l.

by the expression

$$r_s(z) = \int_z^\infty \frac{c_s(z') dz'}{H(z')}, \quad (\text{B22})$$

where

$$c_s(z) = \frac{c}{\sqrt{3(1 + \mathcal{R}(z))}} \quad (\text{B23})$$

is the sound speed in the photo-baryon plasma and

$$\mathcal{R}(z) = \frac{\delta\rho_b(z)}{\delta\rho_\gamma(z)}. \quad (\text{B24})$$

For all the models studied in this paper the energy densities for radiation and baryons evolve in the standard way. Thus, function (B24) takes the usual form  $\mathcal{R}(z) = (3\Omega_b/4\Omega_\gamma)/(1+z)$ , being  $\Omega_\gamma$  the photon density parameter.

The redshift at the drag epoch is  $z_d \sim \mathcal{O}(10^3)$ . For  $z < z_d$  the baryon perturbations effectively decouple from the photon ones and start to grow with dark matter perturbations. The precise value of  $z_d$  depends in a complicated way on the different cosmological parameters. The fitted formula for determining it is given in [144]:

$$\begin{aligned} z_d &= \frac{1291 \omega_m^{0.251}}{1 + 0.659 \omega_m^{0.828}} [1 + \beta_1 \omega_b^{\beta_2}] \\ \beta_1 &= 0.313 \omega_m^{-0.419} [1 + 0.607 \omega_m^{0.674}] \\ \beta_2 &= 0.238 \omega_m^{0.223}. \end{aligned} \quad (\text{B25})$$

Let us point out that many experimental groups do not make use of these fitted formulas (labeled with a subindex ff below), and prefer the complete set of Boltzmann (Boltz) equations, which must be solved numerically. Both approaches can give rise to differences that are around 2–3%. Consequently, if the observational values are computed with a Boltzmann code, then we need to correct them in order to perform the comparison with our theoretical predictions, which make use of the above expressions. In these cases we follow the same procedure applied in [91] based on re-scaling the observational data by  $f_r \equiv r_s(z_d)^{fid}/r_s(z_d)^{fid}_{\text{Boltz}}$ . The two quantities involved in this ratio are computed using the same fiducial  $\Lambda\text{CDM}$  cosmology chosen by the observational teams, but whilst the first is obtained with the fitted formulas (B22)-(B25), the second is obtained with a Boltzmann code. One can also compute the latter using the existing

approximated formulas for the sound horizon at  $z_d$  that are obtained by fitting the data extracted from e.g. the CAMB code, since they are very accurate, with errors less than the 0.1% [192]:

$$r_s(z_d)_{\text{Boltz}} = \frac{55.234(1 + \Omega_\nu h^2)^{-0.3794} \text{Mpc}}{(\Omega_{dm} h^2 + \Omega_b h^2)^{0.2538} (\Omega_b h^2)^{0.1278}}, \quad (\text{B26})$$

where  $\Omega_\nu h^2$  is the neutrino reduced density parameter and depends, of course, on the effective number of neutrino species and the photon CMB temperature, which is taken from [129], see also Sect. III B.

We should make clear that the aforementioned re-scaling does not change the values of the dilation scale factors (B17), (B20) and (B21) furnished by the experimental teams. If they, for instance, deliver their results through the product  $\alpha_\perp (D_A^{fid}/r_s(z_d)^{fid}_{\text{Boltz}})$ , then we just multiply it by  $f_r^{-1}$  in order to keep our fitting procedure consistent. Note that we are also using the fitting formulas (B38) and (B39) in the computation of the decoupling redshift  $z_*$  (see below, Sect. B 4). By the same token, we re-scale  $(H^{fid} r_s(z_d)^{fid}_{\text{Boltz}})/\alpha_\parallel$  on multiplying it by  $f_r$ . But we stress once more that the dilation scale factors, which are the fundamental outputs extracted from the analysis of the BAO signal, are not modified by this re-scaling.

We have studied the changes induced in our fitting results when we use (B26) instead of (B22)-(B25). We show the corresponding values of the sound horizon at the drag epoch,  $r_s(z_d)$ , in Table XIII, and the corresponding new fitting results for the various models in Table XIV. As it can be seen, they are close to the original ones shown in Table I. The statistical significance of the new results is exactly  $4\sigma$  for the RVM and very near to it ( $3.94\sigma$ ) also for the  $Q_{dm}$ . The  $\Delta \text{AIC}$  and  $\Delta \text{BIC}$  values of these models are above 15, which denote very strong evidence in favor of these models as compared to the  $\Lambda\text{CDM}$ . The central fit values did not undergo significant changes with respect to Table I, which again reflects the robustness of our results and conclusions.

We use data from the 6dFGS survey [89],  $D_V(z = 0.106) = (456 \pm 27) \text{Mpc}$ . Also from the SDSS DR7 MGS one [90],  $D_V(z = 0.15) \left( \frac{r_s(z_d)^{fid}}{r_s(z_d)} \right) = (664 \pm 25) \text{Mpc}$ . For

the data of the WiggleZ Dark Energy survey [91],

$$\begin{aligned} D_V(0.44) \left( \frac{r_s(z_d)^{fid}}{r_s(z_d)} \right) &= (1716.4 \pm 83.1) \text{ Mpc} \\ D_V(0.60) \left( \frac{r_s(z_d)^{fid}}{r_s(z_d)} \right) &= (2220.8 \pm 100.6) \text{ Mpc} \\ D_V(0.73) \left( \frac{r_s(z_d)^{fid}}{r_s(z_d)} \right) &= (2516.1 \pm 86.1) \text{ Mpc}. \end{aligned} \quad (\text{B27})$$

We have also taken into account the correlations between the different measurements through the corresponding inverse covariance matrix,

$$C_{\text{BAO/WZ}}^{-1} = b \begin{pmatrix} 2.17898878 & -1.11633321 & 0.46982851 \\ -1.11633321 & 1.70712004 & -0.71847155 \\ 0.46982851 & -0.71847155 & 1.65283175 \end{pmatrix}, \quad (\text{B28})$$

with  $b = 10^{-4} \text{ Mpc}^{-2}$ .

As explained in the data set item DS3), we also use BOSS LSS and anisotropic BAO data, more specifically from the LOWZ ( $z = 0.32$ ) and CMASS ( $z = 0.57$ ) samples [92]. For each of these redshifts the authors provide three data points,  $f(z)\sigma_8(z)$ ,  $D_A(z)/r_s(z_d)$  and  $H(z)r_s(z_d)$ , which are extracted by a thorough study involving RSD measurements of the power spectrum combined with the bispectrum, and the BAO post-reconstruction analysis of the power spectrum. For the LOWZ sample, we have

$$\begin{aligned} f\sigma_8 &= 0.42660 \pm 0.05627 \\ Hr_s(z_d)/(10^3 \text{ km/s}) &= f_r(11.549 \pm 0.385) \\ D_A/r_s(z_d) &= f_r^{-1}(6.5986 \pm 0.1337), \end{aligned} \quad (\text{B29})$$

and for the CMASS sample,

$$\begin{aligned} f\sigma_8 &= 0.42613 \pm 0.02907 \\ Hr_s(z_d)/(10^3 \text{ km/s}) &= f_r(14.021 \pm 0.225) \\ D_A/r_s(z_d) &= f_r^{-1}(9.3869 \pm 0.1030), \end{aligned} \quad (\text{B30})$$

where  $f_r = (151.79 \text{ Mpc}/148.11 \text{ Mpc})$  is the sound horizon re-scaling introduced above. We need to apply such a rescaling because the authors of [92] compute  $r_s(z_d)^{fid}$  with the Boltzmann code, whereas we make use of the fitting formula (B25). The corresponding covariance matrices read, respectively,

$$C_{\text{LOWZ}} = 10^{-3} \begin{pmatrix} 3.1667 & 14.726f_r & 5.0871f_r^{-1} \\ 14.726f_r & 148.099f_r^2 & 28.929 \\ 5.0871f_r^{-1} & 28.929 & 17.883f_r^{-2} \end{pmatrix}, \quad (\text{B31})$$

and

$$C_{\text{CMASS}} = 10^{-3} \begin{pmatrix} 0.84506 & 4.3722f_r & 2.0151f_r^{-1} \\ 4.3722f_r & 50.717f_r^2 & 13.827 \\ 2.0151f_r^{-1} & 13.827 & 10.613f_r^{-2} \end{pmatrix}. \quad (\text{B32})$$

We also use the data from the combined Ly $\alpha$ F analysis at  $z = 2.34$  presented in [93],

$$\begin{aligned} D_A/r_s(z_d) &= 10.93^{+0.35}_{-0.34} \cdot f_r^{-1} \\ D_H/r_s(z_d) &= 9.15^{+0.20}_{-0.21} \cdot f_r^{-1}, \end{aligned} \quad (\text{B33})$$

with  $f_r = (153.4 \text{ Mpc}/149.7 \text{ Mpc})$  and their correlation coefficient,  $\rho_{12} = -0.48$  [94].

### 3. $\mathbf{H}(\mathbf{z})$

The covariance matrix for the  $H(z)$  data is diagonal and therefore,  $C_{H,ij} = \sigma_{H,i}^2 \delta_{ij}$ , (see DS4 above and Table IV). The possibility of having non zero off-diagonal terms in the correlation matrix is not excluded, but they are not available in the literature, and as we know the  $H(z)$  data set plays a secondary role in comparison to the BAO, CMB and LSS sets. The impact of these coefficients should be negligible, and thus the corresponding  $\chi^2$ -function adopts the following simple form:

$$\chi_H^2(\vec{p}) = \sum_{i=1}^{30} \left[ \frac{H(z_i, \vec{p}) - H_{\text{obs}}(z_i)}{\sigma_{H,i}} \right]^2. \quad (\text{B34})$$

The theoretical values for the DVMs are computed with Eqs. (21)-(23), and the ones for the XCDM and CPL parametrizations with (24) and (26), respectively. The observed points and their uncertainties are listed in Table IV.

### 4. CMB

As explained in DS6), we have made use of the CMB data and correlation matrix of the Planck 2015 TT,TE,EE+lowP analysis presented in [125]. The data points are the following:

$$\begin{aligned} R &= 1.7448 \pm 0.0054 \\ l_a &= 301.460 \pm 0.094 \\ \omega_b &= 0.02240 \pm 0.00017 \\ n_s &= 0.9680 \pm 0.0051, \end{aligned} \quad (\text{B35})$$

and the corresponding correlation matrix:

$$\rho_{cmb} = \begin{pmatrix} 1 & 0.53 & -0.73 & -0.80 \\ 0.53 & 1 & -0.42 & -0.43 \\ -0.73 & -0.42 & 1 & 0.59 \\ -0.80 & -0.43 & 0.59 & 1 \end{pmatrix}. \quad (\text{B36})$$

The theoretical expression for the “shift parameter” is given by

$$R(\vec{p}) = \sqrt{\Omega_m} \int_0^{z_*} \frac{dz}{E(z)}, \quad (\text{B37})$$

where  $z_*$  is the redshift at decoupling. Its precise value depends weakly on the parameters, and it is obtained from the fitting formula [193]:

$$z_* = 1048 (1 + 0.00124 \omega_b^{-0.738}) (1 + g_1 \omega_m^{g_2}), \quad (\text{B38})$$

with

$$\begin{aligned} g_1 &= \frac{0.0783 \omega_b^{-0.238}}{1 + 39.5 \omega_b^{0.763}} \\ g_2 &= \frac{0.560}{1 + 21.1 \omega_b^{1.81}}. \end{aligned} \quad (\text{B39})$$

Finally, the formula for the acoustic length  $\ell_a$  is:

$$\ell_a(\vec{p}) = \pi(1 + z_*) \frac{D_A(z_*)}{r_s(z_*)}, \quad (\text{B40})$$

in which the angular diameter distance  $D_A$  is given in (B16) and the expression for the sound horizon in (B22).

---

[1] A.G. Riess *et al.*, *Astron. J.* **116**, 1009 (1998).

[2] S. Perlmutter *et al.*, *Astrophys. J.* **517**, 565 (1999).

[3] G. Hinshaw *et al.* (WMAP Collaboration), *Astrophys. J. Suppl. Ser.* **208**, 19 (2013).

[4] P.A.R. Ade *et al.* (Planck Collaboration): Planck 2013 results. XVI, *Astron. Astrophys.* **571**, A16 (2014).

[5] P.A.R. Ade *et al.* (Planck Collaboration): Planck 2015 results. XIII, *Astron. Astrophys.* **594**, A13 (2016).

[6] P.A.R. Ade *et al.* (Planck Collaboration): Planck 2015 results. XIV, *Astron. Astrophys.* **594**, A14 (2016).

[7] S. Weinberg, *Rev. Mod. Phys.* **61**, 1 (1989).

[8] V. Sahni and A.A. Starobinsky, *Int. J. Mod. Phys. A* **9**, 373 (2000).

[9] T. Padmanabhan, *Phys. Rept.* **380**, 235 (2003).

[10] P.J.E. Peebles and B. Ratra, *Rev. Mod. Phys.* **75**, 559 (2003).

[11] E.J. Copeland, M. Sami and S. Tsujikawa, *Int. J. Mod. Phys. D* **15**, 1753 (2006).

[12] J. Solà, *Cosmological constant and vacuum energy: old and new ideas*, *J. Phys. Conf. Ser.* **453**, 012015 (2013).

[13] A. Einstein, *Kosmologische Betrachtungen zur allgemeinen Relativitätstheorie*, Sitzungsber. Königl. Preuss. Akad. Wiss. phys.-math. Klasse VI 142 (1917) (Submitted: February 8th, 1917).

[14] Y. B. Zeldovich, *Cosmological constant and elementary particles*, *JETP Lett.* **6**, 316 (1967), *Pisma Zh. Eksp. Teor. Fiz.* **6**, 883 (1967); *Cosmological constant and the theory of elementary particles*, *Sov. Phys. Usp.* **11** (1968) 381, republished in *Gen. Rel. Grav.* **40**, 1557 (2008) (edited by V. Sahni and A. Krasinski).

[15] P.W. Higgs, *Phys. Lett.* **12**, 132 (1964); *Phys. Rev. Lett.* **13**, 508 (1964); G.S. Guralnik, C.R. Hagen and T.W.B. Kibble, *Phys. Rev. Lett.* **13** (1964) 585; F. Englert and R. Brout, *Phys. Rev. Lett.* **13** 321 (1964) 321.

[16] A.D. Linde, *JETP Lett.* **19**, 183 (1974).

[17] J. Dreitlein, *Phys. Rev. Lett.* **33**, 1243 (1974).

[18] M.J.G. Veltman, *Phys. Rev. Lett.* **34**, 777 (1975).

[19] G. Gamow, *My World Line, an informal autobiography* (The Viking Press, Inc., New York, 1970), see p. 44.

[20] C. Brans and R.H. Dicke, *Phys. Rev.* **124**, 925 (1961).

[21] P.G. Bergmann, *Int. J. Theor. Phys.* **1**, 25 (1968); K. Nordtvedt, *Astrophys. J.* **161**, 1059 (1970); R. Wagoner, *Phys. Rev. D* **1**, 3209 (1970).

[22] R.D. Peccei, J. Solà, and C. Wetterich, *Phys. Lett. B* **195**, 183 (1987).

[23] M. Endo and T. Fukui, *Gen. Relativ. Gravit.* **8**, 833 (1977); *Gen. Relativ. Gravit.* **14**, 769 (1982).

[24] Y. Fujii, *Phys. Rev. D* **26**, 2580 (1982).

[25] A.D. Dolgov, in *The very Early Universe*, edited by G. Gibbons, S.W. Hawking, and S.T. Tiklos, (Cambridge Univ. Press, Cambridge, 1983), p. 449.

[26] L. Abbott, *Phys. Lett. B* **150**, 427 (1985).

[27] A. Zee, *Phys. Lett. B* **161**, 141 (1985).

[28] S.M. Barr, *Phys. Rev. D* **36**, 1691 (1987); S.M. Barr and D. Hochberg, *Phys. Lett. B* **211**, 49 (1988).

[29] L.H. Ford, *Phys. Rev. D* **35**, 2339 (1987).

[30] N. Weiss, *Phys. Lett. B* **197**, 42 (1987).

[31] P.J.E. Peebles and B. Ratra, *Astrophys. J.* **325**, L17 (1988).

[32] B. Ratra and P.J.E. Peebles, *Phys. Rev. D* **37**, 3406 (1988).

[33] C. Wetterich, *Nucl. Phys. B* **302**, 668 (1988).

[34] C. Wetterich, *Astron. Astrophys.* **301**, 321 (1995).

[35] R.R. Caldwell, R. Dave and P.J. Steinhardt, *Phys. Rev. Lett.* **80**, 1582 (1998).

[36] I. Zlatev, L.M. Wang and P.J. Steinhardt, *Phys. Rev. Lett.* **82**, 896 (1999); *Phys. Rev. D* **59**, 123504 (1999).

[37] L. Amendola, *Phys. Rev. D* **62**, 043511 (2000).

[38] R.R. Caldwell, M. Kamionkowski and N.N. Weinberg, *Phys. Rev. Lett.* **91**, 071301 (2003).

[39] M. Ozer and O. Taha, *Phys. Lett. B* **171**, 363 (1986); *Nucl. Phys. B* **287**, 776 (1987).

[40] O. Bertolami, *Nuovo Cimento B* **93**, 36 (1986).

[41] K. Freese, F.C. Adams, J.A. Frieman, and E. Mottola, *Nucl. Phys. B* **287**, 797 (1987).

[42] J.C. Carvalho, J.A.S. Lima and I. Waga, *Phys. Rev. D* **46**, 2404 (1992).

[43] I. Waga, *Astrophys. J.* **414**, 436 (1993).

[44] J.A.S. Lima and J.M.F. Maia, *Mod. Phys. Lett. A* **08**, 591 (1993).

[45] R.C. Arcuri and I. Waga, *Phys. Rev. D* **50**, 2928 (1994).

[46] A.I. Arbab, *Gen. Relativ. Gravit.* **29**, 61 (1997); *Astrophys. Space Sci.* **246**, 193 (1997).

[47] J.M. Overduin and F.I. Cooperstock, *Phys. Rev. D* **58**, 043506 (1998).

[48] R.G. Vishwakarma, *Class. Quant. Grav.* **18**, 1159 (2001).

[49] M. Bronstein, *Phys. Z. Sowjetunion* **3**, 73 (1933).

[50] P.J.E. Peebles, *Principles of Physical Cosmology* (Princeton Univ. Press, Princeton, 1993).

[51] J. Solà and A. Gómez-Valent, *Int. J. Mod. Phys. D* **24**, 1541003 (2015).

[52] J. Solà, *Int. J. Mod. Phys. A* **31**, 1630035 (2016).

[53] J. Solà, *J. Phys. A* **41**, 164066 (2008).

[54] C. España-Bonet *et al.*, *JCAP* **0402**, 006 (2004); *Phys. Lett. B* **574**, 149 (2003).

[55] S. Basilakos, M. Plionis, and J. Solà, *Phys. Rev. D* **80**, 083511 (2009).

[56] J. Solà, *Cosmologies with a time dependent vacuum*, *J. Phys. Conf. Ser.* **283**, 012033 (2011).

[57] J. Grande, J. Solà, S. Basilakos, and M. Plionis, *JCAP* **1108**, 007 (2011).

[58] S. Basilakos, D. Polarski, and J. Solà, *Phys. Rev. D* **86**, 043010 (2012).

[59] S. Basilakos and J. Solà, *Phys. Rev. D* **90**, 023008 (2014).

[60] A. Gómez-Valent, J. Solà, and S. Basilakos, *JCAP* **1501**, 004 (2015).

[61] A. Gómez-Valent and J. Solà, *Mon. Not. R. Astron. Soc.* **448**, 2810 (2015).

[62] S. Basilakos, *Mod. Phys. Lett. A* **30** (2015) 1540031.

[63] A. Gómez-Valent, E. Karimkhani, and J. Solà, *JCAP* **1512**, 048 (2015).

[64] C.Q. Geng, C.C. Lee, and K. Zhang, Phys.Lett. B**760**, 422 (2016).

[65] C.Q. Geng, C.C. Lee, and L. Yin, *Constraints on running vacuum model with  $H(z)$  and  $f\sigma_8$* , arXiv:1704.02136.

[66] J. Solà, A. Gómez-Valent, and J. de Cruz Pérez, Astrophys. J. **836**, 43 (2017).

[67] J. Solà, A. Gómez-Valent, and J. de Cruz Pérez, Astrophys. J. **811**, L14 (2015).

[68] J. Solà, J. de Cruz Pérez, A. Gómez-Valent, and R.C. Nunes, *Dynamical Cosmic Vacuum against a rigid Cosmological Constant*, arXiv:1606.00450v3 (submitted to Phys. Rev. Lett.).

[69] J. Solà, A. Gómez-Valent, and J. de Cruz Pérez, Mod. Phys. Lett. A**32** 1750054 (2017).

[70] S.M. Turner and M. White, Phys. Rev. D**56**, R4439 (1997).

[71] M. Chevallier and D. Polarski, Int. J. Mod. Phys. D**10**, 213 (2001); E.V. Linder, Phys. Rev. Lett. **90**, 091301 (2003); Phys. Rev. D**70**, 023511 (2004).

[72] L. Amendola and S. Tsujikawa, *Dark Energy* (Cambridge Univ. Press, Cambridge, 2010 and 2015).

[73] Gong-Bo Zhao *et al.*, *The clustering of galaxies in the completed SDSS-III Baryon Oscillation Spectroscopic Survey: Examining the observational evidence for dynamical dark energy*, arXiv:1701.08165.

[74] J.A.S. Lima, S. Basilakos, and J. Solà, Mon. Not. R. Astron. Soc. **431**, 923 (2013).

[75] E.L.D. Perico *et al.*, Phys. Rev. D**88**, 063531 (2013).

[76] J. Solà, Int. J. Mod. Phys. D**24**, 1544027 (2015).

[77] J.A.S. Lima, S. Basilakos, and J. Solà, Gen. Relativ. Gravit. **47**, 40 (2015).

[78] J.A.S. Lima, S. Basilakos, and J. Solà, Eur. Phys. J. C**76**, 228 (2016).

[79] H. Fritzsch and J. Solà, Class. Quant. Grav. **29**, 215002 (2012).

[80] H. Fritzsch and J. Solà, Mod. Phys. Lett. A**30**, 1540034 (2015).

[81] H. Fritzsch, J. Solà, and R.C. Nunes, Eur. Phys. J. C**77** 193 (2017).

[82] V. Salvatelli *et al.*, Phys. Rev. Lett. **113**, 181301 (2014).

[83] R. Murgia, S. Gariazzo, and N. Fornengo, JCAP **1604**, 014 (2016).

[84] Y.H. Li, J.F. Zhang, and X. Zhang, Phys. Rev. D**93**, 023002 (2016).

[85] Y.L. Bolotin, A. Kostenko, O.A. Lemets, and D.A. Yerokhin, Int. J. Mod. Phys. D **24**, 1530007 (2015).

[86] A. A. Costa, X.-D. Xu, B. Wang, and E. Abdalla, JCAP **1701**, 028 (2017).

[87] M. Betoule *et al.*, Astron. Astrophys. **568**, A22 (2014).

[88] L. Amendola, Notes for the course *Statistical Physics* (Heidelberg Univ., 2015).

[89] F. Beutler *et al.*, Mon. Not. R. Astron. Soc. **416**, 3017 (2011).

[90] A.J. Ross *et al.*, Mon. Not. R. Astron. Soc. **449**, 835 (2015).

[91] E.A. Kazin *et al.*, Mon. Not. R. Astron. Soc. **441**, 3524 (2014).

[92] H. Gil-Marín *et al.*, Mon. Not. Roy. Astron. Soc. **465**, 1757 (2017).

[93] T. Delubac *et al.*, Astron. Astrophys. **574**, A59 (2015).

[94] E. Aubourg *et al.*, Phys. Rev. D**92**, 123516 (2015).

[95] F. Beutler *et al.*, Mon. Not. R. Astron. Soc. **423**, 3430 (2012).

[96] M. Feix, A. Nusser, and E. Branchini, Phys. Rev. Lett. **115**, 011301 (2015).

[97] F. Simpson *et al.*, Phys. Rev. D**93**, 023525 (2016).

[98] C. Blake *et al.*, Mon. Not. R. Astron. Soc. **436**, 3089 (2013).

[99] C. Blake *et al.*, Mon. Not. R. Astron. Soc. **415**, 2876 (2011).

[100] C.M. Springob *et al.*, Mon. Not. R. Astron. Soc. **456**, 1886 (2016).

[101] B.R. Granett *et al.*, Astron. Astrophys. **583**, A61 (2015).

[102] L. Guzzo *et al.*, Nature **451**, 541 (2008).

[103] Y.-S. Song and W.J. Percival, JCAP **0910**, 004 (2009).

[104] C. Zhang *et al.*, Res. Astron. Astrophys. **14**, 1221 (2014).

[105] R. Jiménez *et al.*, Astrophys. J. **593**, 622 (2003).

[106] J. Simon, L. Verde, and R. Jiménez, Phys. Rev. D**71**, 123001 (2005).

[107] M. Moresco *et al.*, JCAP **1208**, 006 (2012).

[108] M. Moresco *et al.*, JCAP **1605**, 014 (2016).

[109] D. Stern *et al.*, JCAP **1002**, 008 (2010).

[110] M. Moresco, Mon. Not. R. Astron. Soc. **450**, L16 (2015).

[111] O. Farooq and B. Ratra, Astrophys. J. **766**, L7 (2013).

[112] V. Sahni, A. Shafieloo, and A.A. Starobinsky, Astrophys. J. **793**, L40 (2014).

[113] X. Ding *et al.*, Astrophys. J. **803**, L22 (2015).

[114] X. Zheng *et al.*, Astrophys. J. **825**, L17 (2016).

[115] Y. Chen, S. Kumar, and B. Ratra, Astrophys. J. **835**, 86 (2017).

[116] M.H.P.M. van Putten, Astrophys. J. **837**, 22 (2017).

[117] W.P. Percival *et al.*, Mon. Not. R. Astron. Soc. **353**, 1201 (2004).

[118] S. Alam, S. Ho, and A. Silvestri, Mon. Not. R. Astron. Soc. **456**, 3743 (2016).

[119] S.J. Turnbull *et al.*, Mon. Not. R. Astron. Soc. **420**, 447 (2012).

[120] M.J. Hudson and S.J. Turnbull, Astrophys. J. **751**, L30 (2013).

[121] A. Johnson *et al.*, Mon. Not. R. Astron. Soc. **444**, 3926 (2014).

[122] F. Beutler *et al.*, Mon. Not. R. Astron. Soc. **455**, 3230 (2016).

[123] F.A. Marín *et al.*, Mon. Not. R. Astron. Soc. **455**, 4046 (2016).

[124] P. Mukherjee, M. Kunz, D. Parkinson, and Y. Wang, Phys. Rev. D**78**, 083529 (2008).

[125] Q.G. Huang, K. Wang, and S. Wang, JCAP **1512**, 022 (2015).

[126] J.-P. Uzan, Living Rev. Rel. **14**, 2 (2011); *The big-bang theory: construction, evolution and status*, arXiv:1606.06112.

[127] T. Chiba, Prog. Theor. Phys. **126**, 993 (2011).

[128] S. Nesseris, G. Pantazis, and L. Perivolaropoulos, *Tension and constraints on modified gravity parametrizations of  $G_{eff}(z)$  from growth rate and Planck data*, arXiv:1703.10538.

[129] D. Fixsen, Astrophys. J. **707**, 916 (2009).

[130] G. Mangano *et al.*, Nucl. Phys. B**729**, 221 (2005); G. Mangano, G. Miele, S. Pastor, and M. Peloso, Phys. Lett., B**534**, 8 (2002).

[131] E.W. Kolb and M.S. Turner, *The Early Universe* (Addison-Wesley Publishing Company, 1990).

[132] A.R. Liddle and D.H. Lyth, *Cosmological Inflation and Large-Scale Structure* (Cambridge Univ. Press, 2000).

[133] A.R. Liddle and D.H. Lyth, *The Primordial Density Perturbation* (Cambridge U. Press, 2009).

[134] S. Dodelson, *Modern Cosmology* (Academic Press, 2003).

[135] J. Grande, A. Pelinson, and J. Solà, Phys. Rev. D **79**, 043006 (2009).

[136] V.F. Mukhanov, H.A. Feldman, and R.H. Brandenberger, Phys. Rept. **215**, 203 (1992); C.-P. Ma and E. Bertschinger, Astrophys. J. **455**, 7 (1995).

[137] S. Basilakos and J. Solà, Phys. Rev. D **92**, 123501 (2015).

[138] L.M. Wang and P.J. Steinhardt, Astrophys. J. **508**, 483 (1998).

[139] S. Basilakos and S. Nesseris, Phys. Rev. D **94**, 123525 (2016).

[140] A. Pouri, S. Basilakos, and M. Plionis, JCAP **1408**, 042 (2014).

[141] J.M. Bardeen, J.R. Bond, N. Kaiser, and A.S. Szalay, Astrophys. J. **304**, 15 (1986).

[142] J.A. Peacock and S.J. Dodds, Mon. Not. R. Astron. Soc. **267**, 1020 (1994).

[143] N. Sugiyama, Astrophys. J. Suppl. Ser. **100**, 281 (1995).

[144] D. Eisenstein and W. Hu, Astrophys. J. **496**, 605 (1998).

[145] J.M. Salim and I. Waga, Class. Quant. Grav. **10**, 1767 (1993).

[146] J.A.S. Lima, Phys. Rev. D **54**, 2571 (1996).

[147] D. Pavón, Phys. Rev. D **43**, 375 (1991).

[148] G.W. Gibbons and S.W. Hawking, Phys. Rev. D **15**, 2738 (1977); P.C.W. Davies, Class. Quant. Grav. **4**, L225 (1987).

[149] J.P. Mimoso and D. Pavón, Phys. Rev. D **87**, 047302 (2013).

[150] S. Kumar and R.C. Nunes, arXiv:1702.02143; R.-Y. Guo, Y.-H. Li, J.-F. Zhang, and X. Zhang, arXiv:1702.04189.

[151] H. Gil-Marín *et al.*, Mon. Not. R. Astron. Soc. **460**, 4188 (2016).

[152] A.G. Riess *et al.*, Astrophys. J. **826**, 56 (2016).

[153] A.G. Riess *et al.*, Astrophys. J. **730**, 119 (2011).

[154] G. Chen and B. Ratra, Publ. Astron. Soc. Pac. **123**, 1127 (2011).

[155] W.L. Freedman *et al.*, Astrophys. J. **758**, 24 (2012).

[156] J.L. Sievers *et al.* (Atacama Cosmology Telescope), JCAP **1310**, 060 (2013).

[157] E.D. Valentino, A. Melchiorri, and J. Silk, Phys. Lett. B **761**, 242 (2016).

[158] J.L. Bernal, L. Verde, and A.G. Riess, JCAP **1610**, 019 (2016).

[159] E.D. Valentino, A. Melchiorri, E.V. Linder, and J. Silk, *Constraining dark energy dynamics in extended parameter space*, arXiv:1704.00762.

[160] H. Akaike, IEEE Trans. Autom. Control. **19**, 716 (1974).

[161] N. Sugiura, Communications in Statistics A, Theory and Methods, **7**, 13 (1978).

[162] G. Schwarz, Annals of Statistics **6**, 461 (1978).

[163] K.P. Burnham and D.R. Anderson, *Model selection and multimodel inference* (Springer, New York, 2002).

[164] J. Solà, ed. *Fundamental Constants in Physics and Their Time Variation*, Mod. Phys. Lett. A **30** (2015) Special Issue.

[165] J. Solà, E. Karimkhani, and A. Khodam-Mohammadi, Class. Quant. Grav. **34**, 025006 (2017).

[166] C. Blake *et al.*, Mon. Not. R. Astron. Soc. **418**, 1707 (2011).

[167] S. Alam *et al.*, arXiv:1607.03155.

[168] J.E. Bautista *et al.*, *Measurement of BAO correlations at  $z = 2.3$  with SDSS DR12 Ly $\alpha$ -Forests*, arXiv:1702.00176.

[169] A. Font-Ribera *et al.*, JCAP **1405**, 027 (2014).

[170] H. Gil-Marín *et al.*, arXiv:1606.00439 v1.

[171] A. Pavlov, O. Farooq, and B. Ratra, Phys. Rev. D **90**, 023006 (2014).

[172] O. Avsajanishvili, N.A. Arkhipova, L. Samushia, and T. Kahniashvili, Eur. Phys. J. C **74**, 3127 (2014).

[173] O. Farooq, D. Mania, and B. Ratra, Astrophys. J. **764**, 138 (2013).

[174] E.J. Copeland, A.R. Liddle, and D. Wands, Phys. Rev. D **57**, 4686 (1998).

[175] T. Barreiro, E.J. Copeland, and N.J. Nunes, Phys. Rev. D **61**, 127301 (2000).

[176] A. Poutsidou, C. Skordis, and E.J. Copeland, Phys. Rev. D **88**, 083505 (2013).

[177] C. Wetterich, Nucl. Phys. B **897**, 111 (2015).

[178] A. Poutsidou and T. Tram, Phys. Rev. D **94**, 043518 (2016).

[179] A. Maeder, Astrophys. J. **834**, 194 (2017).

[180] K. Trachenko, Phys. Rev. D **95**, 043522 (2017).

[181] J. Solà, A. Gómez-Valent, and J. de Cruz Pérez (work in preparation).

[182] A. Aghamousa *et al.* (DESI Collaboration), *The DESI Experiment Part II: Instrument Design*, FERMILAB-PUB-16-518-AE, arXiv:1611.00037.

[183] Y. Zhang *et al.*, *Probing dynamics of dark energy with latest observations*, e-Print: arXiv:1703.08293.

[184] N.D. Birrell and P.C.W. Davies, *Quantum Fields in Curved Space* (Cambridge Univ. Press, Cambridge, 1982).

[185] C. Patrignani *et al.* (Particle Data Group), Chin. Phys. C **40**, 100001 (2016).

[186] A. Babic *et al.*, Phys. Rev. D **71**, 124041 (2005).

[187] M. Maggiore, Phys. Rev. D **83**, 063514 (2011).

[188] S. Basilakos, N.E. Mavromatos, and J. Solà, Universe **2**, 14 (2016).

[189] D.J. Eisenstein *et al.* (SDSS Collaboration), Astrophys. J., **633**, 560 (2005).

[190] C. Alcock and B. Packzynski, Nature **281**, 358 (1979).

[191] M. Shoji, D. Jeong, and E. Komatsu, Astrophys. J. **693**, 1404 (2009).

[192] L. Anderson *et al.*, Mont. Not. Roy. Astron. Soc. **441**, 24 (2014).

[193] W. Hu and N. Sugiyama, Astrophys. J. **444**, 489 (1995).